9-27-2017 1:30 PM

An invasive tumor cell subpopulation as a therapeutic target in breast cancer

Tahereh Vakili
The University of Western Ontario

Supervisor
Dr. Eva Turley
The University of Western Ontario

Graduate Program in Biochemistry
A thesis submitted in partial fulfillment of the requirements for the degree in Master of Science

Abstract

Tumor heterogeneity and lack of targeted therapies are major hurdles in triple-negative breast cancer (TNBC) management. Elevated hyaluronan (HA) is a prognostic factor for poor outcome in TNBC. The TNBC MDA-MB-231 cell line contains highly metastatic but slow growing subpopulations that bind high levels of HA. I show these subpopulations express elevated HAS2, RHAMM and PGA3, and are more resistant to doxorubicin but more sensitive to MEK1 targeted therapy than parental cells or low HA binding subpopulations. Data bank mining show HAS2, RHAMM, and PGA3 are significantly associated with chemotherapy-treated BCa. Knockout of RHAMM using CRISPR/Cas9 gene editing reduced localization of active ERK1/2 to nuclei and sensitivity to MEK1 targeted therapy. These results show that RHAMM and likely HA are factors in TNBC subset in susceptibility to MEK inhibition, and that it is a potential biomarker for TNBC patients with sensitivity to MEK1 therapy.

Keywords

Tumor heterogeneity, Hyaluronan, HA, Chemoresistance, CD44, RHAMM, MEK inhibition, Targeted therapy, TNBC, Triple Negative Breast Cancer

Acknowledgments

I would like to express my sincere appreciation to my supervisor, Dr. Eva Turley, for her invaluable guidance, encouragement, and support throughout my time as a graduate student.
My gratitude is also extended to my committee members, Dr. Ann Chambers and Dr. Bonnie Deroo, for sharing their wealth of knowledge with me and providing guidance throughout this project.
I would like to acknowledge my examiners, Dr. James Koropatnick, Dr. David Rodenhiser, and Dr. Madhulika Gupta for taking the time to review my thesis and providing me with constructive criticism.
Special thanks are due to Dr. Vincent Morris for his time and useful advice during the journey of writing my thesis.
Thanks to past and present members of the Turley lab who made my student life a great experience. I would especially like to thank Sallie, Kate, and Sean for making lab life enjoyable. I would like to give special thanks to Jenny Ma for her constant support and kindness throughout my time in the lab. I would also like to thank Dr. Patrick Telmer and Dr. Conny Tolg for all their help and feedback throughout this project.

Lastly, I would like to convey my deepest gratitude to my family for their love and support throughout my life. In particular, my sister Fatemeh, who is the absolute best sister and friend anyone could ask for. I thank my love Farhad, who is always there to encourage and support me through the toughest moments of my life.

This thesis is dedicated to my son Ryan, who slowed down this journey, but filled my life with so much joy.

Table of Contents

Abstract i

Acknowledgments ii

Table of Contents iii

List of Tables vi

List of Figures vii

List of Abbreviations x

Chapter 1 1

1 « Introduction » 1

1.1 Histological and Molecular Subtypes of Breast Cancer 1

1.1.1 Triple Negative Breast Cancers 4

1.1.2 Diagnosis and Treatment of TNBC 6

1.1.3 Tumor Heterogeneity: a Hurdle for TNBC Diagnosis and Treatment 6

1.1.4 Hyaluronan as a Diagnostic and Prognostic Factor in TNBC 7

1.2 Hyaluronan and Its Receptors 9

1.2.1 Biology of Hyaluronan 10

1.2.2 Hyaluronan Receptors 12

1.3 Hyaluronan, CD44, and RHAMM Crosstalk in TNBC 16

1.3.1 Hyaluronan, CD44, and RHAMM in Tumorigenesis 17

1.3.2 Hyaluronan, CD44, RHAMM, and Regulation of Multidrug Resistance 18

1.4 The Raf/MEK/ERK Pathway as a Drug Target in TNBC 22

1.5 Hypothesis and Objectives 25

The objectives for this dissertation were as follows: 25

Chapter 2 27

2 « Materials and Methods » 27

2.1 Cell Culture 27

2.2 Fluorescence-Activated Cell Sorting 27

2.3 Cell Surface Marker and ALDH Activity Analyses 28

2.4 Half Maximal Inhibitory Concentration Assays 29

2.5 Intracellular Doxorubicin Accumulation 29

2.6 HA Synthase 2 Immunofluorescence Staining 30

2.7 HA Production 30

2.8 Flow Cytometry Assays of F-HA Binding and Cell Surface RHAMM and CD44 Expression 31

2.9 Analysis of RNA Expression Levels 31

2.10 Quantitative Real-time RT-PCR 32

2.11 METABRIC analysis 33

2.12 ERK 1/2 Activity and Localization 33

2.13 Generating RHAMM Knockout MDA-MB-231 Cell Line 34

2.14 Statistical Analysis 35

Chapter 3 36

3 « Results » 36

3.1 MDA-MB-231 Breast Cancer Cell Line Comprises Cells with High Levels of HA Binding That are Resistant to Doxorubicin 36

3.2 HA Synthase 2 Expression and Activity is increased in HA^{high} compared to HA^{low} Cells 44

3.3 Intracellular Doxorubicin Accumulation and Distribution Is Similar in HA^{high} and HA^{low} Cells 52

3.4 RHAMM Cell-Surface Display Is Higher in HA^{high} Compared to HA^{low} Cells ... 57

3.5 Cell Surface RHAMM Modulates MDA-MB-231 Cell Proliferation 60

3.6 RHAMM Modulates Intracellular Distribution of Activated ERK1/2 63

3.7 Sensitivity of MDA-MB-231 Cells to MEK1/2 Inhibition Depends on RHAMM Expression 66

Chapter 4 68

4 « Discussion » 68

4.1 RHAMM as a Prognostic Factor for Response to Chemotherapy and Targeted Therapy 68

4.2 The phenotypic stability of HA^{low} and HA^{high} TNBC Phenotypes 73

4.3 The Transcriptome of HA^{low} and HA^{high} Cells 73

4.4 Strategies for Increasing the Purity of Isolated HA^{low} and HA^{high} Subpopulations 74

4.5 Significance and Future Studies 74

4.6 Limitations 75

References 76

Curriculum Vitae 96

List of Tables

Table 1.1. Microarray classification of TNBC. 5

Table 3.1. Genes are differentially expressed in HA^{high} vs. HA^{low} subsets. 45

Table 3.2. IC_{50} of $RHAMM^{-/-}$ MDA-MB-231 cell treated with doxorubicin was 2.5-fold higher than for $RHAMM^{+/+}$ MDA-MB-231 cells. 63

Table 3.3. $RHAMM^{+/+}$ MDA-MB-231 cells are more sensitive to trametinib than $RHAMM^{-/-}$ MDA-MB-231. 67

List of Figures

Figure 1.1. Histological classification of breast cancer. 2

Figure 1.2. Molecular intrinsic classification of breast cancer. 3

Figure 1.3. Chemical structure of hyaluronan. 8

Figure 1.4. Schematic representation of mammalian HAS isoforms structure and a hypothetical model for the HA synthesis. 11

Figure 1.5. Schematic representation of mouse CD44 gene/protein structures. 14

Figure 1.6. Schematic representation of mouse RHAMM gene/protein structures. 15

Figure 1.7. HA: CD44 interaction stabilize multidrug transporters in the plasma membrane. 20

Figure 1.8. HA, CD44, RHAMM and regulation of drug resistance. 21

Figure 1.9. Schematic overview of the Raf/MEK/ERK signaling pathway upon binding HA to CD44 and RHAMM. 24

Figure 1.10. A proposed model for doxorubicin's mechanisms of anti-cancer. 26

Figure 3.1. Isolation of MDA-MB-231 cell subpopulations using fluorescent HA binding levels. 38

Figure 3.2. HA^{high} cells proliferate slower than HA^{low} cells. 39

Figure 3.3. IC_{50} of HA^{high} cell treated doxorubicin was four-fold higher than for HA^{low} cells. 40

Figure 3.4. HA^{high} and HA^{low} subpopulations do not display significant differences cancer-stem-cell markers ($ALDH^+$ $CD44^+$ $CD24^-$). 42

Figure 3.5. Alterations in HAS2 and PGA3 genes are associated with shorter overall survival in breast cancer patients. 46

Figure 3.6. Alterations in HAS2 gene are associated with shorter overall survival in breast cancer patients receiving chemotherapy. 47

Figure 3.7. HA^{high} cells displayed significantly enhanced HAS2 expression compared to HA^{low} cells. 49

Figure 3.8. HAS2 protein level is increased in HA^{high} cells. 49

Figure 3.9. HAS2 protein localizes to the cell membrane in HA^{high} cells to a greater extent than in HA^{low} cells. 50

Figure 3.10. HA^{high} cells produce higher levels of HA than HA^{low} cells. 51

Figure 3.11. Intracellular doxorubicin accumulation and distribution is not significantly different in HA^{high} and HA^{low} subpopulations. 53

Figure 3.12. Treatment of HA^{high} and HA^{low} cells with 4-MU reduced cell viability. 55

Figure 3.13. 4MU did not inhibit HA synthesis in HA^{high} to the level of HA in HA^{low} cells. 56

Figure 3.14. RHAMM cell-surface display was higher in HA^{high} than HA^{low} cells. 58

Figure 3.15. Alterations in HMMR, HAS2, and PGA3 genes is associated with shorter overall survival in breast cancer patients receiving chemotherapy. 59

Figure 3.16. Blocking cell surface RHAMM function significantly inhibited HA^{high} but not HA^{low} cell proliferation. 61

Figure 3.17. $RHAMM^{-/-}$ cells grew significantly more slowly than $RHAMM^{+/+}$ MDA-MB-231 cells. 62

Figure 3.18. $RHAMM^{-/-}$MDA-MB-231 cells exhibit lower ERK1/2 activity than $RHAMM^{+/+}$MDA-MB-231 cells. 64

Figure 3.19. pERK1/2 protein localize in the nuclei in $RHAMM^{+/+}$MDA-MB-231 cells to a greater extent than in $RHAMM^{-/-}$MDA-MB-231 cells. 65

Figure 3.20. HA^{high} cells are inhibited approximately two-fold more by PD98059 compared to HA^{low} cells. 67

Figure 4.1. Schematic representation of the Raf/MEK/ERK and PI3K pathway interconnectivity. 72

List of Abbreviations

4-MU: 4-methylumbelliferon

7-AAD: 7-aminoactinomycin D

ABC: ATP-binding cassette

ALDH: Aldehyde dehydrogenase

ASCO/CAP: American Society of Clinical Oncology/College of American Pathologists

ATCC: American Type Culture Collection

BAAA: BODIPY™- aminoacetaldehyde

Bcl-2: B-cell lymphoma 2

BL1: Basal-like 1

BL2: Basal-like 2

BRCA1: Breast cancer 1, early onset

BSA: Bovine serum albumin

CD44: Cluster of differentiation 44

cDNA: Complementary DNA

C-terminal: Carboxy terminal

DAPI: 4',6-diamidino-2-phenylindole

DEAB: Diethylaminobenzaldehyde

DMEM: Dulbecco's modified eagle medium

DNA: Deoxyribonucleic acid

DRP: Drug resistance protein

ECM: Extracellular matrix

EDTA: Ethylenediaminetetraacetic acid

EGF: Epidermal growth factor

EGFR: Epidermal growth factor receptor

ELISA: Enzyme-linked immunosorbent assay

EMT: Epithelial-mesenchymal transition

ER: Endoplasmic reticulum

ER: Estrogen Receptor

ERK1/2: Extracellular signal-regulated kinase 1/2

FACS: Fluorescence-activated cell sorting

FBS: Fetal bovine serum

FDA: Food and Drug Administration

F-HA: Fluorescent HA

FISH: Fluorescent in situ hybridization

FITC: Fluorescein isothiocyanate

GAG: Glycosaminoglycan

GAPDH: Glyceraldehyde 3-phosphate dehydrogenase

GI50: Growth Inhibitory-50

GlcNAc: N-Acetyl-D-glucosamine

GlcUA: D-glucuronic acid:

GPI: Glycosylphosphatidylinositol

HA: Hyaluronic acid/Hyaluronan

HAS: Hyaluronan synthase

HER2: Human epidermal growth factor receptor-2

HMMR: Hyaluronan-Mediated Motility Receptor

HYAL: Hyaluronidase

IC50: Inhibitory concentration-50

IDC: Invasive ductal carcinoma

IGF-1R: Insulin-like growth factor I receptor

IHC: Immunohistochemistry

IL: Interleukin

IM: Immunomodulatory

JNK: c-Jun N-terminal kinase

kDa: Kilodalton

KO: Knockout

LAR: Luminal Androgen Receptor

M: Mesenchymal

MAPK: Mitogen-Activated Protein Kinase

MEK: MAP/ERK kinase

mRNA: Messenger-ribonucleic acid

MRP: Multidrug resistance protein

MSL: Mesenchymal stem-like

NGF: Nerve growth factor

N-terminal: Amino terminal

OCT: Optimal cutting temperature

p53: Tumor protein p53

PBS: Phosphate buffered saline

PBS: Phosphate buffered saline

PCR: Polymerase chain reaction

PDGF-BB: platelet-derived growth factor-BB

PI3K: Phosphatidylinositol 3′ kinase

PR: Progesterone

RHAMM: Receptor for hyaluronan-mediated motility

RNA: Ribonucleic acid

ROS: Reactive oxygen species

SE: Standard error

SH2: Src homology 2 domain

SH3: Src homology 3 domain

SiRNA: Small interfering ribonucleic acid

TBS: Tris-buffered saline

TGFβ: Transforming growth factor β

TNBC: Triple-negative breast cancer

UDP: Uridine diphosphate

Chapter 1

1 « Introduction »

Breast cancer is the leading cause of cancer-related death among women in both advanced and less developed countries[1]. In Canada, breast cancer is the third most common cancer, accounting for 13% of all cancers and 25% of cancers among females. An estimated 26,300 and 230 new cases of female and male breast cancer, respectively, are expected to be diagnosed in Canada in 2017[2].

Despite high incidence rates, the female breast cancer mortality rate has substantially declined since its peak in 1987. The age-standardized mortality rates (ASMR) has dropped 44%, from 41.7 deaths per 100,000 in 1988 to a projected rate of 23.2 deaths per 100,000 in 2017[2]. The downward trend is likely due to a combination of advances in screening or prevention, improved diagnosis, and more effective treatment protocols.

Breast cancer is comprised of a group of heterogeneous diseases that differ significantly in their molecular, pathological, and clinical features. Several breast cancer classification systems have been developed and evolved over many decades, some of which are being used in prognosis and treatment in clinics and some of which currently are in preclinical development[3].

1.1 Histological and Molecular Subtypes of Breast Cancer

Clinically, breast cancer classification is based on tumor histology. It is sub-typed primarily into in situ carcinoma where the tumor is limited to the epithelial component of the breast, and invasive/infiltrating carcinoma where the tumor has invaded the stroma. In situ carcinomas are further categorized by their growth pattern and cytological features into ductal carcinomas (originating from the inner lining epithelium of the ducts) and lobular carcinomas (originating from the lobules that supply the ducts with milk). Similar to in situ carcinomas, invasive carcinomas have been classified into several subtypes. The main subtypes include invasive

ductal, invasive lobular, ductal lobular, tubular, colloid (mucinous), and medullary. Invasive ductal carcinoma (IDC) is, by far, the most common form of invasive breast cancer. It accounts for 55% of breast cancer incidence upon diagnosis and 70-80% of invasive lesions[4]. IDCs are a heterogeneous group of tumors classified according to cytoarchitectural features such as nuclear pleomorphism, glandular/tubule formation, and mitotic rate[5]. IDC is sub-typed as well-differentiated (grade 1), moderately-differentiated (grade 2), and poorly-differentiated (grade 3)[3, 5] (Figure 1.1). Differentiation describes how much or how little tumor cells look like the normal cells they came from. Here, well-differentiated IDCs look more like normal ductal cells and tend to grow and spread more slowly than poorly-differentiated counterparts[3].

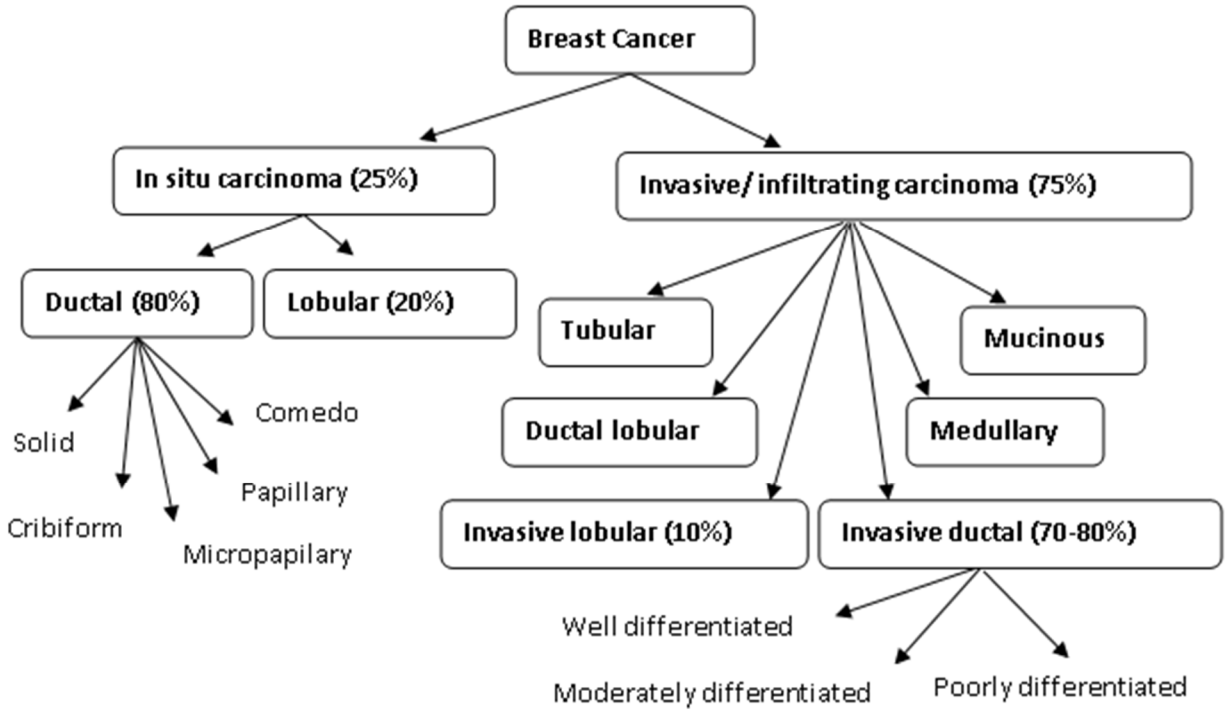

Figure 1.1. Histological classification of breast cancer.

Histological subtyping, which is most commonly used by clinicians, dissects the heterogeneity found in breast cancer based on architectural features and growth patterns (Figure reproduced from Malhotra *et al.*[3]).

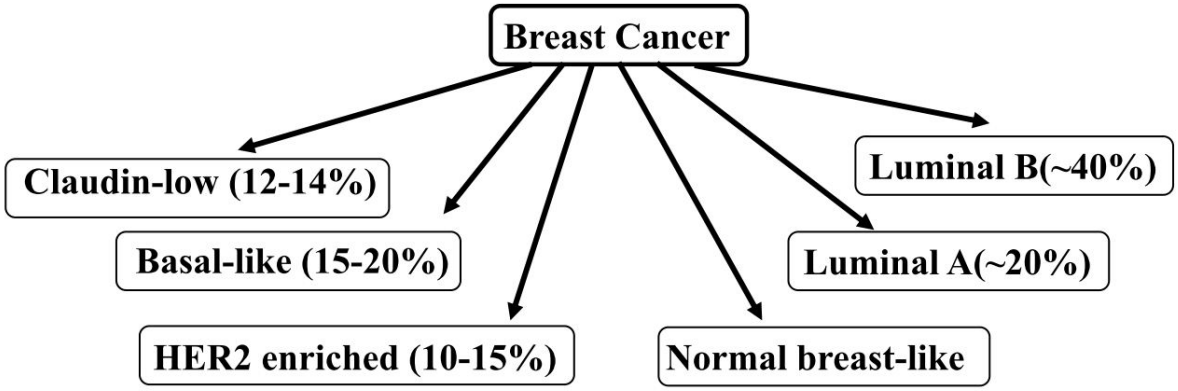

Figure 1.2. Molecular intrinsic classification of breast cancer.

This categorization is not currently used in clinical practice but is more practical in identifying molecular targets (Figure reproduced from Malhotra *et al.*[3]).

While histological subtyping of breast cancer has prognostic value, understanding the molecular basis for these classifications provides an opportunity to discover molecular targets and predict a response to them. Molecular subclassification focuses on gene expression signatures. Perou *et al.* in 2000, first categorized distinct molecular subtypes based on gene expression profiles into *ER-positive luminal-like A* and *B, basal-like*, *ErbB2-positive* and *normal-like* subgroups[6]. More recent studies identified a new subtype classified as "*claudin-low*"[7, 8] with reduced expression of Claudin proteins, components of epithelial tight junctions (Figure 1.2). This classification is based on the intrinsic molecular subtypes of breast cancer identified by microarray analysis of patient tumor samples[6-10].

The above classifications emphasize that breast cancer is not a single entity, but a complex and heterogeneous disease with distinct molecular and clinical characteristics. Despite the molecular heterogeneity of breast cancer, histological subtypes remain the mainstay of routine clinical diagnosis. However, these subtypes are of limited utility, since most of the breast cancers (approximately 75%) belong to a single subtype, invasive ductal carcinoma (IDC) of no special type. It has been shown that that combination of molecular/functional biomarkers with clinical

variables results in a system that is more robust and capable than any one system alone. Therefore, there is a need for designed genomic based clinical trials to advance the molecular subtypes to the level of clinical practice.

1.1.1 Triple Negative Breast Cancers

The advancement of "omics technologies" such as genomics and proteomics has provided exceptional insights into the molecular complexity of breast cancer[10-13]. Nevertheless, clinical decisions still rely primarily on the assessment of three markers: the expression of the endocrine receptors for estrogen (ER) and progesterone (PR) and the aberrant expression of human epidermal growth factor receptor-2 (HER2; also known as ErbB2). Triple-negative breast cancer (TNBC) is a clinical designation that applies to all the breast cancer phenotypes lacking expression of ER, PR, and HER2, and which therefore do not respond to therapies directed against these receptors. TNBC accounts for approximately 15% of breast cancers cases[14]. It is usually aggressive, with higher grade or more frequent lymph node metastasis, and it is usually more prevalent in younger, pre-menopausal, and especially African-American/Hispanic women[15]. TNBC patients also experience higher rates of distant metastases and lower five-year disease-free survival (DFS) rates than patients with other breast cancer subtypes, despite showing a better initial response to chemotherapy[16]. Therefore, with the remarkably high rates of relapse, developing improved treatments for TNBC is one of the highest priorities in current breast cancer research.

TNBC is itself a heterogeneous entity and can further be subclassified based on gene expression analyses. Thus, improved understanding of the biological characteristics and clinical behaviours of subtypes within TNBC is necessary for designing of clinical trials and developing personalized treatments. Lehmann *et al.*[17], using gene expression profiling of 587 TNBC samples, identified six molecular subtypes; *Basal-like 1 (BL1)*, *Basal-like 2 (BL2)*, *Immunomodulatory (IM)*, *Mesenchymal (M)*, *Mesenchymal stem-like (MSL)*, and *Luminal androgen receptor (LAR)* (Table 1.1).

Of note, triple-negative (TN) and basal-like (BL) breast cancer definitions have been commonly used interchangeably to describe breast cancers that do not express ER and PR, and overexpress/amplify HER2 gene. Despite a significant overlap (approximately 70%) between TNBC and basal-like breast cancer, gene expression data suggest that these two subtypes are not equivalent[18].

Table 1.1. Microarray classification of TNBC.

Subtypes	**Genetic signature**
Basal-like 1	Enriched in cell cycle and DNA damage response (ATR–BRCA pathway) gene
Basal-like 2	Enriched in growth factor signaling pathways (EGF, MET, NGF, Wnt/β-catenin, IGF-1R), glycolysis, gluconeogenesis, and myoepithelial markers
Immunomodulatory	Enriched in immune cell processes; immune cell signaling such as TH1/TH2, NK cell, and B cell receptor pathway, cytokine signaling such as IL-12, and IL-7 pathway, antigen processing/presentation, and signaling through core immune signal transduction pathways such as NFKB, TNF, and JAK/STAT signaling
Mesenchymal	Enriched in components of cell motility, cell differentiation, and growth pathways such as Wnt, anaplastic lymphoma kinase pathway, and TGF-β signaling, EMT
Mesenchymal stem-like	Similar to *Mesenchymal* but low levels of proliferation, and claudins 3, 4, and 7 genes, Angiogenesis genes
Luminal androgen receptor	Enriched in androgen receptor gene, displays luminal gene expression pattern

Six molecular subtypes of TNBC based on gene expression profiling of 587 TNBC samples[17, 19]

Abbreviations: DNA, deoxyribonucleic acid; EGFR, epidermal growth factor receptor; EMT, epithelial-mesenchymal-transition; IGF-1R, insulin-like growth factor I receptor; IL, interleukin; MET, hepatocyte growth factor; NGF, nerve growth factor.

1.1.2 Diagnosis and Treatment of TNBC

As mentioned earlier, in spite of the molecular heterogeneity of TNBC, clinical decisions (diagnosis and treatment) still rely primarily on the presence of the endocrine receptors for estrogen and progesterone and the aberrant expression of HER2. Immunohistochemistry (IHC) is currently the main hormone receptor assessment. Based on American Society of Clinical Oncology/College of American Pathologists (ASCO/CAP) guidelines, ER and PR assays should be considered positive if at least 1% of tumor cells in the sample demonstrate positive nuclear staining by immunohistochemistry[20]. HER2 status is determined by IHC and usually, an additional fluorescent *in situ* hybridization (FISH), which assesses HER2 gene amplification, is used to confirm IHC results[21].

Treatment of patients with TNBC has been challenging as this type of tumor does not express PR, ER, and HER2 receptors, and as a result, cannot be managed with presently targeted therapies such as the anti-HER2 monoclonal antibody Trastuzumab, and hormonal (endocrine) therapy. Hormonal therapy includes preventing the production of estrogen and progesterone and/or blocking their receptors signalling in breast cancer cells. With the lack of FDA approved targeted therapies available for TNBC, mono- or combination chemotherapy remains the only systemic treatment option for patients in the neoadjuvant, and adjuvant (the administration of therapeutic agents before or after the main treatment, respectively), or metastatic settings.

1.1.3 Tumor Heterogeneity: a Hurdle for TNBC Diagnosis and Treatment

TNBC presents a significant challenge for the treatment and management with chemotherapy mainly because of the vast intertumor and intratumor heterogeneity. Intertumor heterogeneity refers to heterogeneity between tumors from different patients or different lesions from the same patient. By contrast, intratumor heterogeneity refers to heterogeneity within one tumor at any given time. Tumor cells can show three different levels of heterogeneity. Firstly, tumor cells can contain distinct genetic alterations. Secondly, cells with the same genetic landscape can have different epigenetic alterations and states of differentiation. Thirdly, tumor cells can be influenced by a complex and diverse microenvironment generated by stromal cell heterogeneity

that supports tumor growth, reduces immune surveillance, and impede penetration of therapeutic drugs.

Decoding the molecular basis of tumor heterogeneity could bring insights to more effective therapeutic strategies. Therefore, it is necessary to identify prognostic factors that are associated with poor outcome and are potentially involved in treatment resistance. These factors can be used as probes to sort tumor cells into distinct and homogeneous subsets for investigating their responses to treatments.

While both genetic and phenotypic markers are available to characterize tumor heterogeneity, phenotypic markers can be more informative than genetic changes. The genotype to phenotype map is not simple and genetic heterogeneity may not translate directly to phenotypic heterogeneity. Therefore, tumor phenotypes, which reflect genetic diversity as well as microenvironmental dynamics of the tumor, may provide a powerful diagnostic and prognostic tool.

1.1.4 Hyaluronan as a Diagnostic and Prognostic Factor in TNBC

Hyaluronan (HA), a polymer of alternating *N*-acetylglucosamine and glucuronic acid disaccharides (Figure 1.3), is a suitable prognostic/diagnostic factor for several reasons. First, elevated production of HA has been shown to provide many different cancer cell lines with drug resistance[22]. Second, HA accumulation within breast cancer cells and peritumor stroma is a predictor of poor outcome[23] as well as an indicator of the conversion of the pre-invasive form of breast cancer, ductal carcinoma in situ, to an early invasive form of breast cancer[24, 25].

Veiseh *et al*. in 2014[25] revealed a novel type of breast cancer phenotypic heterogeneity based on the level of HA binding which was linked to pre-disposition to invade and metastasize. These authors showed that binding levels of a fluorescent HA probe (F-HA) to human breast cancer cell lines of different molecular subtypes (basal-like such as MDA-MB-231 and T4-2, and luminal such as MCF-7 and SKBR3) were heterogeneous. The most malignant cell line, the TNBC MDA-MB-231, exhibited the highest HA binding heterogeneity. Fluorescence-Activated

Cell Sorting (FACS) identified MDA-MB-231 subpopulations that bind high levels of F-HA (HA^{high}) were unexpectedly different from those binding little or no probe (HA^{low}). HA^{high} cells proliferated slowly but were highly invasive *in vitro* and metastatic *in vivo*, while HA^{low} cells were more proliferative but poorly invasive, and did not form detectable metastases. These results are consistent with evidence linking high levels of HA to poor outcome of breast cancer patients. Furthermore, elevated expression of HA receptors, which link HA to the cell surface and mediate HA signaling instructions, have also been implicated in breast cancer aggression[26].

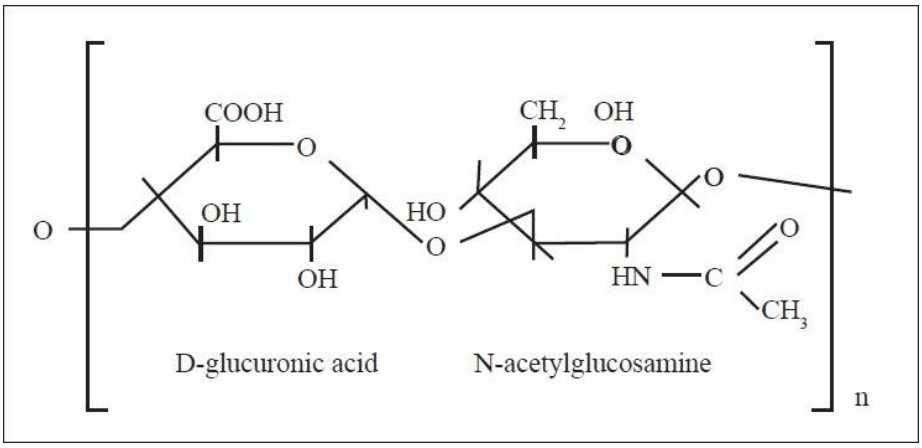

Figure 1.3. Chemical structure of hyaluronan.

Repeating disaccharide unit of HA molecule consisting of D-glucuronic acid and N-acetylglucosamine, linked with alternating β-1,4 and β-1,3 glycosidic bonds (Figure adapted from Bansal *et al.*[27]).

1.2 Hyaluronan and Its Receptors

HA was isolated from the vitreous body of bovine eyes in 1934 by Meyer and Palmer[28]. Its chemical structure, which consists of repeating disaccharide units of N-acetylglucosamine (GlcNAc) and D-glucuronic acid (GlcUA) linked with alternating β-1,4 and β-1,3 glycosidic bonds: $[-\beta(1,4)\text{-GlcUA-}\beta(1,3)\text{-GlcNAc-}]_n$[29] (Figure 1.3), was revealed 20 years later by Weissmann *et al*.[29]. Under normal physiological conditions, HA can consist of up to 2,000-25,000 disaccharides with a relative molecular mass of 1-10 MDa (each disaccharide is approximately 400 daltons) and chain lengths of 2-25 μm (the average length of a disaccharide is approximately 1 nm)[30]. The molecular mass of HA extracted from tissues ranges from 10^4-10^7 Da[31, 32]. While HA is distributed in all tissues and body fluids of the human body, it is abundantly expressed as a native homeostatic form in soft connective tissue and skin[33].

At physiological pH, HA is highly negatively charged due to ionization of the carboxyl group of the glucuronic acid[34]. The HA molecule is hydrophilic and based on its size can fold into different conformations in water. Biophysical studies show that large HA (> 10^3 kDa) forms a random coil, whereas very small (*e.g.*, 10 kDa) HA form a rod high molecular weight HA[35, 36]. Twists in the HA chain form hydrophobic patches, which allow interactions with cell membranes, other HA chains, proteoglycans and other extracellular macromolecules that are important in the organization of extracellular and pericellular matrices[37]. These hydrodynamic characteristics of HA help to regulate the porosity and malleability of these matrices, which are crucial factors in determining whether cells invade tissues during development, tissue remodeling and cancer progression. In addition, a HA viscous meshwork protects cells against mechanical forces and excludes large macromolecules; also, it slows the diffusion of substances unable to penetrate the network[38]. In the body HA occurs in the salt form, hyaluronate, and serves to lubricate, hydrate, or space-fill tissues such as joints and connective tissue[39, 40]. Besides the viscoelastic and hydrating properties, HA has various signaling activity by binding to its extracellular and intracellular binding proteins/receptors which will be discussed later. During disease or tissue remodeling HA is degraded, as a result of free radicals or hyaluronidase activity, into fragments that differ structurally and functionally from large HA[41, 42]. Also, different sizes of HA binds to different receptors and therefore the signaling outcome varies in response to the size of HA bound[36].

1.2.1 Biology of Hyaluronan

The production of HA is a complex, tightly regulated, and multi-step process. HA is synthesized by three distinct HA synthases that are found in vertebrates, certain bacteria, and chlorella virus PBCV-1[43]. The HA synthase genes in humans include three members: HAS1, HAS2, and HAS3. The structures of the three genes are well-conserved with highly homologous amino acid sequences, but the genes are located on separate chromosomes; HAS1 is located on chromosome 19q13.4; HAS2 resides on chromosome 8q24.12; HAS3 is on chromosome 16q22.1[44]. HAS1 gene has five exons, whereas HAS2 and HAS3 have four[45]. HAS1 and HAS3 have been shown to have splice variants. HAS1 has been shown to have splice variants in Waldenström's macroglobulinemia[46], multiple myeloma[47] and bladder cancer[48]. HAS3 has two separate variant transcripts (4.9kb and 2.0kb) coding for proteins[49]. HASs are plasma membrane proteins with seven transmembrane domains, two of which are located at the N-terminal end and five at the C-terminal end (Figure 1.4 A) connected by a large cytoplasmic loop[43, 50]. The enzymes need Mg^{2+} or Mn^{2+} in addition to the two substrates UDP-glucuronic acid and UDP-N-acetylglucosamine. The expression of HAS isoforms is regulated in a different manner. Transcriptional regulation of the three HAS genes varies with respect to developmental stage and tissue type as well as in response to growth factors and cytokines. The three mammalian HAS isoforms differ in kinetic characteristics and produced HA size. HAS2 synthesizes very large HA molecules (> 2×10^3kDa), whereas smaller sizes of HA are synthesized by HAS1, and HAS3 (2×10^2-2×10^3 kDa)[51].

The cellular synthesis of HA is a unique process; unlike most glycosaminoglycans, it is not made in the cell's Golgi network. Polymerization of HA takes place at the inner surface of the plasma membrane[52], and the growing HA chain may be extruded or translocated through the plasma membrane, possibly through channels generated by oligomerization of HASs into the extracellular space[53, 54] (Figure 1.4 B).

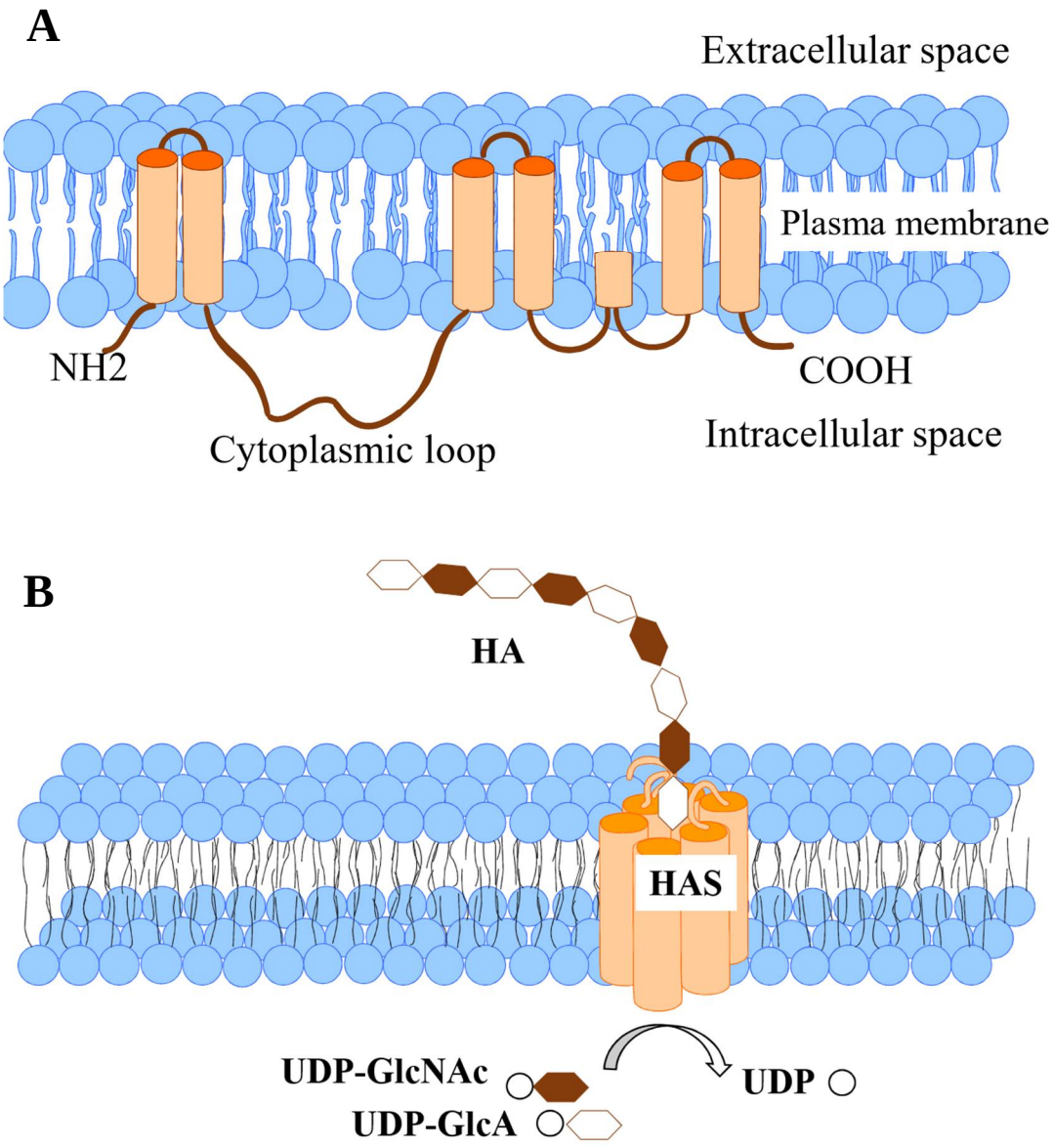

Figure 1.4. Schematic representation of mammalian HAS isoforms structure and a hypothetical model for the HA synthesis.

(A) All mammalian HAS enzymes have seven membrane-spanning domains; two located at the N-terminal end and five at the *C*-terminal end. **(B)** The HAS enzymes use GlcNAc and GlcA from the UDP-sugars to polymerize HA. They also transport the growing HA chains out of the cell through a channel-like structure after polymerization at the inner surface of the plasma membrane (Figure reproduced from Itano *et al.*[51]).

1.2.2 Hyaluronan Receptors

HA was long considered to be an inert component acting only as “glue” or “space filler” for the extracellular matrix. It is now established, however, that HA has many biological and instructive functions[55]. Through its interactions with specific receptors, HA regulates several important cellular processes such as proliferation, migration, differentiation, angiogenesis, and tumor progression[56]. HA signaling properties are influenced by HA fragment size. For example, high molecular weight HA has mediated antiangiogenic and immunosuppressive effects, whereas HA fragments promote angiogenesis and inflammation[57-60]. HA fragmentation can occur as a result of direct action of reactive oxygen and nitrogen species or hyaluronidase activity (*e.g.*, Hyal1 and Hyal2)[41, 42]. Furthermore, HA signaling properties is cell-specific depending on specific receptor expression, specific signaling pathways, and cell cycle.

HA receptors bind HA via either a common domain called the link module, or a B(X7) B consensus motif, where “B” represents arginine/lysine and “X” represents any non-acidic amino acid[61, 62]. The best-characterized HA receptors for functions in breast cancer are CD44 and RHAMM (receptor for hyaluronic acid-mediated motility), which upon the binding to HA induce the transduction of a range of intracellular signals, directly or by activating other receptors[30].

HA can be tethered to the cell surface through interaction with receptors such as CD44 and proteoglycan molecules, which are highly negatively charged and repel each another, causing HA to extend out exhibit the cell surface in a brush-like configuration. As mentioned before, HA can also be retained at the cell surface by sustained transmembrane interactions with its synthases. HA retention can form a pericellular matrix/coat that as a protective barrier.

1.2.2.1 Biology of CD44

CD44, the primary cell surface receptor for HA[63], is a single pass transmembrane glycoprotein, also referred to as P-glycoprotein 1[64]. In human, it is encoded by a single gene located on chromosome 11p13[65, 66]. The CD44 molecule consists of the extracellular domain (ectodomain), the transmembrane domain, and the intracellular domain (cytoplasmic tail)[66]. This glycoprotein was first discovered as a homing receptor for lymphocytes[67, 68] called CD44H, which is also known as the standard isoform (CD44s) as it is the simplest variant. CD44 is subjected to alternative splicing. The CD44s, with a molecular weight of 85-90 kDa in SDS-PAGE, is the smallest form of CD44 and is expressed in most cell types[69]. Alternative splicing happens at specific sites within the extracellular domain generating more than 20 isoforms with a molecular weight of 85-200 kDa[70-72]. CD44s is encoded by nine non-variable exons, exons 1-5 and 16-20, while the variants of the receptor also include variable exons 6 to 15 (alternatively designated v2- 10, exon v1 is not expressed in the human being)[72-74] (Figure 1.5).

The extracellular region of CD44 can be divided into a distant conserved region, (with 85% sequence identity between mammals) and a non-conserved region proximal to the plasma membrane. The conserved region comprises N-glycosylation sites and the HA-binding link module, while the non-conserved region contains sites for alternative splicing, O-glycosylation with or without the addition of chondroitin sulphate or heparan sulphate[75]. Depending on cell type and state of the cell, CD44 undergoes different posttranscriptional modifications such as phosphorylation[76], palmitoylation[77], and proteolytic cleavage[78, 79] or oligomerization[80]. CD44s is widely expressed in a variety of normal tissues including all cell types of blood, lung, and epidermis, whereas CD44 variants are expressed on a tissue- and differentiation-specific manner[71, 81].

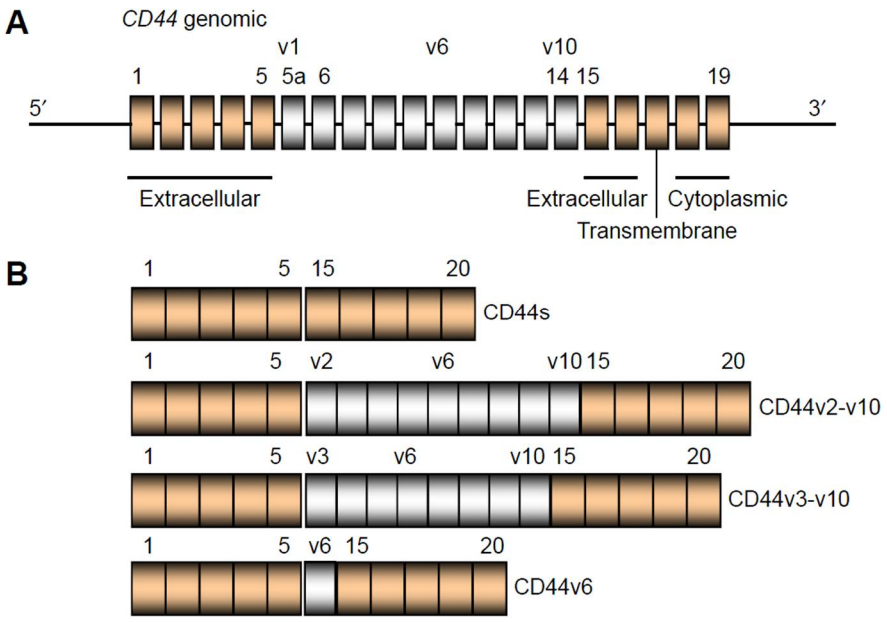

Figure 1.5. Schematic representation of mouse CD44 gene/protein structures.

(A) The CD44 gene is comprised of 10 constant exons (exons 1–5 and 15–19) shown in tan that encode the extracellular, transmembrane, cytoplasmic tail domains, and 10 variable exons- 9 variable exons in human- for the extracellular domain (shown in silver). The exon 5a or exon v1 is not expressed in humans. **(B)** Protein structures of the standard (CD44s) and variant CD44 (CD44v) proteins. Alternative splicing of CD44 predominantly involves variable insertion of 10 extra exons (v1-v10) between exons 5 and 15. CD44v contains amino acid sequences between those encoded by exons 5 and 15 (exons 5a–14) The relative sizes of the exons and introns are not drawn to scale (Figure adapted from Inoue *et al.*[82]).

1.2.2.2 Biology of RHAMM

RHAMM, (receptor for hyaluronic acid-mediated motility), was first isolated and cloned from subconfluent migrating cardiac fibroblasts as a cell surface HA receptor involved in cell locomotion, but lacking a signal peptide for export through the Golgi ER[83, 84]. Although RHAMM was first located at the cell surface, it was also later discovered to also occur as an intracellular protein, within the cytoplasm and in the nucleus[85-88]. The cell surface form of RHAMM is designated as CD168[89]. The *HMMR* (Hyaluronan-Mediated Motility Receptor) gene that encodes for RHAMM is located on chromosome 5q33.2 in humans and four different

isoforms, generated by alternative splicing of its messenger RNA, are found both on cell surfaces and inside the cells[90, 91]. The constitutively expressed and most common RHAMM mRNA transcript encodes the largest intracellular RHAMM protein, 85 kDa in human, that has been designated as v5[92]. Full-length RHAMM is encoded by 18 exons, and three variant forms are encoded by alternatively spliced exon 4, 5, or 13 (Figure 1.6)[93, 94]. Full-length RHAMM and its isoforms do not have the link module domain and GPI tail to integrate into the cell membrane[90]. At the cell surface, RHAMM binds to HA and a number of receptor tyrosine kinases (RTKs) and non-TK receptors, including PGFR[91], TGFβ receptor-1[95], CD44[96, 97], CD44-EGFR (epidermal growth factor receptor) complexes[98, 99], bFGFR[100], and RON[101]. All RHAMM isoforms have two positively charged $B(X)_7B$ motifs on its carboxyl terminal that are required for HA binding[62]. TGFβ-1, RON, and the YAP-HIPPO pathway promote RHAMM expression, while p53 and BRCA1 suppress its expression[89, 95, 101-108]. Under the homeostatic condition, RHAMM expression is tightly regulated and is absent or only present at low concentrations. However, RHAMM mRNA and protein expression are transiently increased in response to injury and during inflammation and cancer[109].

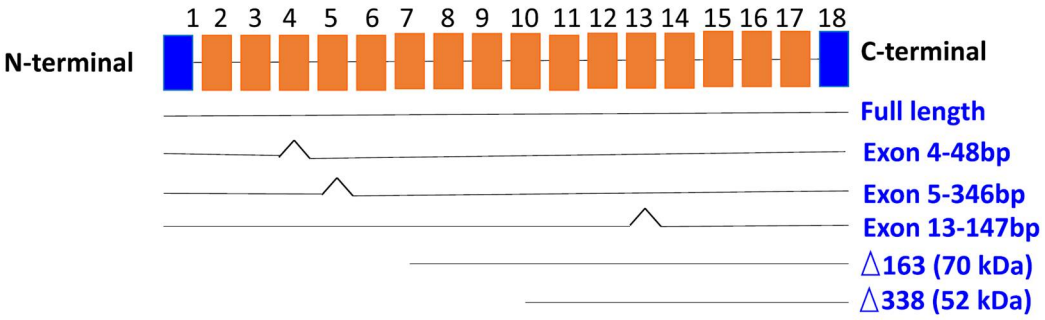

Figure 1.6. Schematic representation of mouse RHAMM gene/protein structures.

The RHAMM gene is comprised of 18 exons. Full-length RHAMM encodes a 794-amino acid protein sequence (85kDa protein with a 725-amino acid sequence in human). It contains two tubulin-binding sites, at the N-terminus and C-terminus (exons 4 and 16), for binding to interphase and mitotic spindle microtubules, respectively. Three isoforms are generated by alternative splicing of exon 4, 5, or 13. The C-terminal of RHAMM contains HA and ERK binding sites. The relative sizes of the exons and introns are not drawn to scale (Figure adapted from Misra *et al.*[110]).

1.3 Hyaluronan, CD44, and RHAMM Crosstalk in TNBC

HA plays complex roles in TNBC, some of which result from its physicochemical properties and some of which depend upon receptor mediated signaling[110-112]. The former is mechanical, relating to purely physical interactions regulating cell-cell adhesion, cell migration, growth, and differentiation. Furthermore, HA can physically protect cells against immune attack, and small molecule therapeutics by forming pericellular coats[30, 113-115]. The latter is biological in nature, involving the interaction of HA with its cell membrane receptors to induce signaling pathways and subsequent genes' expression. HA induces several signaling pathways upon binding to its receptors. Both CD44 and RHAMM, which are known to have roles in cancer pathogenesis, mediate HA signaling[90]. While CD44 and RHAMM can interact independently with HA, in some cases, they exhibit both cooperative and interchangeable functions. For example, interactions at the cell surface between CD44 and RHAMM have been shown to activate signaling cascades which promote cancer cell motility[89]. Sometimes, RHAMM can compensate for loss of CD44 in binding HA, which should be considered in experiments with CD44-null mice[116].

As has been mentioned earlier, all CD44 isoforms contain a link module HA-binding site in their extracellular domain. When HA binds to CD44, it brings CD44 in close proximity to signaling receptors such as ErbB2, EGFR, or TGF-β type 1 receptors, allowing for direct association and interaction between receptors and their signaling complexes in a tightly localized lipid raft[117]. In response to HA binding, and depending on the cellular context, the intracellular domain of CD44 variants selectively interacts with many regulatory and adaptor proteins and modulates specific signaling pathways[118, 119]. Therefore, the binding of CD44 to HA affects cell adhesion to extracellular matrix components and is also involved in the stimulation of aggregation, proliferation, migration, and angiogenesis[119-122].

Mitogen-activated protein kinase (MAPK) cascades are the major signal transducing pathways that are activated by HA: HA receptor interactions. Activation of upstream molecules such as EGFR stimulates the activation of downstream MAPK kinases that are involved in a variety of fundamental cellular processes such as proliferation, differentiation, motility, stress response, apoptosis, and survival. Each kinase phosphorylates and, thereby, activates the next member in

sequence. The most relevant of all, for intracellular mechanisms involved in TNBC, are the activated extracellular signal-regulated kinase/mitogen-activated protein kinase (ERK/MAPK), c-Jun N-Terminal Kinase/c-Jun (JNK/c-Jun), as well as the phosphoinositol-3-kinase/ Protein kinase B (PI3K/Akt) pathways[118, 119]. ERK is one of the proteins that is phosphorylated on tyrosine as a result of HA/RHAMM interactions[123].

HA and its receptors CD44 and RHAMM have been implicated in all steps of breast cancer progression such as migration, invasion, adhesion, and proliferation. In this thesis, emphasis is placed upon their contribution to cell proliferation and drug resistance.

1.3.1 Hyaluronan, CD44, and RHAMM in Tumorigenesis

HA, and its receptors CD44 and RHAMM, contribute to tumorigenesis through their effects on cell proliferation. Some of these effects are the result of the physical properties of HA and some are mediated by binding of HA to CD44 and RHAMM and the subsequebt activation of cellular proliferation[124, 125].

HA facilitates cancer cell proliferation by the formation of highly hydrated matrices that facilitate enhanced cell proliferation[124]. Increased HA synthesis in cancer cells results in the formation of hydrated and less dense matrix that facilitate tumor cell motility and invasion[126]. However, HA has a dual effect on cell proliferation; high molecular weight HA (HMW-HA) has a protective effect against cancer cell proliferation and tumorigenesis. For example, HMW-HA treatment has been shown to inhibit growth in a human colon carcinoma xenograft after chemotherapy[127]. On the other hand, LMW-HA promotes progression of breast cancer (MDA-MB-231 cells)[128].

Furthermore, HA can promote proliferation by activating several signaling cascades in cancer cells. HA promotes the interaction of CD44 and EGFR resulting in activation of MAPK pathway and further induction of cell proliferation[124].

The functional roles of CD44 and RHAMM in tumorigenesis are largely a consequence of their ability to bind HA and activate signaling pathways that are implicated in breast cancer progression. CD44 has dual functions in both tumor cell proliferation and growth inhibition, dependent on biological conditions. CD44 promotes or inhibits cell proliferation when cells are at low density or confluent, respectively. Also, the dual functions of CD44 in cancer depend on expression of specific variant isoforms of CD44v, which regulate tumor-initiating cells in subpopulations of cancer cells[129]. Expression of distinct variants of CD44 is linked with progression and metastasis of cancer cells as well as patient prognosis[130, 131]. Similarly, RHAMM has dual functions to maintain cell behavior. Overexpression of RHAMM was found in highly proliferative cells in breast cancer and multiple myeloma[132], whereas loss of RHAMM is linked to peripheral nerve sheath tumor progression[133].

Several studies have addressed RHAMM contribution to cell proliferation[98, 134, 135]. Mohapatra *et al.*[134] showed that interfering with RHAMM functions, either by using soluble recombinant RHAMM protein or by suppressing its function by using dominant negative mutant or antisense RHAMM, results in decreased levels of Cdc2 and Cyclin B1 proteins and consequently a G2/M arrest in H-ras transformed fibroblasts. Soluble RHAMM causes G2/M arrest in ras-transformed fibroblasts without affecting their progression through S-phase[135]. Moreover, it has been shown that RHAMM induces proliferative activities of cementifying fibroma cells through a mechanism that involves the interaction of CD44 and EGFR[90].

1.3.2 Hyaluronan, CD44, RHAMM, and Regulation of Multidrug Resistance

Drug resistance in tumor cells can arise in numerous ways, such as through decreased access to or uptake of anti-cancer drugs, increased anti-cancer drug efflux, and activation of repair and detoxifying systems[30]. Classic multidrug resistance generally results from elevated drug export through the ATP-dependent efflux pumps, such as MDR (multidrug resistance), MRP (multidrug-resistance protein) and other members of the ATP-binding cassette (ABC) transporter families[136]. Moreover, it is known that alterations in cell survival and apoptotic signalling

pathways are related to drug resistance in cancer cells[22]. Therefore, therapeutic interventions that induce downstream events in the apoptotic cascade might help to overcome drug resistance in patients[137, 138].

HA and its receptors are involved in promotion and regulation of multidrug resistance in a variety of cancer cell types via both receptor-dependent and/or -independent pathways[139, 140 141]. First, HA can bind to its cell surface receptors such as CD44 and RHAMM to form a coat of HA on cancer cells. This pericellular HA coat promotes drug resistance by preventing/decreasing the uptake of cytotoxic drugs. Results of clinical studies have demonstrated the enhanced efficacy of chemotherapeutic agents in cancer patients pretreated with bovine hyaluronidase[142].

Furthermore, the interaction of HA and CD44 in cancer cells has been strongly implicated in the development of drug resistance[139, 140]. It has been reported that HA: CD44 interactions promote expression of multidrug transporter1 (MDR1)[143], P-glycoprotein, and multidrug resistance protein 2 (MRP2), stimulating chemoresistance in breast cancer cells[141]. Slomiany *et al.*[144, 145] showed that treatment of cells with HA oligosaccharides induces rapid internalization of the drug transporters, BCRP and P-glycoprotein. They concluded that the effect of HA on transporter expression may be mediated by stabilization of these transporters in the plasma membrane rather than on synthesis. HA can be tethered to its receptors such as CD44 and RHAMM at the plasma membrane and stabilizes actin-linked CD44-transporter complexes in lipid microdomains (Figure 1.7).

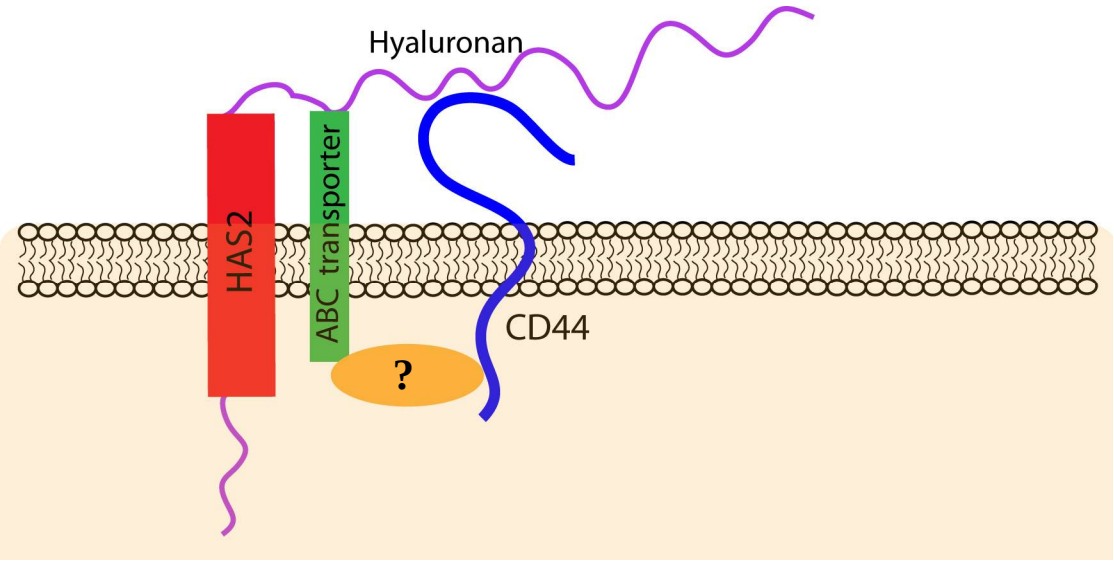

Figure 1.7. HA: CD44 interaction stabilize multidrug transporters in the plasma membrane.
HA is synthesized by HAS2 and binds to CD44 at the plasma membrane whereby it stabilizes CD44-transporter complexes in lipid microdomains. The interaction between CD44 and multidrug transporters is not direct and the orange oval depicts unidentified proteins (Figure reproduced from Toole *et al*.[146]).

Finally, HA and its receptors alter drug resistance by stimulating cell-survival signalling pathways (Figure 1.8). Increased HA production was found to stimulate drug resistance in drug-sensitive cancer cells. In addition, disruption of endogenous HA-induced signaling suppresses drug resistance in several cancer cell lines, including TNBC MDA-MB-231[22]. HA: CD44 interactions promote resistance to a variety of chemotherapeutic drugs, by activation of PI3K signaling that supports cell survival via AKT and induces multidrug transporter[22, 143]. PI3K signaling modulates multidrug resistance (MDR) transporter expression and function and phosphorylates Akt (p-Akt) to activate cell-survival signaling. Moreover, the HA: CD44 interaction induces c-Jun signaling pathway which plays a crucial role in oncogenic microRNA-21 production resulting in survival protein (Bcl-2/IAP) and MDR1 upregulation and consequently chemoresistance in TNBC[118]. MicroRNAs (miRNAs) (of about 21–25 nucleotides) are single-stranded RNAs that are involved in the modulation of gene expression at the posttranslational level. Furthermore, HA: CD44: RHAMM multidrug resistance can be promoted through the mammalian Hippo signaling pathway. Upon binding HA to CD44, the HIPPO pathway becomes blocked, which results in increased apoptosis resistance[147, 148]. In a feedback

loop, activated YAP, one of the Hippo pathway component, binds to the promoter of RHAMM, thereby inducing RHAMM transcription[149, 150].

Although RHAMM can be involved in CD44/HA effect in chemoresistance, to my knowledge, no study has yet investigated the direct role of RHAMM in multidrug resistance.

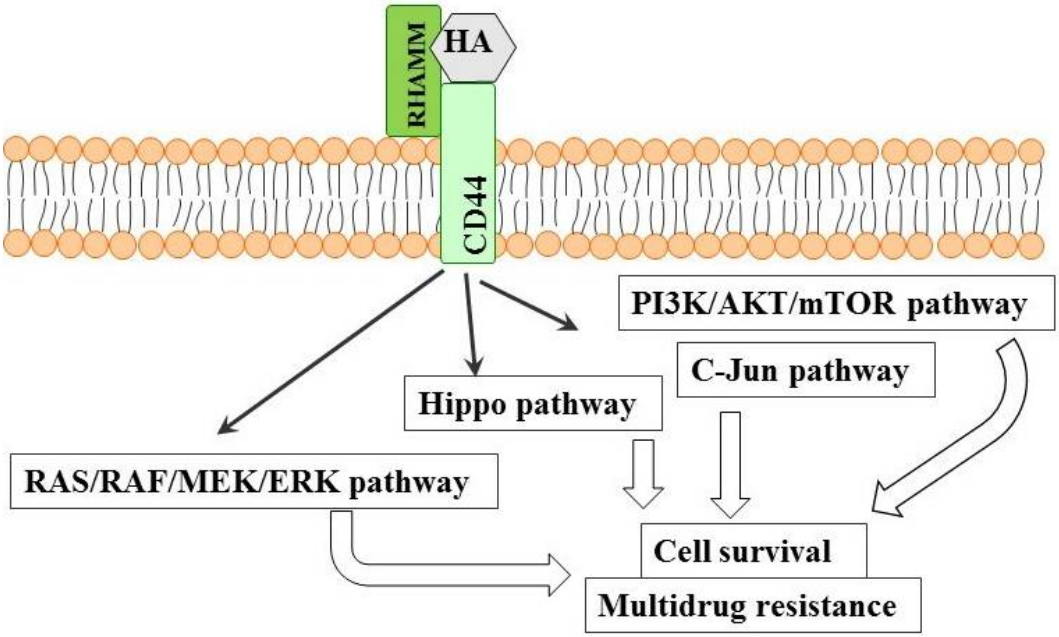

Figure 1.8. HA, CD44, RHAMM and regulation of drug resistance.

HA/CD44/ RHAMM complex activates a couple of signaling pathways that lead to increased cell survival and multidrug resistance.

1.4 The Raf/MEK/ERK Pathway as a Drug Target in TNBC

Interactions between HA and its receptors, CD44 and RHAMM, result in a ligand-clustering and activation of several signaling pathways including the Raf/MEK/ERK pathway. Both CD44 and cell-surface RHAMM function as co-receptors to activate receptor tyrosine kinases (RTKs) such as EGFR, c-MET, and PDGFR. Intracellular RHAMM forms complexes with approximately 20% of total cellular MEK1:ERK1/2 kinases[91], as determined by co-immunoprecipitation analyses (Figure 1.9). RHAMM contains recognition sequences for ERK1/2 and direct binding and site-directed mutation assays show that intracellular RHAMM binds directly to ERK1 but only indirectly with ERK2 and MEK1. RHAMM's function in ERK1/2:MEK1 complexes appears to be as a scaffold protein that directs these complexes to subcellular compartments (*e.g.*, nucleus, membrane extensions) and affects the kinetics of ERK1/2 activation.

The Raf/MEK/ERK is a kinase cascade whose targets are cytoskeletal proteins and transcription factors (Figure 1.9). Upon ligand activation of growth factor receptors, Ras associates with GTP and activates Raf (Raf-1, B-Raf and A-Raf) which phosphorylates the upstream kinase activator of ERK1/2 *(i.e.*, mitogen-associated/extracellular regulated kinase-1 [MEK1]). MEK1 activates extracellular signal-regulated kinases 1 and 2 (ERK1 and ERK2) on specific threonine and tyrosine residues (at Thr202/Tyr204 for human ERK1 and Thr185/Tyr187 for human ERK2). ERK1/2 are highly related proteins that knockout experiments show can perform different functions[151]. When expressed together, ERK1/2 either phosphorylate and activate a variety of substrates in the cytoplasm including transcription factors that then translocate into the nucleus, or themselves translocate into the nucleus where they directly participate in transcriptional complexes[152], particularly those regulating genes that are involved in apoptosis and cytotoxic drug resistance.

The ability of the Raf/MEK/ERK pathway to promote expression of genes involved in apoptosis and cytotoxic drug resistance promotes cell survival during therapy. For example, this pathway phosphorylates apoptotic regulatory machinery including Bcl-2, Bad, Bim, Mcl-1, and caspase 9[152, 153]. Furthermore, increased expression of Raf increases the levels of both the MDR1 drug pump and the anti-apoptotic Bcl-2 protein in MCF-7 breast cancer cells[154, 155], which has been associated with drug resistance in these cells.

The Raf/MEK/ERK kinase cascade also regulates breast cancer cell motility, necessary for invasion and metastasis[156, 157]. Invasive/highly motile breast cancer cell lines such as MDA-MB-231 utilize cell surface RHAMM and CD44 to coordinate an HA-dependent autocrine mechanism that sustains ERK1/2 signaling leading to cell motility[156]. Therefore, Raf/MEK/ERK signaling is key to breast cancer progression as it contributes to cytotoxic drug resistance and increased motility and invasion in MDA-MB-231 cells.

A large body of clinical observations validates the important role of the Raf/MEK/ERK in breast cancer. The pathway is deregulated in approximately a third of human cancers, particularly those of epithelial origin. The pathway is associated with breast cancer progression as the increased ERK1/2 activity is linked to shorter disease-free survival, and is prognostic for recurrence-free survival in patients with breast cancer[158, 159]. Elevated levels of active ERK/MAPK have been shown to be a marker of breast cancer metastasis and predict metastasis to the lymph nodes[160].

This association is particularly apparent in TNBC. In TNBC, the MAPK pathway is more commonly activated[161, 162] particularly in metastatic sites when compared to other breast cancer subtypes[160, 163]. Eralp *et al.*[162] showed that a higher level of MAPK expression is associated with shorter disease-free survival and increased anthracycline resistance in patients with TNBC tumors. Bartholomeusz *et al.*[159] reported that TNBC patients with ERK2-overexpressing tumors have a higher risk of death than those with low ERK2-expressing tumors.

Given the wealth of preclinical data and clinical observations regarding the Raf/MEK/ERK pathway in cell survival and cytotoxic drug resistance, triggering this pathway would be a reasonable approach to eradicate invasive tumor cells that are resistant to chemotherapeutic drugs.

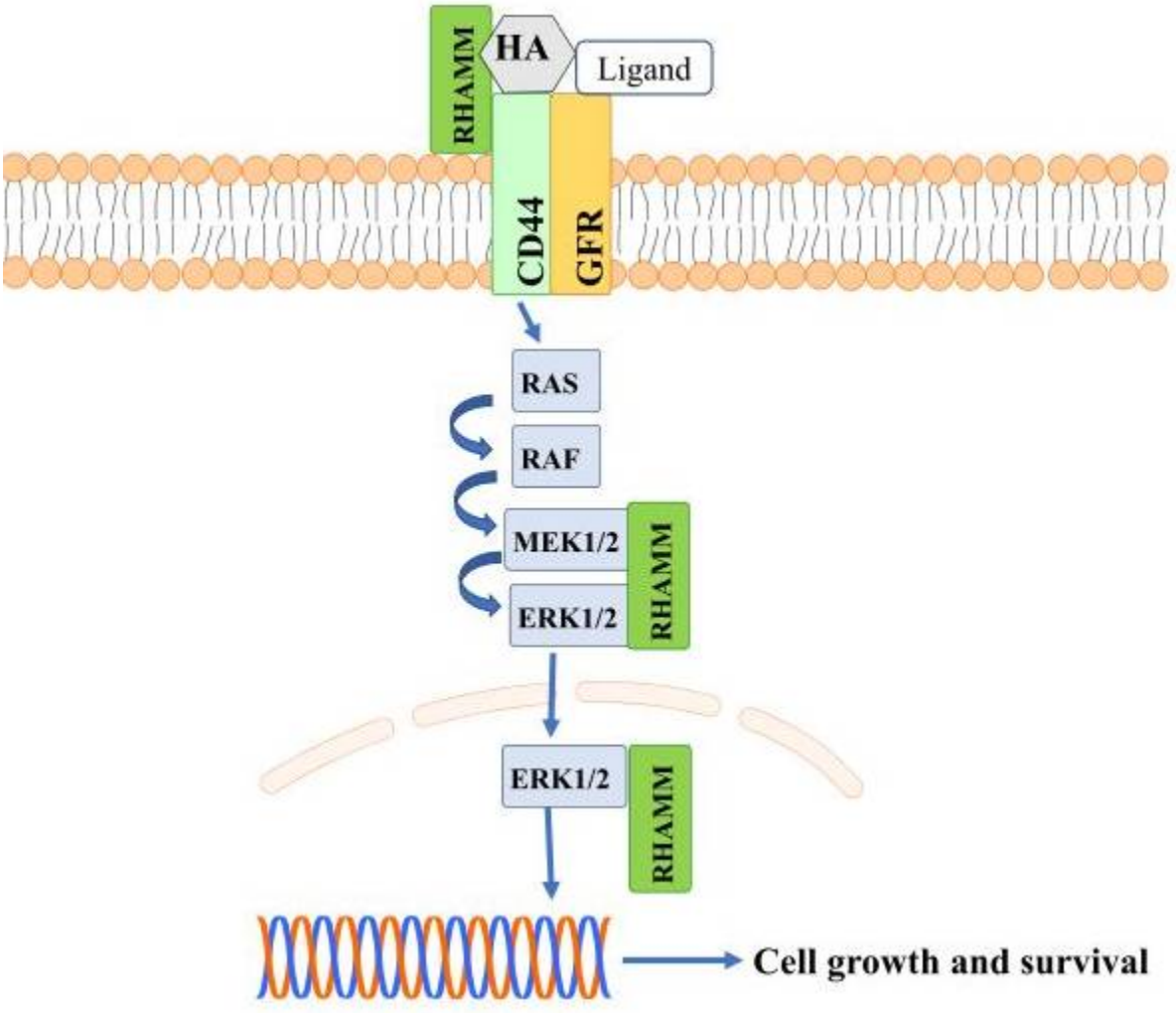

Figure 1.9. Schematic overview of the Raf/MEK/ERK signaling pathway upon binding HA to CD44 and RHAMM.

External stimuli, including binding HA to CD44 and RHAMM, initiate the activation of Ras, a small GTPase, through membrane-associated signaling complexes. Ras facilitates the heterodimerization and activation of Raf intracellular kinases, which starts a kinase cascade through MEK and ERK. This results in the activation of transcription factors that drive genomic signature programs of dysregulated cell cycle progression, proliferation, survival, migration, invasion.

1.5 Hypothesis and Objectives

Since elevated HA production/binding and low cell proliferation rate are linked to chemoresistance, I hypothesized that the HA^{high} subset is more resistant to chemotherapy than the HA^{low} subset and serves as a model for targeted therapy.

The objectives for this dissertation were as follows:

1. To compare sensitivity of HA^{high} and HA^{low} tumor cell subpopulations to chemotherapy *in vitro*
2. To compare sensitivity of HA^{high} and HA^{low} tumor cell subpopulations to targeted therapy *in vitro*

I used the MDA-MB-231 cell line, which models TNBC and exhibits a high degree of HA binding heterogeneity[25], to assess response to chemotherapy (doxorubicin) and to identify potential targeted therapies. MDA-MB-231 was originally isolated from the pleural effusion of a Caucasian breast adenocarcinoma patient. It belongs to the Claudin-low intrinsic subtype which is characterized by the low expression of tight-junctions related genes (E- cadherin, claudin-3, -4, and 7) and high expression of mesenchymal and stem-like biological processes (CD44/CD24 mRNA Ratio: 1.37, and CD49f/EpCAM mRNA Ratio: 1.17)[164, 165]. MDA-MB-231 cells harbour K-Ras, H-Ras and BRAF mutations.

Doxorubicin (trade name: Adriamycin PFS), an anthracycline antibiotic, is the most widely used agent in the treatment of (TNBC) breast cancer, both as a single agent as well as in combination with other drugs. Also, it is considered the most active single agent in breast cancer. Doxorubicin's mechanism of anticancer action is not well understood. It is proposed that doxorubicin slows or blocks cell proliferation by intercalating into DNA helix and disrupting topoisomerase II and consequently inhibiting DNA replication and repair. Doxorubicin also is capable of increasing generation of free radicals leading to DNA and cell membrane damage (Figure 1.10). Intercalating into DNA and producing of free radicals are unlikely to be clinically

relevant as the concentration of doxorubicin required to produce these effects is much higher than that achievable in patients (1.4 to 34.4 μmol/L)[166-168]. Inhibition of topoisomerase II by doxorubicin at clinically achievable concentrations causes DNA breaks[168].

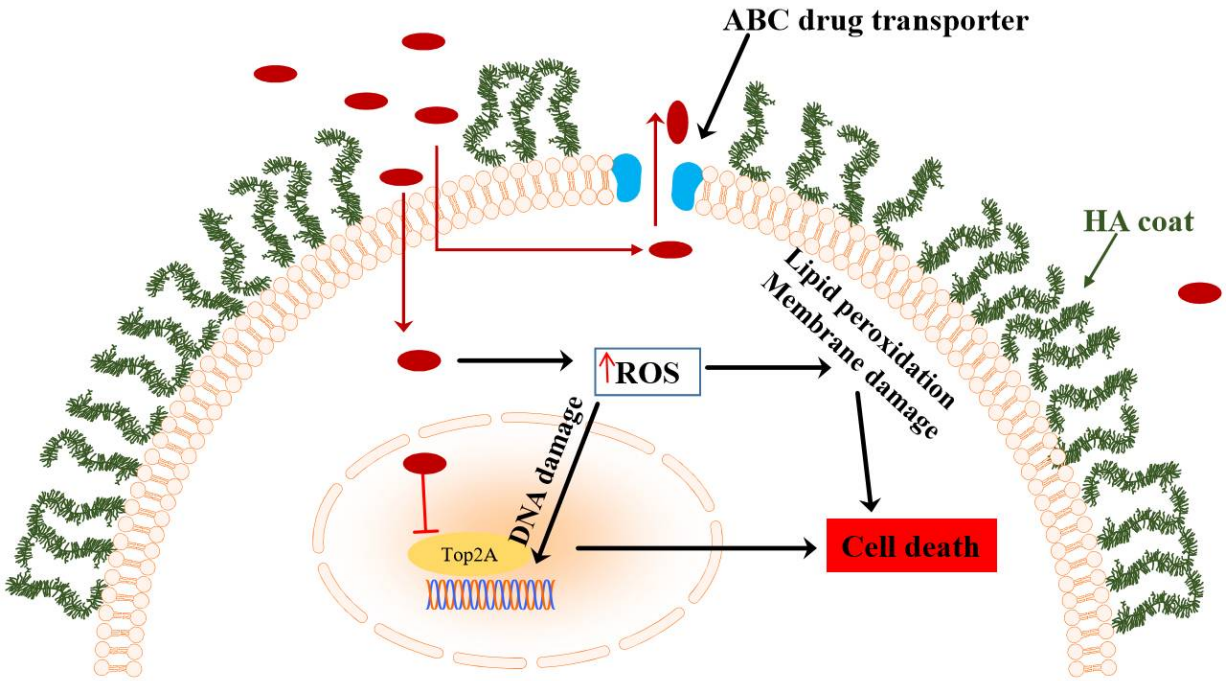

Figure 1.10. A proposed model for doxorubicin's mechanisms of anti-cancer.

Doxorubicin exerts its cytotoxicity through several different mechanisms. It inhibits topoisomerase II (TOP2A) by intercalating into DNA. Also, it causes the formation of free radicals that leads to the cell membrane and/or DNA damage followed by cell death.

Chapter 2

2 « Materials and Methods »

2.1 Cell Culture

Human breast cancer MDA-MB-231 cell line was purchased from American Type Culture Collection (ATCC; Manassas, USA). RHAMM$^{-/-}$ MDA-MB-231 cells generated by CRISPR/Cas9 gene editing system were obtained from Dr. James B. McCarthy (University of Minnesota, Minneapolis, MN). Cell lines were grown on 75 cm^2 or 175 cm^2 tissue culture plastic flasks (Sarstedt Inc.) in low glucose (1.0 g/L) Dulbecco's Modified Eagle Medium (DMEM) (Wisent BioProducts, St. Burno, Quebec, Canada) supplemented with 10% (v/v) Fetal Bovine Serum (FBS) (Wisent BioProducts) and 50 µg/mL Gibco™ Penicillin-Streptomycin (Invitrogen, Life Technologies, Burlington, ON, Canada) in a 37˚C humidified atmosphere of 5% CO_2. Cells were passaged every 3 days at 80% confluence using 0.25% trypsin-0.5 mM EDTA (Wisent BioProducts).

2.2 Fluorescence-Activated Cell Sorting

Fluorescent HA (F-HA) probe was synthesized following established procedures (Veiseh *et al.* 2014)[25]. Briefly, 200 µL of polydisperse 132 kDa Sodium Hyaluronate (1%, Lifecore) were added to 300 µL Alexa fluor 647 hydrazide dye (1 mg/mL, Life Technologies) in 1 mL of conjugation buffer (20 mM MES, 30% EtOH, 0.0028 g/mL 1-Ethyl-3-(3-dimethylaminopropyl) carbodiimide. After overnight incubation of the mixture at room temperature (20-27˚C), unconjugated dye was removed by dialyzing the mixture in 3 mL slide-a-lyzer cassettes (10,000 MWCO, Thermoscientific) against 1X PBS (10 mM PO_4^{3-}, 137 mM NaCl, and 2.7 mM KCl) four times using 2 liters per dialysis for 24 hours for each dialysis. In preparation for Fluorescence-Activated Cell Sorting (FACS), 50-60% confluent MDA-MB-231 cells were detached from tissue culture flasks with 2 mM EDTA, centrifuged at 1,200 rpm for 3 minutes and suspended at 1×10^6 cells in 1 mL PBS followed by incubation with 133 µg/mL F-HA for 45

minutes in the dark on ice. After 3X washes with PBS, cells were suspended at a concentration of 10×10^6 cells/mL for sorting using a BD FACSaria™ III flow cytometry machine (BD Biosciences, Franklin Lakes, NJ). Cells were sorted to HA^{low} and HA^{high} based on the fluorescent intensity (5-8% of minimum and maximum signal selection). The HA^{low} gate was set based on the corresponding unstained control sample. The HA^{high} gate was set on the upper shoulder of the stained cell population and was verified to be a discrete cell cluster separated from the main cell population. To determine the post-sort purity of HA^{high} and HA^{low}cells, 200 events were recorded from each isolated cell populations back on the sorter.

2.3 Cell Surface Marker and ALDH Activity Analyses

To compare the proportion of stem-like ($ALDH^{high}CD44^{+}$) and non-stem-like ($ALDH^{low}CD44^{-}$) cell populations in HA^{high} and HA^{low} subpopulations, ALDH activity and cell surface expression of CD44 and CD24 were assessed. The ALDEFLUOR® assay kit (StemCell Technologies, Vancouver, BC) was used to isolate the population with a high ALDH enzymatic activity. The basis for this assay is that uncharged ALDH substrate (BODIPY-aminoacetaldehyde [BAAA]) is taken up by living cells via passive diffusion. Once inside the cell, BAAA is converted into negatively-charged BODIPY-aminoacetate (BAA) by intracellular ALDH. BAA-is retained inside the cell, causing the cell to become highly fluorescent. Only cells with an intact cell membrane can retain BAA-, so only viable cells can be identified. The ALDEFLUOR® assay was performed essentially as described by Ginestier *et al*[169].

MDA-MB-231 cells at 50% confluency in DMEM+10% FBS were released from the tissue culture surface using 2 mM EDTA. After 2X washing with 1X PBS, cells were suspended in ALDEFLUOR® assay buffer containing ALDH substrate (BAAA, 1×10^6 cells/mL), and incubated for 45 minutes at 37˚ C to allow substrate conversion. As a negative control, an aliquot was treated with 50 mmol/l diethylaminobenzaldehyde (DEAB), a specific ALDH inhibitor. To compare the expression of cell surface CD44 and CD24 in HA^{high} and HA^{low} subpopulations, 1×10^6 cells/mL assay buffer were incubated with CD24-PE antibody (clone ML5; BD Biosciences Canada, Mississauga, ON) (1:1000), together with CD44-PE/Cy7 antibody (1:1000) (Clone IM7.8.1, Life Technologies) and Alexa Fluor 647-HA (133 µg/mL) for 30 minutes in the

dark on ice. Finally, cells were washed three times with 1 mL 1X PBS before flow cytometry analyses. Cell fluorescence intensity was determined using a FACS Calibur II flow cytometer and the Cellquest™ Pro software (BD Biosciences, Franklin Lakes, NJ). Flow data were analyzed using FlowJo® V10 software (Tree Star, Inc., Ashland, OR, USA). I considered ALDH activity as the primary sort criteria and $CD44^{+}CD24^{-}$ phenotype as the secondary sort criteria.

2.4 Half Maximal Inhibitory Concentration Assays

To determine the half maximal inhibitory concentration of doxorubicin, and MEK inhibitors PD98059 and trametinib, cells (96K cells/96 well plates) were plated and 24 hours later exposed to a single dose of agents for 72 hours. Metabolically viable cells were quantified using alamarBlue® as per the manufacturer's instructions (Invitrogen, Life Technologies). Briefly, 1/10th volume of alamarBlue reagent was added to wells and incubated for 4 hours at 37°C in a cell culture incubator. The fluorescent signal intensity which is directly proportional to cell number was measured at 590 nm on the Wallac 1420 VICTOR 2 plate reader (Perkin-Elmer, Waltham, MA). Finally, results are analyzed by plotting fluorescence intensity versus compounds concentration.

2.5 Intracellular Doxorubicin Accumulation

To assess the intracellular accumulation of doxorubicin, HA^{high} and HA^{low} cells were plated on coverslips coated with 5% fibronectin at approximately 50% confluence (48K cells/24 well plates). After 24 hours, cells were incubated with 0.5 µM doxorubicin for 2 hours, as literature-reported doxorubicin accumulation in nuclei and cytoplasm of MDA-MB-435 cells was highest at 2 hours[170], at 37°C. Then the cells were washed twice with ice-cold PBS. Coverslips were mounted with 40 µL ProLong® Gold Antifade Mountant with DAPI (Molecular probes, Life Technologies) and images were captured using an Olympus Confocal microscope and FluoView™ FV1000 software. Doxorubicin fluorescence was excited at 488 nm, and the emission was collected through a 530 nm long-pass filter. Cell images (>40 per group) were analyzed as mean intracellular doxorubicin fluorescent intensity using ImageJ software (NIH,

Bethesda, MD). To compare intracellular accumulation of doxorubicin in HA^{high} and HA^{low} cells by flow cytometry, 50-60 subconfluent cells were incubated with 0.5 µM doxorubicin for 2 hours at 37°C. Then, cells were released from tissue culture surface using 2 mM EDTA and washed 2X ice-cold PBS before analysis by flow cytometry.

2.6 HA Synthase 2 Immunofluorescence Staining

Cells were plated on coverslips coated with 5% fibronectin at approximately 50% confluence (48K cells/24 well plates). On the following day, cells were fixed (1 mL 3.7% paraformaldehyde/coverslip for 10 minutes at room temperature (20-27˚C)), permeabilized (1 mL 1% BSA/0.3% Triton X-100 in TBS for 15 minutes at room temperature (20-27˚C)), and blocked overnight at 4˚C (1 mL 5% FBS in TBS/coverslip). Then cells were incubated with 200 µL HAS2 (S-15) antibody (sc-34067) from Santa Cruz (Dallas, USA) for 1 hour at room temperature (20-27˚C) followed by 3X washes with PBS/1% BSA and incubation with Alexa Fluor 488 secondary antibody (ab150129) for 1 hour at room temperature (20-27˚C) on rocker (400 rpm). After 4X washing, coverslips were mounted with 40 µL ProLong® Gold Antifade Mountant with DAPI per coverslip (Molecular Probes, Life Technologies) and fluorescent images were collected using an Olympus Confocal microscope and FluoView™ FV1000 software. Cell images (>40 per group) were analyzed as mean fluorescent intensity using ImageJ software (NIH, Bethesda, MD).

2.7 HA Production

To measure the amount of HA secretion, tissue culture supernatants were collected from 50-60% subconfluent cultures after 48 hours culture, and metabolically viable cells were quantified using alamarBlue for normalization. HA concentration in supernatants was quantified by a sandwich ELISA kit (K-4800, Echelon Biosciences Inc., Salt Lake City, UT) per the manufacture's protocol. Briefly, HA^{high} and HA^{low} cell culture supernatants and standards (100 µL) were incubated in ELISA wells for 1 hour at room temperature (20-27˚C). After 3X washing with 200 µL/well 1X TBS buffer (50 mM Tris-Cl, pH 7.6, 150 mM NaCl), wells were incubated with 100

µL of HA detector solution for 1 hour at room temperature (20-27˚C). Then, wells were washed 3X 200 µL/well 1X TBS buffer followed by incubation with 100 µL TMB solution/well (K-TMB1; for approximately 20-30 minutes until blue color develops. Finally, 50 µL of 1N H_2SO_4 solution was added to each well and after tapping plate to mix, OD was recorded at 450 nm and HA concentrations were determined by interpolating relative sample OD values to the standard curve. The kit measures HA larger than 10 disaccharides (4500 Da).

2.8 Flow Cytometry Assays of F-HA Binding and Cell Surface RHAMM and CD44 Expression

To compare the expression of cell surface RHAMM and CD44 in HA^{high} and HA^{low} subpopulations, cells at 50% confluency in DMEM supplemented with 10% FBS were released from the tissue culture surface using 2 mM EDTA. After further washing, 1×10^6 cells/1 mL PBS were incubated with 1:20 monoclonal mouse anti-RHAMM (6B7B7) for 30 minutes on ice. Cells were washed twice with 1 mL 1X PBS and were incubated with Rat anti-mouse Alexa Fluor 488 (1:2000) secondary antibody, together with Rabbit anti-mouse CD44-RPE conjugate (1:1000) (Clone IM7.8.1, Life Technologies) and Alexa Fluor 647-HA (133 µg/mL) for 30 minutes in the dark on ice. Finally, cells were washed three times with 1 mL 1X PBS before flow cytometry analyses. Cell fluorescence intensity was determined using a FACSCalibur II™ flow cytometer and the Cellquest™ Pro software (BD Biosciences, Franklin Lakes, NJ). Flow data were analyzed using FlowJo® V10 software (Tree Star, Inc., Ashland, OR, USA).

2.9 Analysis of RNA Expression Levels

Total RNA was extracted using TRIzol Reagent (Invitrogen, Life Technologies) as per the manufacturer's instructions. Briefly, after removing growth media, cells were washed with cold PBS and directly lysed in the culture dish by addition of 1 mL TRIzol/10 cm^2. After passing the cell lysate through a pipette several times, chloroform was added (1/5 of the volume of TRIzol used) and the lysate was mixed. The RNA-containing aqueous phase was recovered after centrifuging for 15 minutes at 12,000×g. The aqueous phase was mixed with 100% isopropanol

(1/2 of the volume of TRIzol used), incubation for 10 minutes at room temperature (20-27˚C) and centrifuged at 12,000×g for 10 minutes. The pellet was washed with 75% ethanol (the equal volume of TRIzol used), air dried, and resuspended in RNase-free water (20-50 µL). RNA quantity and quality were determined by absorbance at 260 nm and 260/280 nm using an ND-1000 spectrophotometer (NanoDrop Technologies, Wilmington, DE). Absorbance ratios of 1.8–2.0 were considered of acceptable purity. RNA samples were sent to the London Regional Genomics Centre (Robarts Research Institute, London, Ontario, Canada) for expression profiling. RNA quality was reassessed using the Agilent 2100 Bioanalyzer (Agilent Technologies Inc., Palo Alto, CA) and the RNA 6000 Nano kit (Caliper Life Sciences, Mountain View, CA). Single-stranded complementary DNA was prepared from 200 ng of total RNA as per the Ambion WT Expression Kit for Affymetrix GeneChip Whole Transcript WT Expression Arrays (Applied Biosystems, Carlsbad, CA) and the Affymetrix GeneChip WT Terminal Labeling kit and Hybridization User Manual[171] (Affymetrix, Santa Clara, CA). Total RNA was first converted to cDNA, followed by *in vitro* transcription to make cRNA. Single-stranded cDNA (5.5 ug) was synthesized; end labelled and hybridized, for 16 hours at 45°C, to Human Gene 2.0 ST arrays. All liquid handling steps were performed by a GeneChip Fluidics Station 450 and GeneChips were scanned and images were captured using the GeneChip Scanner 3000 7G (Affymetrix, Santa Clara, CA) using Command Console v3.2.4. Probe level (.CEL file) data were generated using Affymetrix Command Console v3.2.4. Probes were summarized to gene level data in Partek Genomics Suite v6.6 (Partek, St. Louis, MO) using the RMA (Robust Multi-chip Average) algorithm[172]. Partek was used to determine gene level ANOVA p-values and fold changes.

2.10 Quantitative Real-time RT-PCR

Quantitative Real-time RT-PCR was used to verify gene expression results obtained from mRNA microarray analysis. cDNA was synthesized using Random Primers (Invitrogen, Life Technologies) in a first strand cDNA synthesis reaction using Superscript™ II Reverse Transcriptase (Invitrogen, Life Technologies) as per the manufacturer's instructions. Briefly, a mixture of 1 µg total RNA, 1 µL Oligo (dT) 12-18 (500 µg/mL), and 1 µL dNTP Mix (10 mM each) was heated at 65°C for 5 minutes and cooled on ice for 5 min. After a brief centrifuge to

collect the content of the tube, 4 µL of 5X First-Strand Buffer (250 mM Tris-HCl (pH 8.3 at room temperature), 375 mM KCl, 15 mM $MgCl_2$) and 2 µL of 0.1 M DTT (Dithiothreitol) were added and incubated at 42°C for 2 minutes. Finally, 1 µL of Superscript™ II Reverse Transcriptase was added and incubated at 42°C for 50 minutes followed by heating at 70°C for 15 minutes.

PCR reactions were performed using SYBR® Green QPCR Master Mix (Agilent Technologies, Mississauga, ON, Canada) and a Stratagene Mx3000P instrument (Agilent Technologies). Human-specific primers set used were F: 5´ TTGGGGGAGATGTCCAGA 3´ and R: 5´ CGCTTCGTAGGTCATCCAC 3´ for HAS2, and F: 5'-ACCCACTCCTCCACCTTTGA-3' R: 5'-CTGTTGCTGTAGCCAAATTCGT-3' for GAPDH (Thermo Fisher scientific, Burlington, CA). The following cycle conditions were used: 3 minutes at 95°C, 20 seconds at 95°C, 20 seconds at 60°C, 1 minute at 95°C, 30 seconds at 60°C, and 30 seconds at 95°C. Relative expression levels were calculated by the standard curve method and analyzed using Stratagene Mx3000P software as well as Microsoft Excel. GAPDH served as an endogenous reference.

2.11 METABRIC analysis

Datasets from the METABRIC (Molecular Taxonomy of Breast Cancer International Consortium) analysis of breast cancer samples were downloaded from the Memorial Sloan-Kettering Cancer Center's cbioPortal for Cancer Genomics (http://www.cbioportal.org/)[173, 174]. Raw data were analyzed using the DNACopy package to generate gene-level copy-number variation (CNV). METABRIC transcriptomics samples were generated using the Illumina HumanHT-12 v3 platform (Illumina Human WG-v3) and the CNA using Affymetrix SNP 6.0.

2.12 ERK 1/2 Activity and Localization

Total ERK1/2 and phosphorylated ERK1/2 (Thr202/Tyr204) were determined using ELISA kit (ab176660) as manufacturers' instructions. Briefly, 50 µl of $RHAMM^{-/-}$ and $RHAMM^{+/+}$ MDA-MB-231 cell lysates and standards as well as 50µl of the Antibody Cocktail (affinity tag labelled

capture antibody and a reporter conjugated detector antibody 1:1) were incubated in ELISA wells for 1 hour at room temperature (20-27˚C) on a plate shaker set to 400 rpm. After 3X washing with 350 µL/well 1X wash buffer, wells were incubated with 100 µL of TMB for 15 minutes in the dark on a plate shaker set to 400 rpm. Finally, 100 µL of stop solution was added to each well and after 1 minute mixing on a plate shaker (400 rpm), OD was recorded at 450 nm. Total ERK1/2 and phosphorylated ERK1/2 protein concentrations were determined based on ODs. To determine the localization of activated ERK1/2, cells were plated on coverslips coated with 5% fibronectin at approximately 50% confluence for immunofluorescence staining. On the following day, cells were fixed (1 mL 3.7% paraformaldehyde/coverslip for 10 minutes at RT), permeabilized (1 mL 1% BSA/0.3% Triton X-100 in TBS for 15 minutes at room temperature (20-27˚C)), and blocked overnight at 4˚C (1 mL 5% FBS in TBS/coverslip). Then cells were incubated with 200 µL Phospho-p44/42 MAPK (Erk1/2) (Thr202/Tyr204) (197G2) Rabbit mAb for 1 hour at room temperature on rocker (400 rpm) followed by 4X 1 mL TBS/1%BSA/coverslip washes. Then, coverslips were mounted with 40 µL ProLong® Gold Antifade Mountant with DAPI per coverslip (Molecular Probes, Life Technologies) and fluorescent images were collected using an Olympus Confocal microscope and FluoView™ FV1000 software. Cell images (>40 per group) were analyzed as mean fluorescent intensity using ImageJ software (NIH, Bethesda, MD).

2.13 Generating RHAMM Knockout MDA-MB-231 Cell Line

The RHAMM$^{-/-}$ MDA-MB-231 cell line was generated by transfection with paired guide RNAs (5’ GTATTGTATTTGATTAGAAT 3’, and 5’ GAATTTGAGAATTCTAAGCT 3’ in plasmid pCR4-TOPO-U6-HPRT-gRNA), that bind in exons 3 and 6, respectively. Briefly, in a 6 well plate, the gRNA1 (2 ug) and gRNA2 (2 ug) were co-transfected with the plasmid expressing the CAS9 enzyme (pT3.5 Caggs-FLAG-hCas9) (2 ug) as well as two plasmids for puromycin and GFP selection, pcDNA-PB7 (0.5 ug) and pPBSB-CG-LUC-GFP(Puro) (+CRE) (0.5 ug). Transfection was performed using the UltraCruz® Transfection Reagent (sc-395739) from Santa Cruz Biotechnology as per the manufacturer’s instructions. Cells were plated clonally in 96 well plates 48 hours post-transfection in the presence of 0.6 ug/mL puromycin. Clones were screened initially by genomic PCR to detect clones harboring the genomic deletion using the Platinum™

Pfx DNA Polymerase system (Invitrogen) with the following primers: 5'AGATACTACCTTGCCTGCTTCA3' and 5'ACCTGCAGCTTCATCTCCAT3'. Subsequently, clones with the genomic deletion were also screened by western blot.

RHAMM$^{-/-}$ MDA-MB-231 cell line was generated by the laboratory of Dr. James B. McCarthy (University of Minnesota, Minneapolis, MN). The guide RNAs were designed and the plasmids constructed by the laboratory of Dr. Brandon Moriarity (University of Minnesota, Minneapolis, MN). All additional plasmids listed for CAS9 expression and CRISPR selection were kindly provided by Dr. Brandon Moriarity.

2.14 Statistical Analysis

Data were expressed as mean ± SEM. Statistical differences between two means were assessed using a two-tailed Student *t*-test with significance set at $p< 0.05$ as indicated. Statistical differences between survival curves of two groups were assessed using a log-rank test with significance set at $p< 0.05$ as indicated.

Chapter 3

3 « Results »

3.1 MDA-MB-231 Breast Cancer Cell Line Comprises Cells with High Levels of HA Binding That are Resistant to Doxorubicin

Veiseh *et al.*[25] previously showed that the MDA-MB-231 and other human breast cancer cell lines contain subpopulations that either bind high (HA^{high}) or low (HA^{low}) levels of HA. HA^{high} subpopulations isolated from MDA-MB-231 parental cells by FACS display significantly higher local invasion and lung micrometastases *in vivo* but proliferate more slowly *in vitro* and as xenografts *in vivo* than HA^{low} or parental cells. These results raise the possibility that HA^{high} subsets are more resistant to chemotherapy than HA^{low} since slow proliferation allows cells to escape death from traditional chemotherapeutic agents such as doxorubicin, which predominantly acts on rapidly proliferating cells[98, 175-178]. To begin to address this possibility, I first attempted to repeat the results of Veiseh *et al.*[25], who sorted MDA-MB-231 breast cancer cells into the above two subpopulations using an Alexa Fluor^{647} HA probe (F-HA probe). I prepared the F-HA probe (see section 2.2) and showed that this permitted the isolation of HA^{low} and HA^{high} MDA-MB-231 subpopulations by FACS similar to that reported by Veiseh *et al.*[25] (Figure 3.1). The HA^{low} gate was set based on the corresponding unstained control sample (Figure 3.1 A, B). In all experiments, with varying frequencies, a small but reproducible population of cells separated from the main population/cluster of stained cells which was gated as the HA^{high} cells (Figure 3.1 B). Each of HA^{low} and HA^{high} subpopulations was composed of 5-8% of the total population. The post-sorting purity of each HA^{low} and HA^{high} populations varied between 82-98% (Figure 3.1 C, D). Both HA^{high} and HA^{low} subpopulations were then analyzed for their differences in proliferation.

The proliferation of HA^{low} and HA^{high} subpopulations *in vitro* was measured by an alamarBlue assay. In agreement with the results of Veiseh *et al.*[25], the FACS-isolated HA^{high} cells exhibited

approximately 57% lower proliferation than HA^{low} cells in 2D culture (Figure 3.2), which was statistically significant ($P<0.05$).

I, therefore, next assessed the resistance of these two subpopulations to chemotherapy. I chose doxorubicin as a chemotherapeutic reagent since it is often used in breast cancer treatment[179-182]. Cell viability was determined in fluorescence units and was plotted against doxorubicin concentration after exposure of cells to increasing concentrations of the drug in order to determine the half maximal inhibitory concentration (IC_{50}), which is a measure of drug efficacy, The IC_{50} for HA^{high} cells was four-fold higher than for HA^{low} cells (HA^{high} IC_{50}: 0.08 µM, HA^{low} IC_{50}: 0.02 µM, $p<0.05$) (Figure 3.3). These results show that HA^{high} cells are less sensitive to doxorubicin than HA^{low} cells.

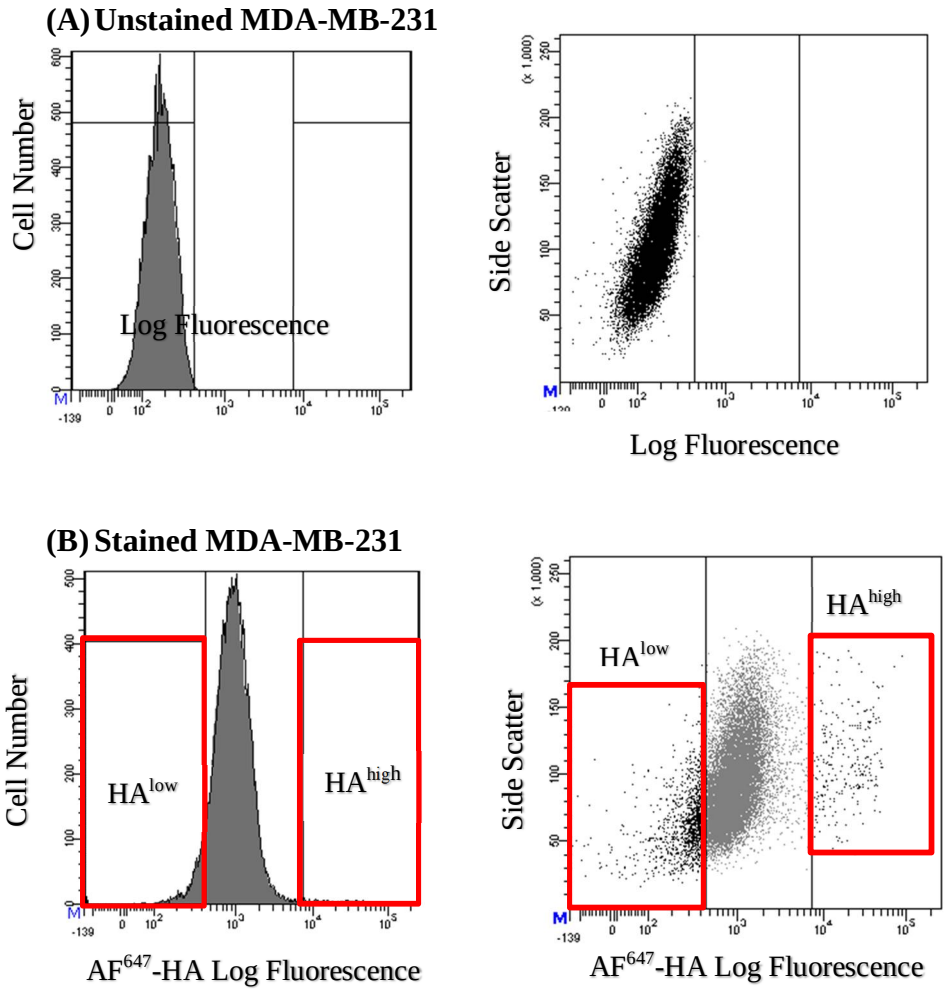

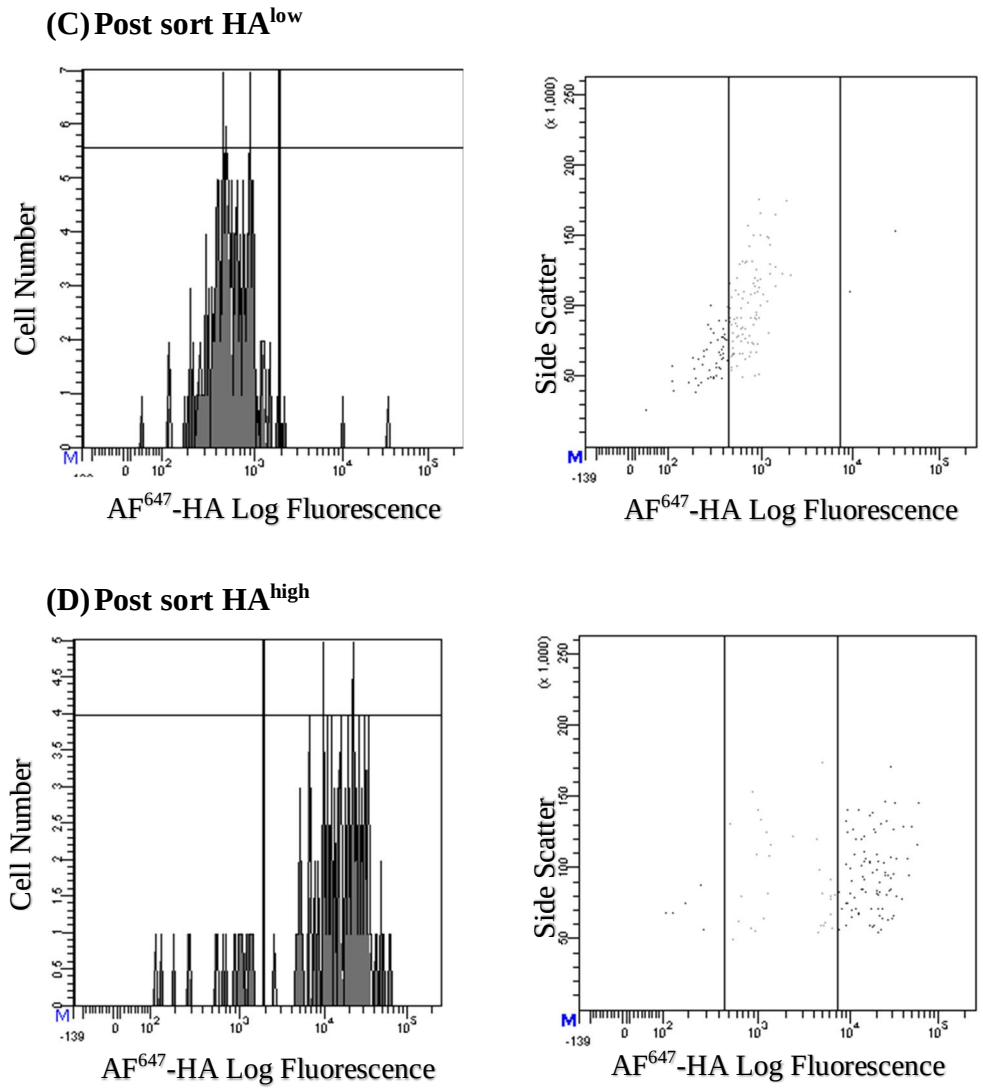

Figure 3.1. Isolation of MDA-MB-231 cell subpopulations using fluorescent HA binding levels. Single cells (minimum of 1×10^6 cells in 1 mL PBS) were exposed to Alexa Fluor^{647}-HA probe for 45 minutes on ice and sorted using FACS. The cell sorting flow cytometry histograms (Left) and dotplots (Right) represent **(A)** unstained **(B)** stained **(C)** post sort low (HA^{low}) and **(D)** post sort high (HA^{high}) fluorescence MDA-MB-231 cells. Fluorescence intensity is shown on the x-axis and the number of events (histograms)/side scatter (dotplots) on the y-axis. F-HA–binding profile spans from 0 to 10^5 fluorescent units. Each red boxed area shows 5-8% selection of the total parental line. Post sort purity of HA^{low} and HA^{high} cells is 96.6% and 83.6%, respectively.

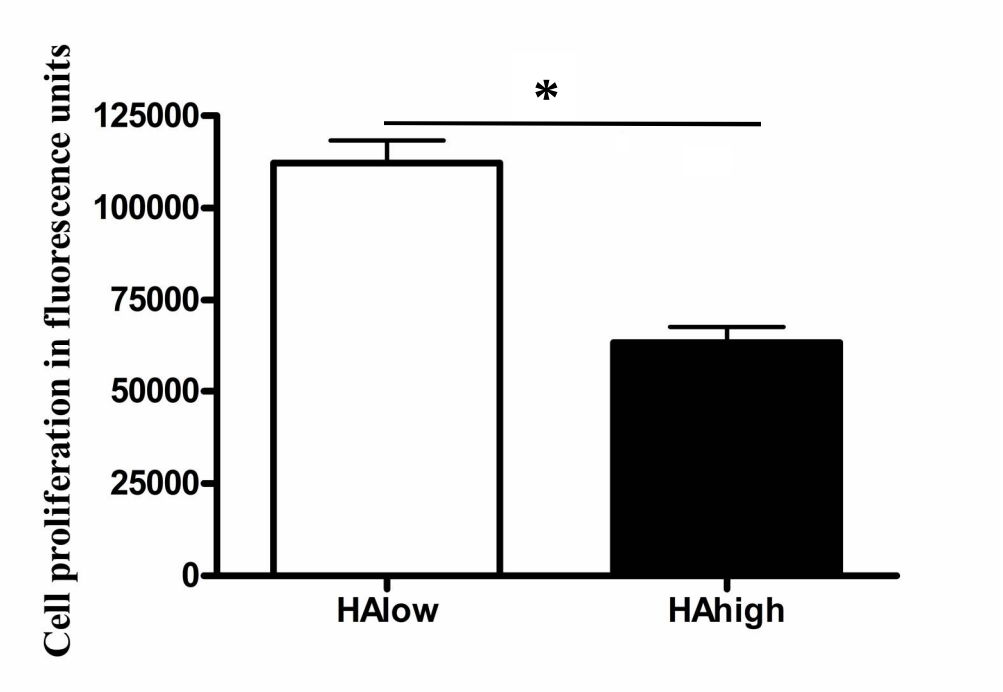

Figure 3.2. HA^{high} cells proliferate slower than HA^{low} cells.

Cells were plated at 1000 cells per well in 96-well plates for 72 hours and incubated with alamarBlue reagent for 4 hours before reading fluorescent at 590 nm. Fluorescence intensity was proportional to the number of viable cells. Mean ± SEM; n=8 replicates, *$p<0.05$ as determined by Student's t-test. The data represent one of 3 experiments performed with similar results.

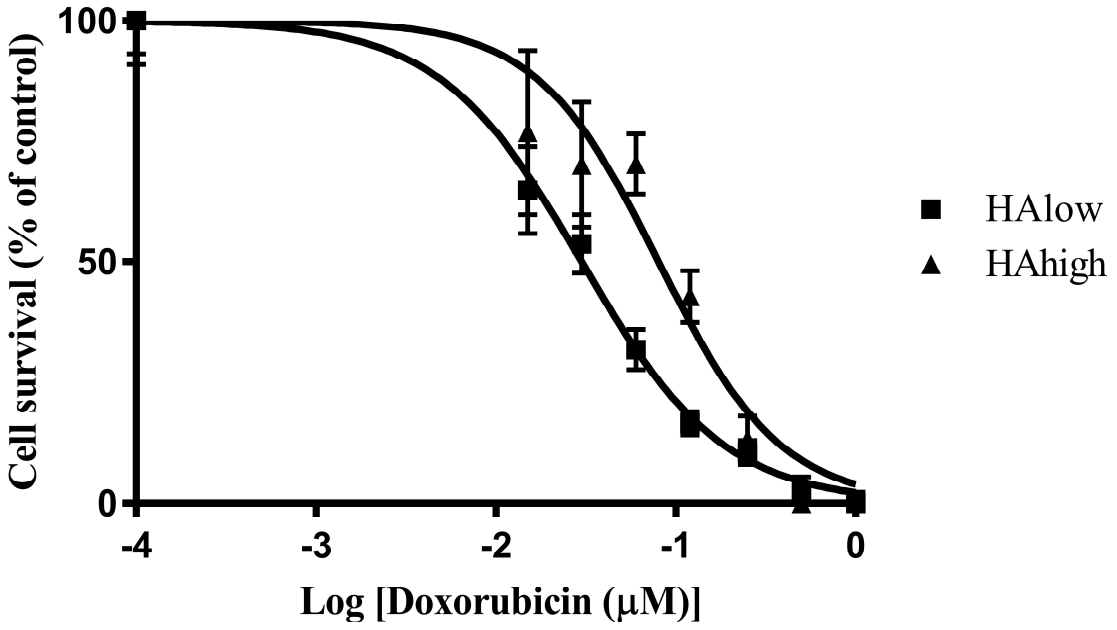

Figure 3.3. IC_{50} of HA^{high} cell treated doxorubicin was four-fold higher than for HA^{low} cells.
Cells were plated at 1000 cells per well in 96-well plates and 24 hours later treated with doxorubicin for 72 hours and incubated with alamarBlue reagent for 4 hours before reading the fluorescent signal at 590 nm. Fluorescence intensity was proportional to the number of viable cells and the number of viable cells. Mean ± SEM; n=8 replicates. The data represent one of 3 experiments with similar results. IC_{50} values, the concentration of doxorubicin which kills 50% of cells, were determined via nonlinear regression using GraphPad Prism 4.0 software. HA^{low} cells with IC_{50}: 0.02 μM were more sensitive to doxorubicin compared to HA^{high} cells with IC_{50}: 0.08 μM ($P<0.05$).

The characteristics of HA^{high} tumor cells including their slow proliferation, increased aggression and resistance to chemotherapy resemble the phenotype of "cancer stem cells" or "tumor-initiating cells" that have been identified in breast cancers[183, 184]. Notably parental MDA-MB-231 tumor cells exhibit a $CD24^{-}CD44^{+}$ surface phenotype that was used by Al-Hajj *et al.*[185] to prospectively isolate stem-like cells from primary tumours and pleural effusions[186-188]. A complementary approach for identifying stem-like cells is measuring functional activity of aldehyde dehydrogenase (ALDH), an enzyme involved in stem cell self-protection[169, 189]. In order to further characterize the nature of the HA^{high} subsets, I first assessed HA^{high} and HA^{low} cells for functional activity of ALDH, and then quantified cell surface display of prospective cancer stem cell markers CD44/CD24 in $ALDH^{+}$ HA^{high} and $ALDH^{+}$ HA^{low} subpopulations. There was no significant difference in the proportion of $ALDH^{+}$ $CD44^{+}$ or $CD24^{-}$ cells in either subpopulation HA^{high} (80.4%) and HA^{low} (88.8%) subpopulations (Figure 3.4 A, C). Also, the proportions $CD44^{+}/CD24^{-}$ cells in $ALDH^{+}$ HA^{high} and $ALDH^{+}$ HA^{low} subpopulations were not significantly different (99.8% and 99.7%, respectively) (Figure 3.4 B, D).

Collectively, these results show that slowly proliferating HA^{high} cells do not appear to be tumor-initiating cells according to the currently accepted definition, high ALDH activity and $CD24^{-}$ $CD44^{+}$ surface phenotype, although they share chemoresistant behavior with tumor-initiating or cancer stem cells.

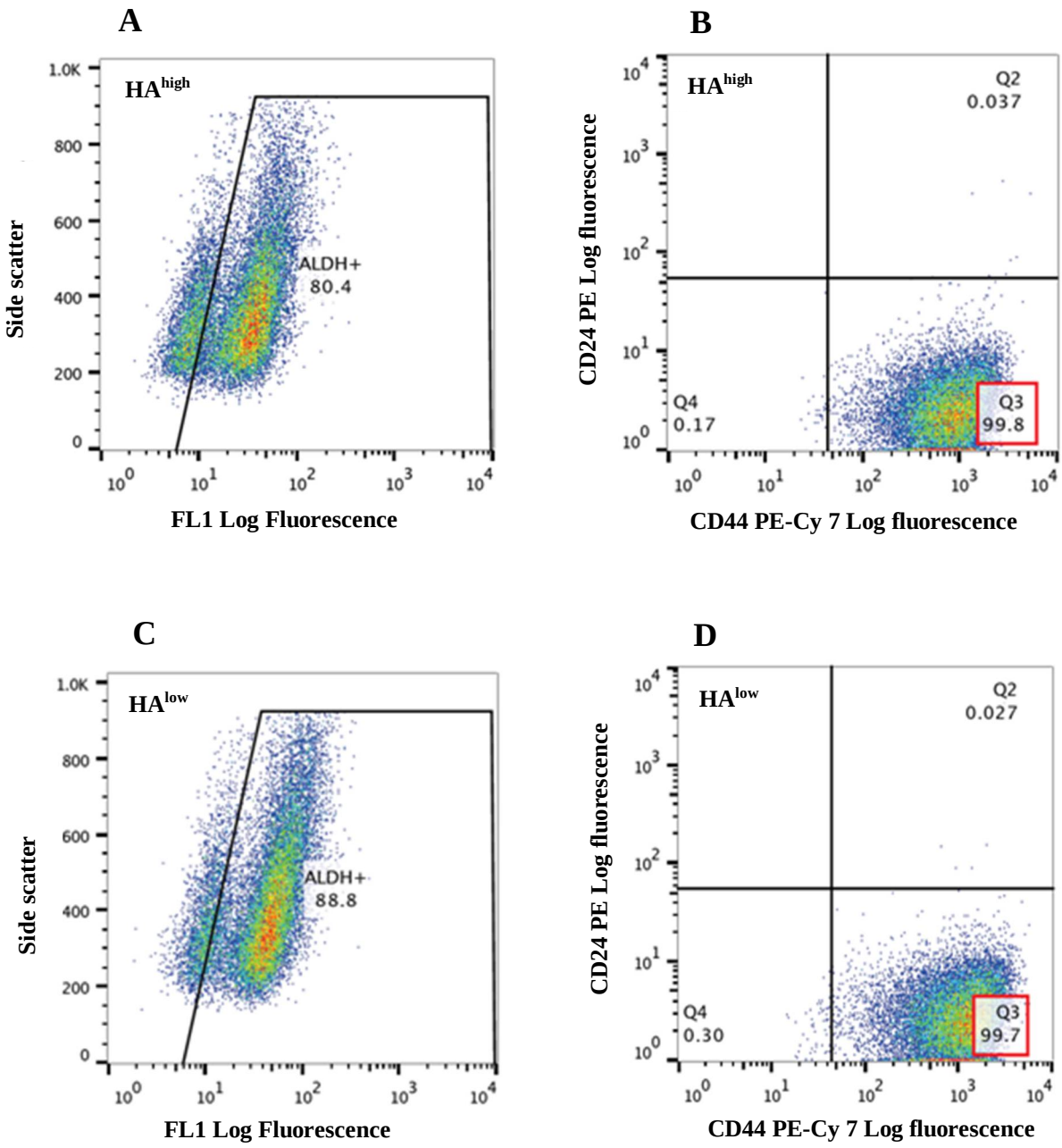

Figure 3.4. HA^{high} and HA^{low} subpopulations do not display significant differences cancer-stem-cell markers ($ALDH^+$ $CD44^+$ $CD24^-$).

Subpopulations of HA^{high} and HA^{low} cells were separated, then those with elevated ALDH display were selected for subsequent analysis of surface CD44 and CD24 levels. (**A, C)** Flow cytometry dot plots of ALDH activity in sorted HA^{high} and HA^{low} subpopulations. Cells which fell within the $ALDH^+$ region were considered to represent subpopulations of cells with enhanced ALDH activity relative to the rest of

the cell population. **(B, D)** Flow cytometry dot plots of CD44-PE Cy7 versus CD24-PE expression in $ALDH^+$ HA^{high} and $ALDH^+$ HA^{low} subpopulations. Cells which fell within the square region Q3 were considered to express the phenotype of interest ($CD44^+CD24^-$). A total of at least 0.5×10^6 cells of each single- (ALDH or CD24 or CD44), double- (ALDH and CD24, ALDH and CD44, CD24 and CD44), or triple-stained (ALDH, CD44, and CD24) and unstained groups was used. A minimum of 20,000 events was collected per sample.

3.2 HA Synthase 2 Expression and Activity is increased in HA^{high} compared to HA^{low} Cells

To begin to identify potential mechanisms for the observed differences in proliferation and doxorubicin sensitivity, I performed a genome-wide mRNA expression profile of HA^{high} and HA^{low} subpopulations using Human Gene 2.0 ST arrays. A comparison of the transcriptome expression patterns (more than 53,000 genes) between HA^{high} and HA^{low} unexpectedly revealed only six significant ($p<0.05$) differences in gene expression levels (Table 3.1).

To examine the clinical relevance of the genes (RNU5A-1, PTGES, METTL7A, PGA3, MIR4655, and HAS2) whose expression levels were significantly altered in HA^{high} cells compared to HA^{low} cells (Table 3.1), I made use of data from a METABRIC dataset that was available in the cBioPortal database[173, 174]. I investigated genetic alterations and genome-wide mRNA expression of the mentioned genes in a cohort of 2509 cases of human breast cancer tumors in the METABRIC study and compared overall survival of patients with and without alterations in the query genes[173, 174]. There was no identified alteration in the RNU5A-1 gene in the dataset. The result showed that the gene set of PTGES, METTL7A, PGA3, MIR4655, and HAS2 and their mRNA expression were altered in 33% (824/2509) (Figure 3.5 A). The only genes associated with poor outcome were HAS2 and PGA3 (log-rank test, $p<0.05$) (Figure 3.5 B, C). Alterations in HAS2 (Figure 3.6) were associated with shorter overall survival in a subgroup of 412 breast cancer cases treated with chemotherapy from the METABRIC dataset (log-rank test, $p<0.05$).

Table 3.1. Genes are differentially expressed in HA^{high} vs. HA^{low} subsets.

Gene Symbol	Protein/RNA name	Protein/RNA Function	Fold Change in HA^{high} vs. HA^{low} mRNA	P-value
RNU5A-1	U5A small nuclear 1 RNA	Involved in splicing of introns from primary genomic transcript, and the regulation of RNA polymerase II or other transcription factors and in the maintenance of telomeres	1.746	0.0152
PTGES	Prostaglandin E synthase	Isomerase that catalyzes the conversion of PGH2 into the more stable prostaglandin E2 (PGE2).	1.657	0.0182
METTL7A	Methyltransferase like 7A	Catalysis of the transfer of a methyl group to an acceptor molecule	1.558	0.0375
PGA3	Pepsin A-3	A protease with particularly broad specificity; although bonds involving phenylalanine and leucine are preferred, many others are also cleaved to some extent.	1.518	0.036
MIR4655	MicroRNA 4655	MicroRNAs are involved in post-transcriptional regulation of gene expression in multicellular organisms by affecting both the stability and translation of mRNAs.	-1.609	0.0149
HAS2	HA synthase 2	Catalyzes the addition of GlcNAc or GlcUA monosaccharides to the nascent hyaluronan polymer.	1.542	0.0003

Genome-wide mRNA expression profiling was performed using Human Gene 2.0 ST arrays shows only 6 genes are significantly up/downregulated between HA^{high} and HA^{low}, $p<0.05$. Three technical replicates of RNA samples were used for mRNA transcriptome profiling.

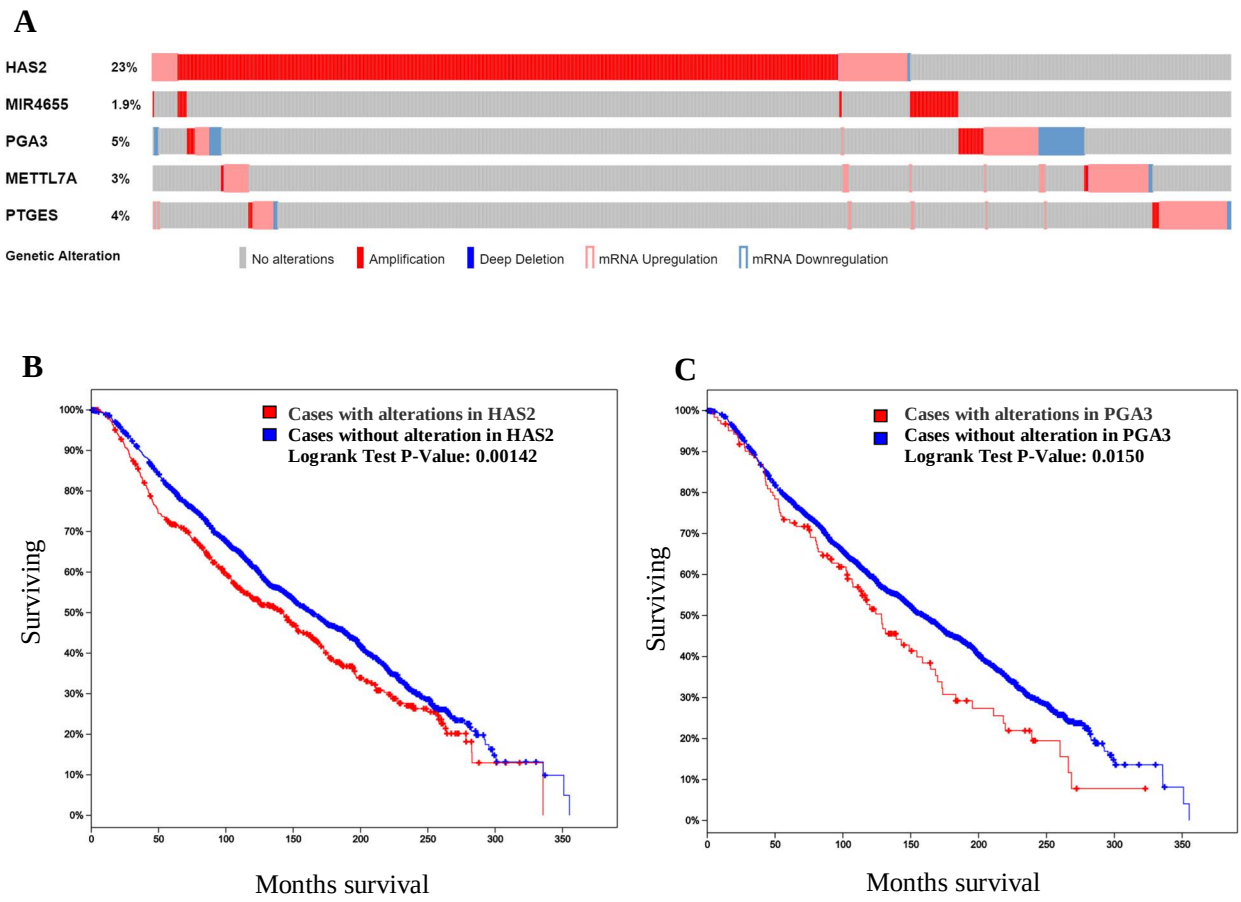

Figure 3.5. Alterations in HAS2 and PGA3 genes are associated with shorter overall survival in breast cancer patients.

(A) Gene copy-number calls at the PTGES, METTL7A, PGA3, MIR4655, and HAS2 loci and their mRNA expression status (up/down regulation) are depicted for 2509 primary breast tumor samples (Amplification = filled red box; deep deletion = filled blue box; mRNA upregulation = red outline; mRNA downregulation = blue outline). Overall survival Kaplan–Meier curve of 2509 breast cancer patients harboring **(B)** HAS2 and **(C)** PGA3 alterations (Logrank Test P-Value< 0.05). Data derived using the METABRIC study from cBioPortal.org[173, 174].

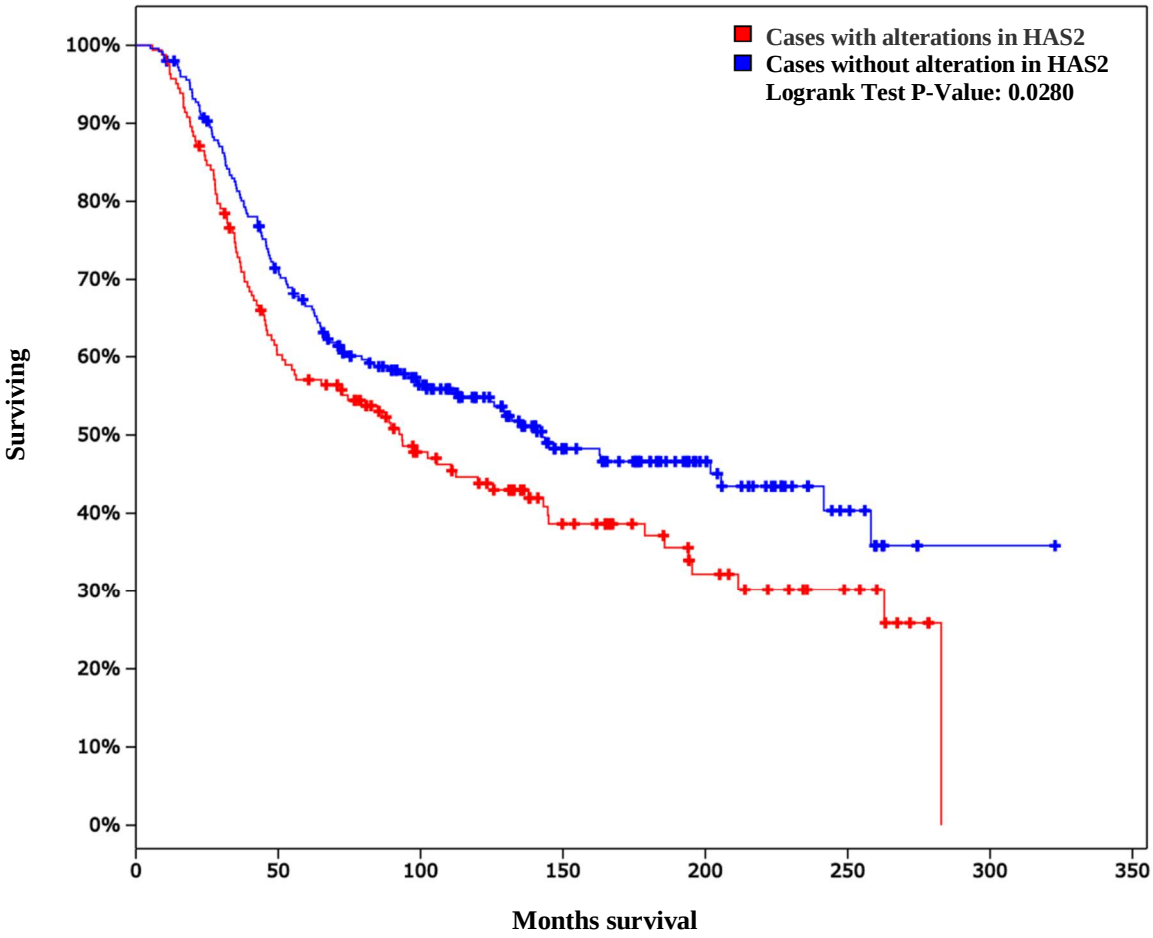

Figure 3.6. Alterations in HAS2 gene are associated with shorter overall survival in breast cancer patients receiving chemotherapy.

Overall survival Kaplan–Meier curve of 412 chemotherapy-treated breast cancer patients harboring HAS2 alterations (Logrank Test P-Value<0.05). Data derived using the METABRIC study from cBioPortal.org[173, 174].

Therefore, I focused on assessing of HAS2 expression and activity in HA^{high} vs. HA^{low} subsets because first, its mRNA expression level showed a significant increase in HA^{high} vs. HA^{low} cells (Table 3.1) and second, its genetic and transcriptional alterations were associated with shorter overall survival in BCa patients treated with chemotherapy. Moreover, HAS2 and its product, the polysaccharide HA, have been linked to TNBC aggression and chemoresistance[23, 190-194].

To validate the array observation, I performed real-time quantitative RT-PCR on RNA isolated from HA^{high} and HA^{low} cells and measured the expression of HAS2. RT-PCR results revealed a significant upregulation of HAS2 in HA^{high} vs. HA^{low} subsets ($p<0.05$) (Figure 3.7).

Since the expression of many genes including HAS2 is regulated at the protein level[195-198] and post-transcriptional changes modulate HAS2 distribution and consequently, its activity, immunofluorescence (IF) staining of HAS2 protein was performed to determine the expression and subcellular localization of HAS2 in HA^{high} and HA^{low} subpopulations. Although there are small differences in HAS2 mRNA expression, HAS2 protein levels were increased approximately 2-fold in HA^{high} cells compared to HA^{low} cells ($P<0.05$) (Figure 3.8 and figure 3.9). Interestingly, in HA^{high} cells, HAS2 aggregated at the cell membrane in approximately 90% of cells; whereas HAS2 is largely distributed in cytoplasmic vesicles in approximately 90% of HA^{low} cells (Figure 3.9).

Since plasma membrane residence of HAS2 is required for its synthetic activity[199], I next quantified the synthesis of HA in HA^{high} and HA^{low} subpopulations. As expected from the membrane localization of HAS2, HA^{high} cells show an approximately three-fold higher amount of secreted HA than HA^{low} cells due to higher expression and activation of HAS2 (Figure 3.10).

These results show that HA^{high} cells express higher levels of HAS2 mRNA, protein and synthase activity than HA^{low} cells. HA has previously been linked to multidrug pump activity[143, 145, 200, 201]. Since this mechanism could account for the increased resistance of HA^{high} cells to doxorubicin, this possibility was next assessed.

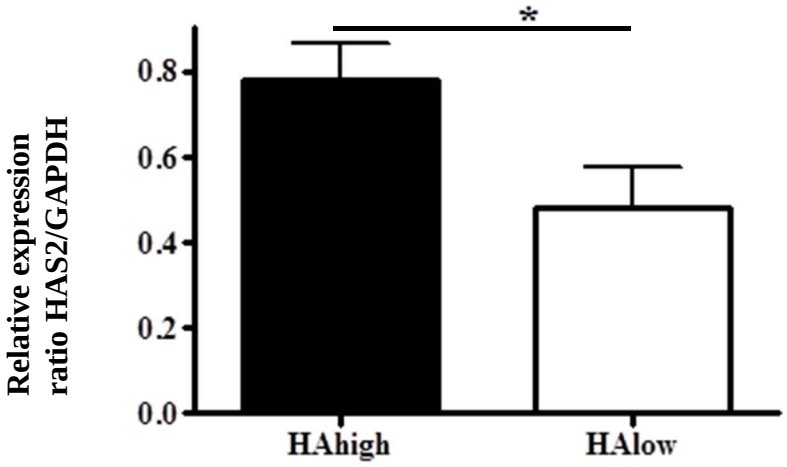

Figure 3.7. HA^{high} cells displayed significantly enhanced HAS2 expression compared to HA^{low} cells.
mRNA expression of HAS2 in HA^{high} and HA^{low} samples was validated by quantitative real-time RT-PCR analysis. Reverse transcription was performed using total RNA isolated from three independent samples. Mean ± SEM; n=6 replicates, *p<0.05 as determined by Student's t-test. The data represent one of 2 experiments performed with similar results.

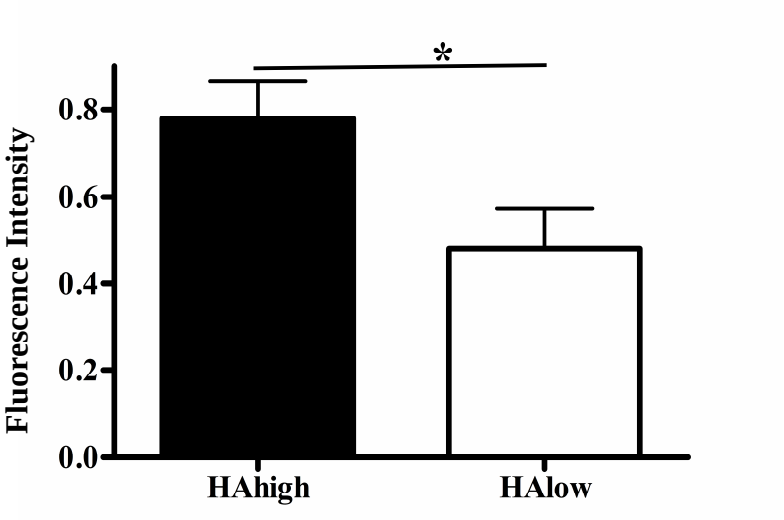

Figure 3.8. HAS2 protein level is increased in HA^{high} cells.
Cells were plated at 2000 cells per fibronectin-coated coverslip in 24-well plates for 24 hours and stained for HAS2 protein. Immunofluorescence images were captured (>40 per group) and fluorescence intensity which is proportional to HAS2 protein expression was quantified using ImageJ software. Mean ± SEM, *P<0.05 as determined by Student's t-test.

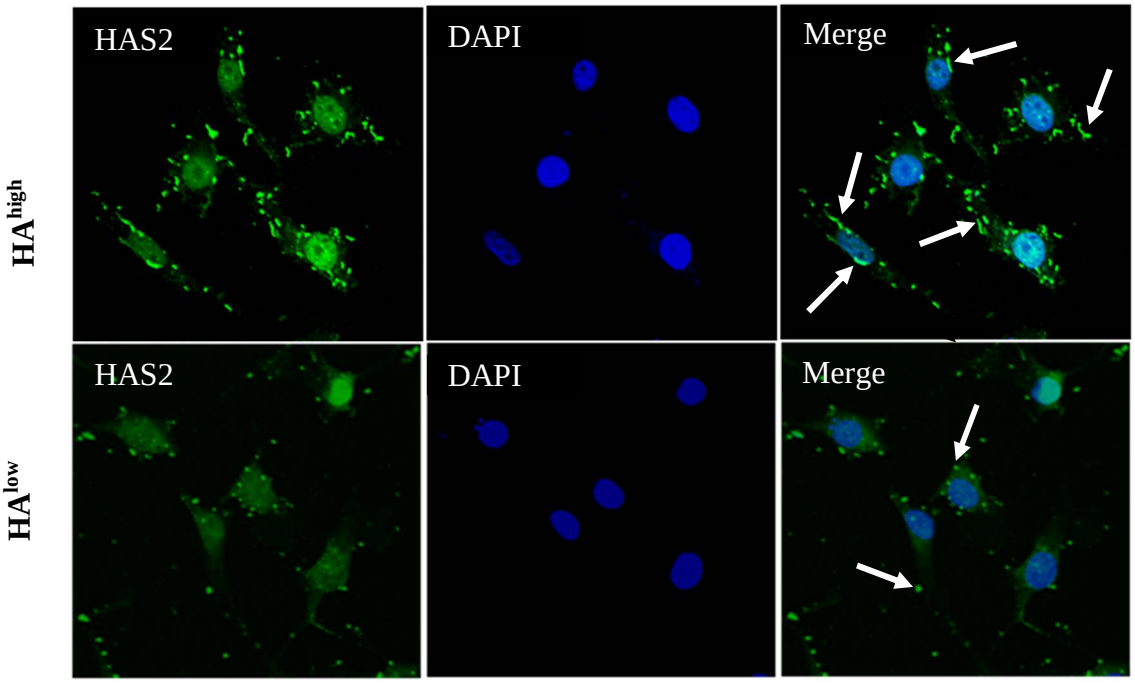

Figure 3.9. HAS2 protein localizes to the cell membrane in HA^{high} cells to a greater extent than in HA^{low} cells.

In immunofluorescence images, HAS2 protein (shown in green) shows 2-fold greater intensity in HA^{high} than HA^{low} cells. Also, HAS2 is more localized (approximately 90% of cells) in the plasma membrane (shown by arrows) for HA^{high} cells and the cytoplasm (shown by arrows) for HA^{low} cells.

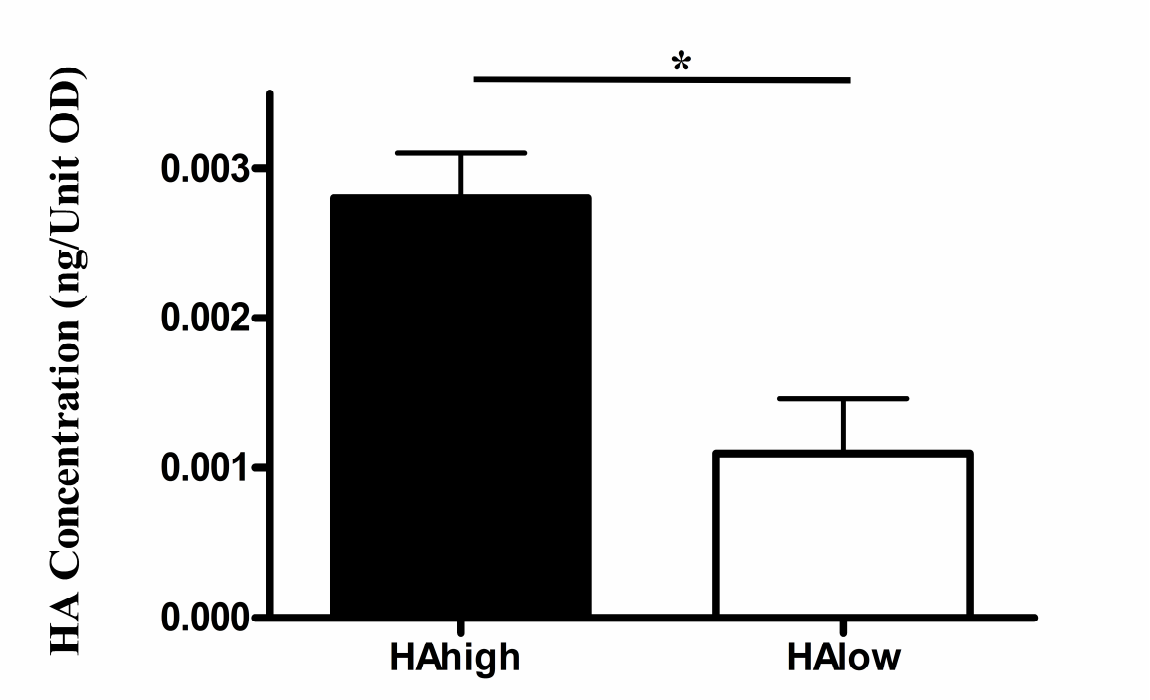

Figure 3.10. HA^{high} cells produce higher levels of HA than HA^{low} cells.

Culture media was collected 48 hours after plating and the amount of secreted HA was quantified by ELISA. Results were normalized to the number of cells. Mean ± SEM; n=8 replicates, *$p<0.05$, Student's t-test was used to determine statistical significance. The data represent one of 2 experiments with similar results.

3.3 Intracellular Doxorubicin Accumulation and Distribution Is Similar in HA^{high} and HA^{low} Cells

Decreased effectiveness of chemotherapy drugs can be due to several reasons including decreased access to or uptake of drugs, activation of repair and detoxification mechanisms and increased drug export[136]. Doxorubicin easily enters cells through passive diffusion and is pumped out of cells by ATP-dependent efflux pumps, such as P-glycoproteins. HA promotes drug resistance by both decreasing drug uptake and increasing drug efflux. The HA coat provides a physical barrier that can decrease drug uptake[202]. HA increases drug efflux by binding to CD44 on tumor cell surface and regulating expression of drug transporters or mediating their stabilization in the plasma membrane, depending upon the cancer cell type[22, 143, 200]. The best approach to determining if HA^{high} cells exhibit altered multidrug pump activity is to expose subsets to doxorubicin and compare abilities to export this fluorescent drug by monitoring intracellular accumulation. To compare the net uptake and efflux of doxorubicin in HA^{low} cells with HA^{high} cells, I measured intracellular doxorubicin related fluorescence intensity by both flow cytometry (Figure 3.11 A) and confocal imaging (Figure 3.11 B) following 2 hours of treatment with the drug *in vitro*. The net uptake and efflux of doxorubicin by HA^{high} cells was not detectably different compared to HA^{low} cells (Figure 3.11 A, B). Confocal cell images showed that in both HA^{high} and HA^{low} subpopulations doxorubicin similarly accumulated in the nuclei ($p>0.05$) (Figure 3.11 B). These results suggest that the greater doxorubicin sensitivity of HA^{low} cells was not due to differences in import or export of the drug.

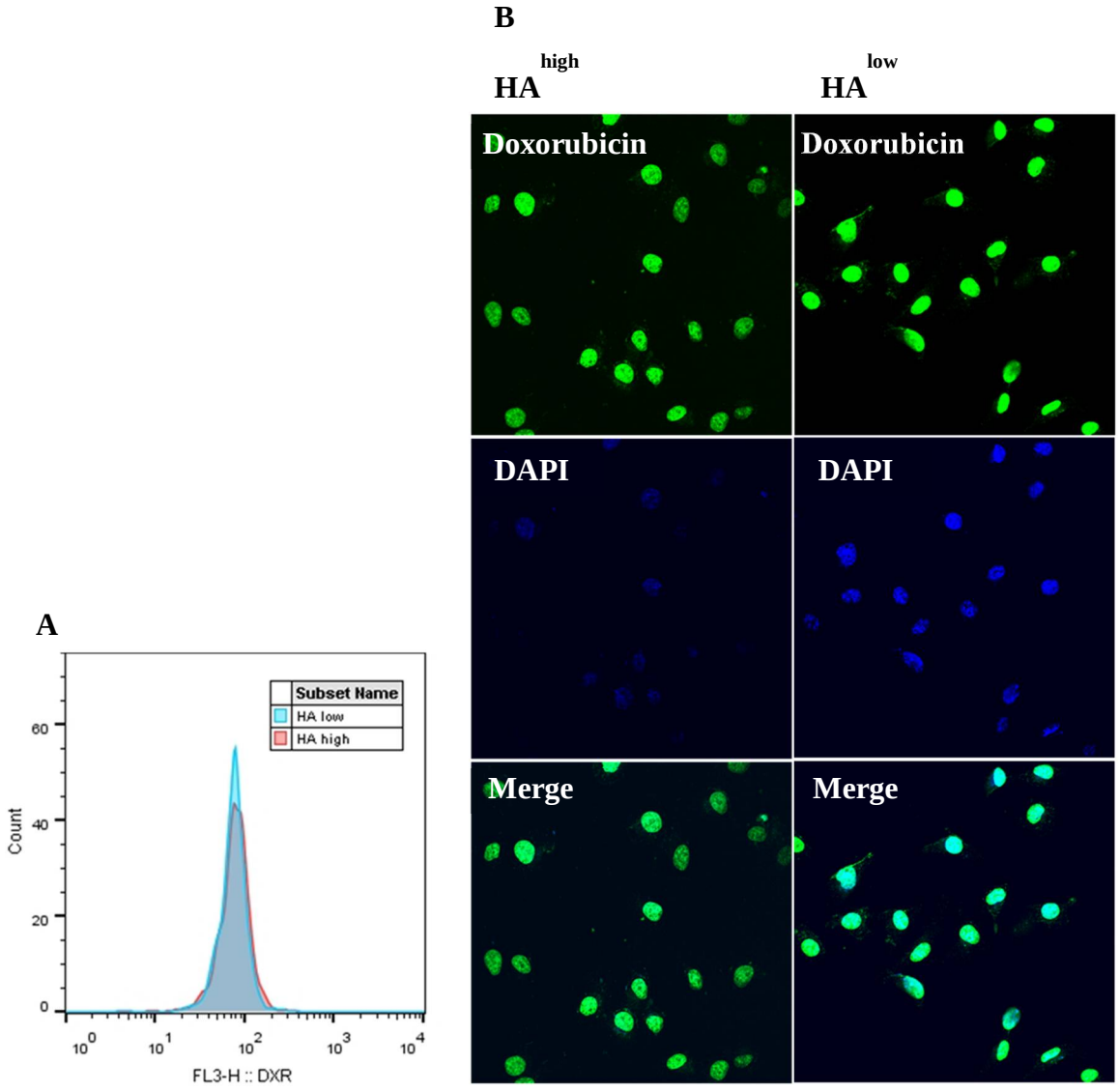

Figure 3.11. Intracellular doxorubicin accumulation and distribution is not significantly different in HA^{high} and HA^{low} subpopulations.

(A) Flow cytometric analyses of HA^{high} and HA^{low} cells show intracellular doxorubicin accumulation was not significantly different, $P<0.05$. **(B)** *In vitro* fluorescence microscopy images (>40 per group) show HA^{high} and HA^{low} cells at 2 hours after doxorubicin treatment. In both subpopulations, doxorubicin is in both nucleus and cytoplasm, but predominantly nucleus. Intracellular fluorescence intensity, which is a measure of doxorubicin accumulation in cells, was quantified by ImageJ software.

The effect of HA on chemoresistance has also been linked to other mechanisms. HA alters cell proliferation differently depending on its molecular weight and concentration[203, 204]. For example, high molecular weight HA such as used for synthesizing the F-HA probe reduces proliferation of some cells[205, 206], and since chemotherapeutic drugs such as doxorubicin target rapidly proliferating cells, slowly proliferating cells survive[98, 175, 176]. Therefore, to determine if HA is in fact directly supporting chemoresistance to doxorubicin, its synthesis was inhibited. To inhibit HA synthesis, I used 4-Methylumbelliferone (4-MU) which is extensively used in experimental models of cancers including TNBC to block HA synthesis[207, 208]. 4-MU suppresses HA synthesis by both depletion of cellular UDP-glucuronic acid, HAS and other glycosyltransferases' precursors, and downregulation of HAS2 and/or HAS3 in tumor cells[209]. It appears 4MU selectively blocks plasma membrane-located HAS[209] and not other Golgi-located glycosyltransferases because[210-212] because 4MU does not accumulate in the Golgi, where other glycosyltransferases are primarily located.

4MU reduced HA^{high} and HA^{low} cell viability in a dose-dependent manner (Figure 3.12). 4-MU (2.0 mM) exhibited the greatest effect on HA^{high} and HA^{low} cell viability (44.3 and 18.3%, respectively, $p<0.05$), following 24 hours of 4MU treatment. HA^{high} cells were more sensitive to 4MU than HA^{low} cells. However, the amount of HA released into the culture medium did not decrease in the presence of 4-MU at any concentration (Figure 3.13) and I could not exclude that 4MU was affecting cell viability via an HA-independent mechanism[209, 213]. Therefore, I concluded that inhibiting HA synthesis was not an option for these particular cells. Furthermore, inhibition of HAS2 through knockdown (small interfering RNA) or knockout (CRISPR-Cas9) is challenging due to the ability of HAS1 or 3 to compensate for HAS2 loss[214-216]. Since HA acts on cell proliferation by binding to HA receptors such as CD44 and RHAMM to activate signaling pathways controlling cell proliferation[90, 124, 217-223], I next considered interrupting HA signaling by blocking these receptors rather than by blocking hyaluronan synthases.

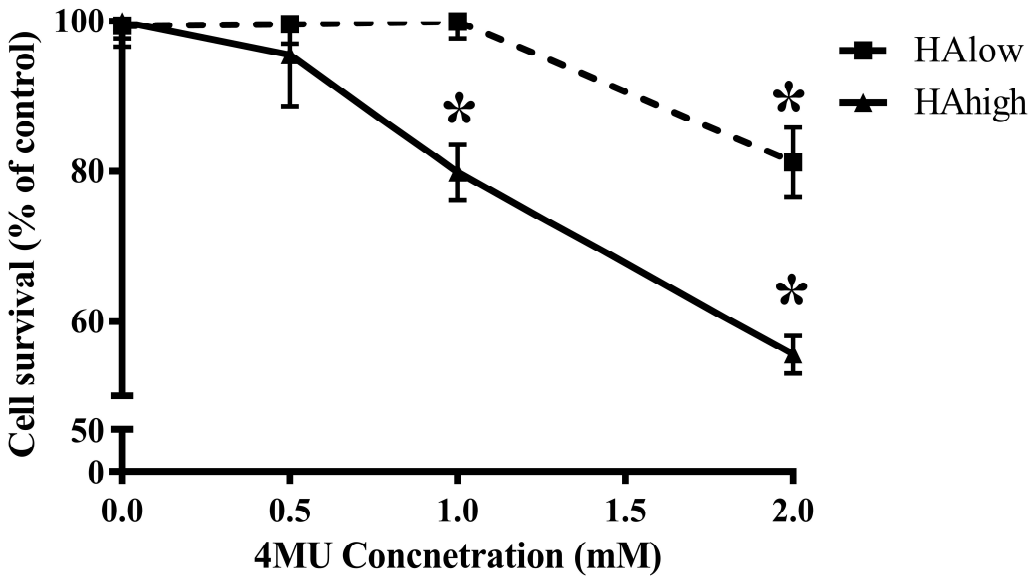

Figure 3.12. Treatment of HA^{high} and HA^{low} cells with 4-MU reduced cell viability.

HA^{high} and HA^{low} cells were plated at 2000 cells per well in 96-well plates and 24 hours later treated with 4MU for 24 hours and incubated with alamarBlue reagent for 4 hours before reading the fluorescent signal at 590 nm. Fluorescence intensity was proportional to the number of viable cells. Mean ± SEM; n=8 replicates, *$p<0.05$ as determined by Student's t-test. The data represent one of 3 experiments with similar results.

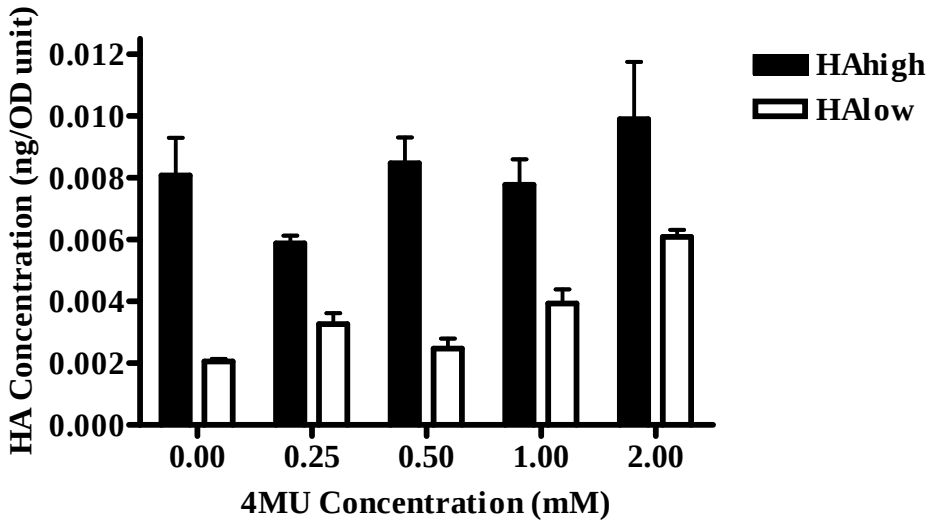

Figure 3.13. 4MU did not inhibit HA synthesis in HA^{high} to the level of HA in HA^{low} cells.

Culture media was collected 24 hours after treating the HA^{high} and HA^{low} cells with 4MU and the amount of secreted HA was quantified by ELISA. Results were normalized to the number of cells. Mean ± SEM; n=8 replicates. The data represent one of 2 experiments with similar results.

3.4 RHAMM Cell-Surface Display Is Higher in HA^{high} Compared to HA^{low} Cells

Since blocking HA production to directly assess its role in chemotherapy was not straightforward, I next assessed if blocking HA receptor signaling affected sensitivity to chemotherapy. In order to decide between CD44 and RHAMM, I first identified which of these receptors was most highly expressed/displayed by the HA^{high} subpopulation. This approach would also allow me to identify aberrant HA receptor signaling involved in TNBC aggression, which may contribute to TNBC chemoresistance and which may identify suitable candidates for targeted therapy, which is currently lacking in TNBC[224]. Previous studies by Turley and others[156, 225] had shown that MDA-MB-231 cells express high levels of the HA receptors CD44 and RHAMM, which strongly activate the Raf/MEK/ERK pathway promoting motility and proliferation[156]. This association is particularly relevant to TNBC because MEK-ERK1/2 signaling is linked to aggressive, chemoresistant TNBC[162]. For these experiments, I performed a multiplexed flow cytometry analysis that allowed me to evaluate the cell surface signature using a combination of F-HA, and immunofluorescence conjugated anti-CD44 and anti-RHAMM antibodies. Results showed that CD44 is similarly displayed on both HA^{high} and HA^{low} subpopulations but high RHAMM display was unique to HA^{high} cells (Figure 3.14). RHAMM is a multifunctional protein the expression of which is increased in aggressive breast cancers and TNBC[25, 89, 132, 218, 226]. It has been reported that RHAMM regulates cell migration and metastatic growth, and contributes to chemoresistance[218, 227]. Moreover, genetic alterations in HMMR beside HAS2 and PGA3 genes were associated with shorter overall survival rate in a subgroup of chemotherapy treated patients from the METABRIC dataset (Logrank Test P-Value <0.05)(Figure 3.15). These reports and analyses as well as my demonstration of high cell surface RHAMM display in HA^{high} subpopulations led me to assess the consequence of blocking RHAMM function on MDA-MB-231 cells proliferation and therapy resistance.

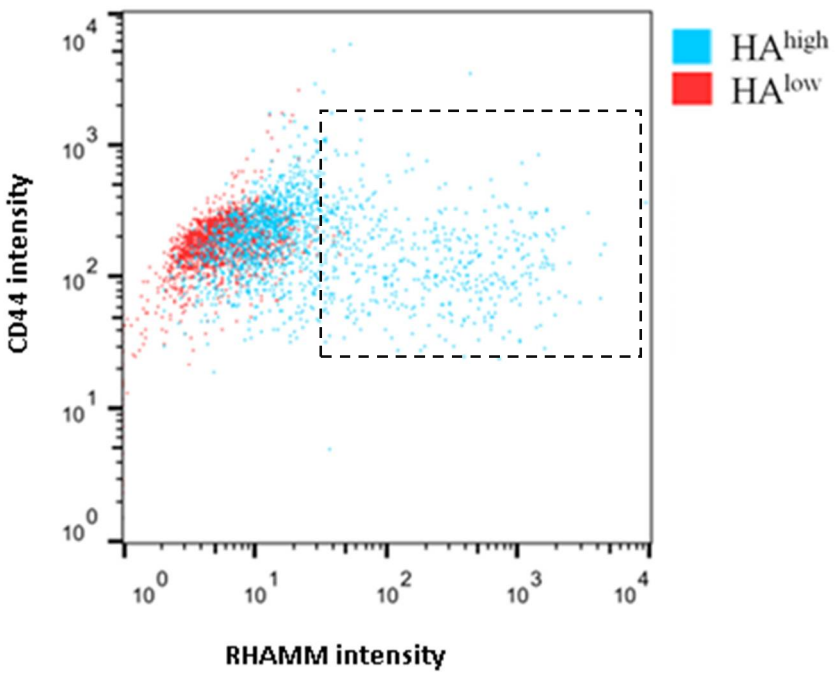

Figure 3.14. RHAMM cell-surface display was higher in HA^{high} than HA^{low} cells.

Cell surface coexpression of RHAMM and CD44 in HA^{high} and HA^{low} subpopulations was compared using triple staining with F-HA to detect HA binding levels, anti-RHAMM and anti-CD44 antibodies to detect RHAMM and CD44 display, respectively. A total of at least 1×10^6 cells of each single- (F-HA or RHAMM or CD44), double- (F-HA and RHAMM, F-HA and CD44, RHAMM and CD44), or triple-stained (F-HA, CD44, and RHAMM) and unstained groups was used. Triple-color flow cytometry dot plot shows both HA^{high} and HA^{low} subpopulations display a similar range in levels of CD44; however, RHAMM display is higher in HA^{high} compare to HA^{low} cells. The dashed square represents HA^{high} cells expressing higher levels of RHAMM cell surface.

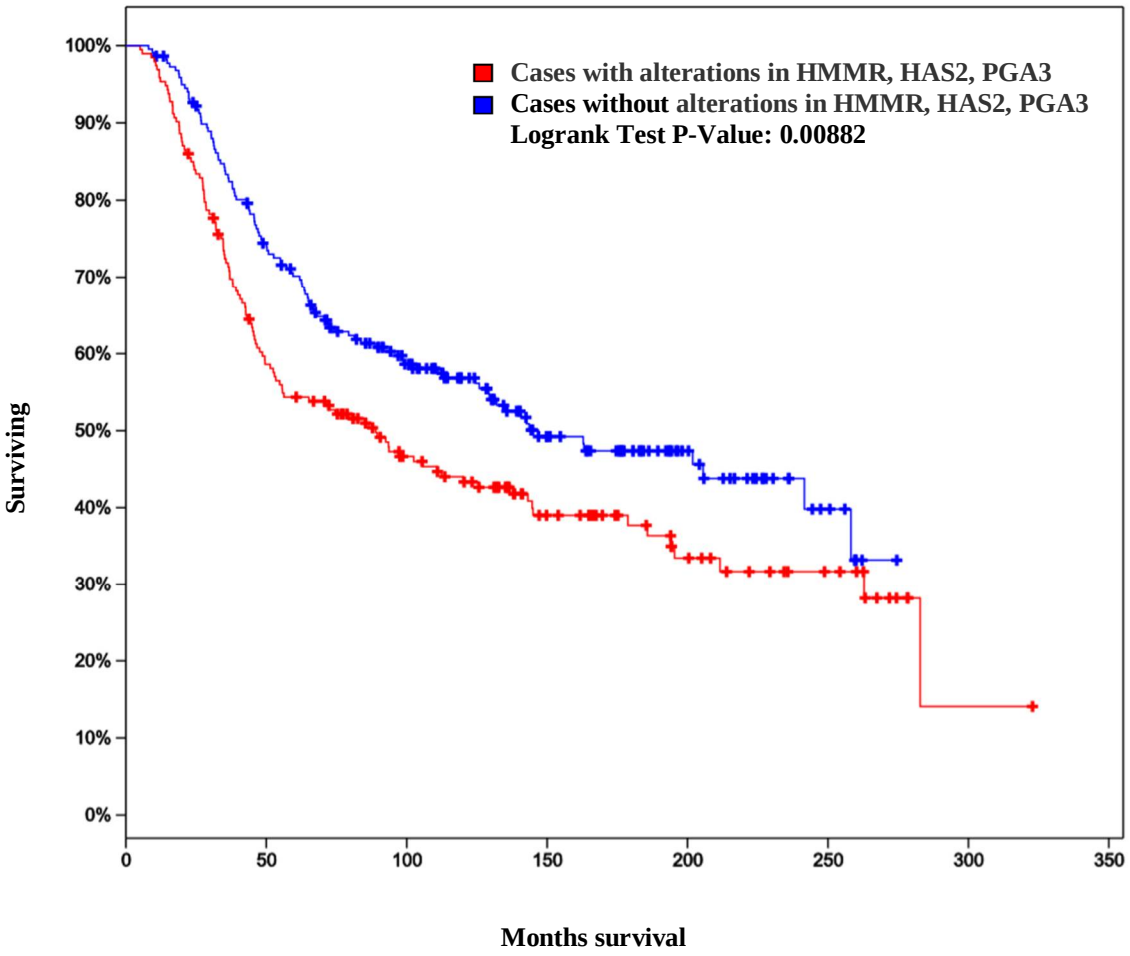

Figure 3.15. Alterations in HMMR, HAS2, and PGA3 genes is associated with shorter overall survival in breast cancer patients receiving chemotherapy.

Overall survival Kaplan–Meier curve of 412 chemotherapy-treated breast cancer patients harboring HMMR, HAS2, and PGA3 alterations (Logrank Test P-Value<0.05). Data derived using the METABRIC study from cBioPortal.org[173, 174].

3.5 Cell Surface RHAMM Modulates MDA-MB-231 Cell Proliferation

Previous studies have reported that RHAMM mediates HA-stimulated cell proliferation and migration through the Raf/MEK/ERK pathway signaling[227, 228]. To begin to assess the role of cell surface RHAMM in chemoresistance, I showed that blocking cell surface RHAMM signaling using rabbit polyclonal function blocking anti-RHAMM antibody significantly suppressed HA^{high} but not HA^{low} cells proliferation (Figure 3.16), confirming the role of extracellular RHAMM in modulating of HA^{high} cell proliferation. Previous analyses have shown that this antibody specifically affects RHAMM function in that it inhibits migration of $RHAMM^{+/+}$ but not $RHAMM^{-/-}$ cells[97]. Since the antibody also did not significantly affect the proliferation of HA^{low} cells that display very low levels of surface RHAMM, its effect on the proliferation of HA^{high} cells is likely to be specific. To confirm and extend this observation, the effect of RHAMM deletion on MDA-MB-231 cell proliferation was investigated. RHAMM expression was deleted in MDA- MB- 231 cells using CRISPR/Cas9 gene editing. CRISPR/Cas9 targeting RHAMM was designed to delete exons 3 and 6 in the RHAMM gene of MDA-MB-231 cells. Clone H8 that did not express RHAMM mRNA or protein was isolated (Figure 3.17 A). $RHAMM^{-/-}$ MDA-MB-231 cells were a kind gift from Dr. James B. McCarthy (University of Minnesota, Minneapolis, MN). AlamarBlue assays showed that $RHAMM^{-/-}$ MDA-MB-231 cells proliferated more slowly than $RHAMM^{+/+}$ cells (Figure 3.17 B, C).

Next, I tested $RHAMM^{-/-}$ and $RHAMM^{+/+}$ MDA-MB-231 cells sensitivity to doxorubicin. The IC_{50} was approximately two-fold higher in $RHAMM^{-/-}$ MDA-MB-231 cells than $RHAMM^{+/+}$ MDA-MB-231 cells ($RHAMM^{-/-}$ MDA-MB-231 IC_{50}: 0.05 µM, $RHAMM^{+/+}$ MDA-MB-231 IC_{50}: 0.02 µM, $P<0.05$) (Table 3.2) showing $RHAMM^{+/+}$ MDA-MB-231 cells were more sensitive to doxorubicin than $RHAMM^{-/-}$ MDA-MB-231 cells. Collectively, these results suggest that HA binding and RHAMM mediate resistance to doxorubicin and this correlates with the regulation of cell proliferation.

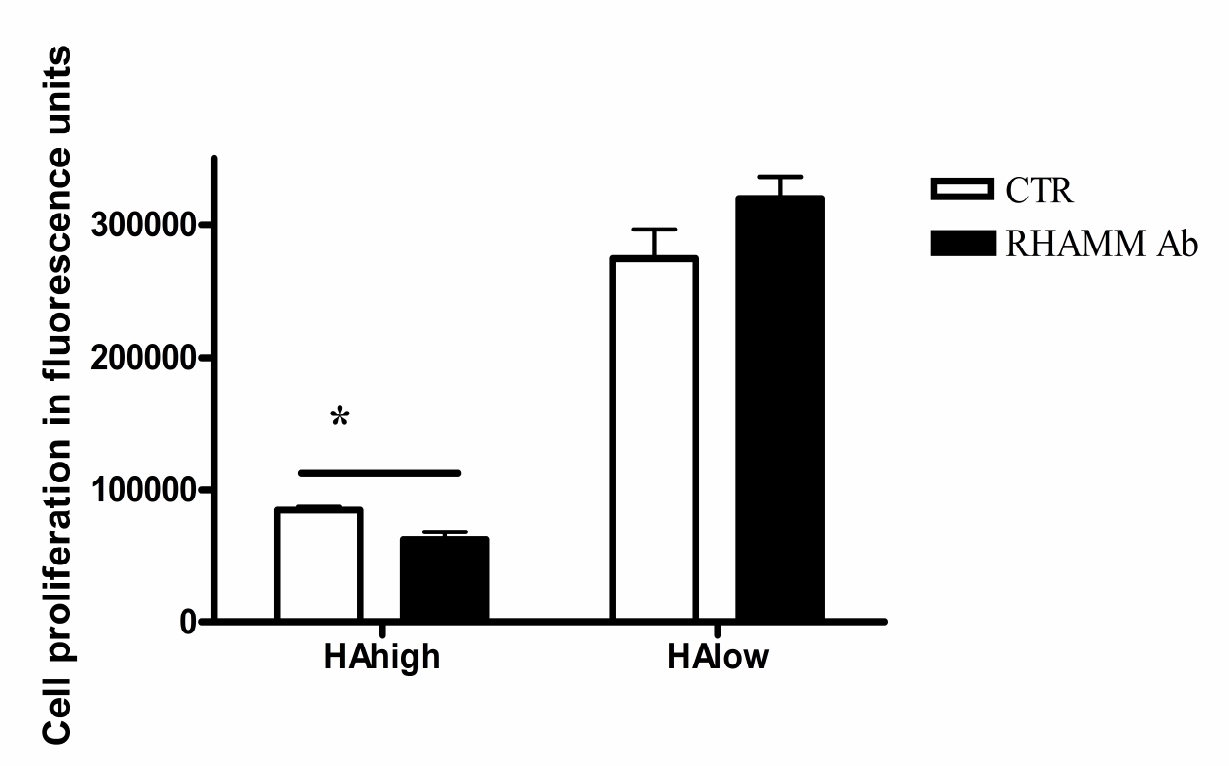

Figure 3.16. Blocking cell surface RHAMM function significantly inhibited HA^{high} but not HA^{low} cell proliferation.

Cells (96K cells/96 well plates) were plated and 4 hours later exposed to a single dose (1:20) of rabbit polyclonal antibody against exon 3 RHAMM for 72 hours and incubated with alamarBlue reagent for 4 hours before reading absorbance (590 nm). Mean ± SEM; n=8 replicates, *P<0.05 using Student's t-test. The data represent one of 2 experiments with similar results.

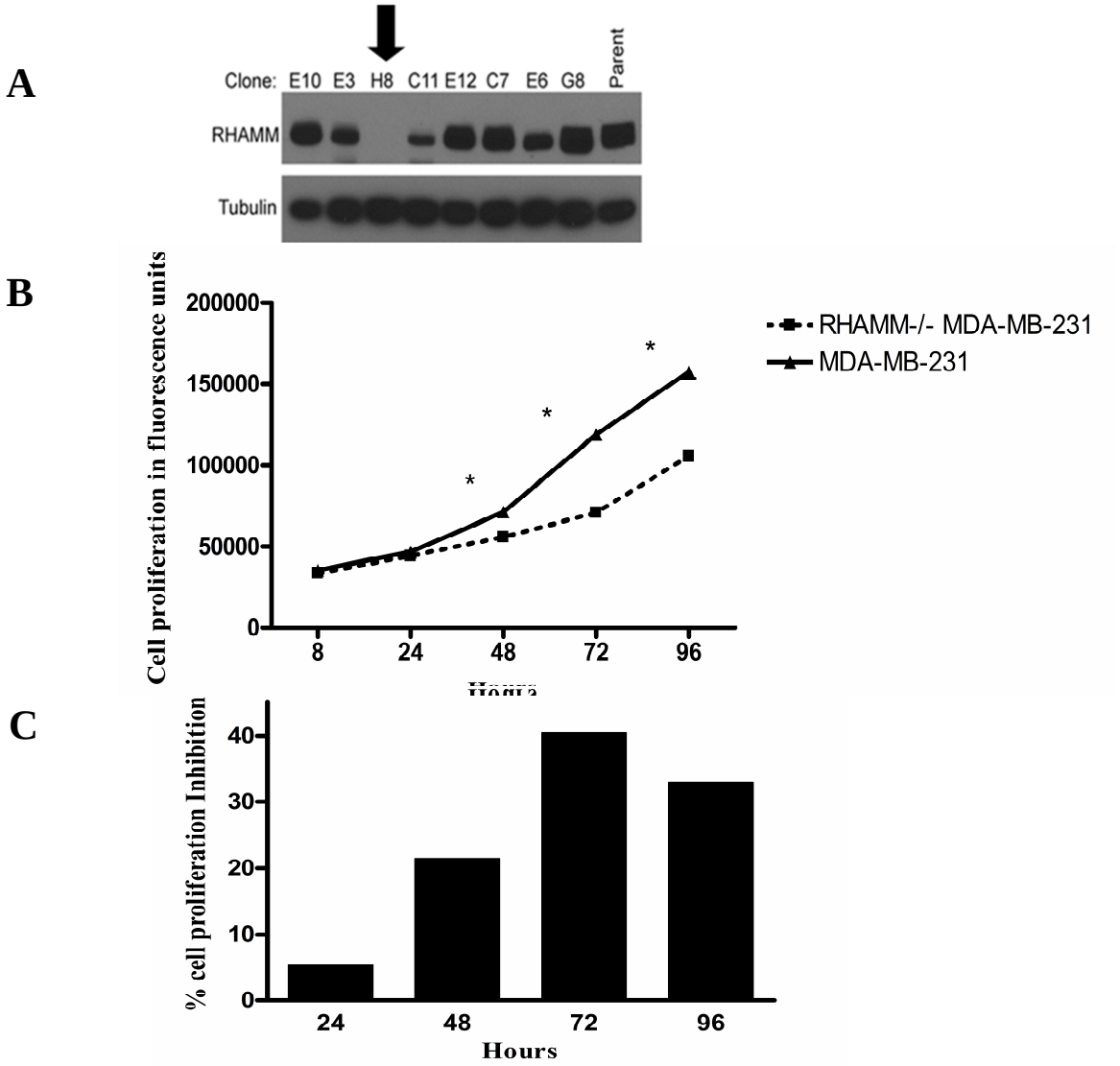

Figure 3.17. RHAMM$^{-/-}$ cells grew significantly more slowly than RHAMM$^{+/+}$ MDA-MB-231 cells.

A) Western blot validation of RHAMM deletion (in clone 8) using the CRISPR/CAS-9 gene editing system. RHAMM$^{-/-}$ MDA-MB-231 cells obtained from Dr. James B. McCarthy laboratory (University of Minnesota, Minneapolis, MN). **B, C)** RHAMM$^{-/-}$ cells grew significantly more slowly than RHAMM$^{+/+}$ MDA-MB-231 cells. Cells were plated at 1000 cells per well in 96-well plates and incubated with alamarBlue reagent for 4 hours before reading absorbance (590 nm) at 8, 24, 48, 72, and 96 hours following plating. Mean ± SEM; n=8 replicates, *P<0.05 using Student's t-test. Figure C shows % cell proliferation inhibition in RHAMM$^{-/-}$ compared to RHAMM$^{+/+}$ MDA-MB-231 cells. The data represent one of 3 experiments with similar results.

Table 3.2. IC_{50} of $RHAMM^{-/-}$ MDA-MB-231 cell treated with doxorubicin was 2.5-fold higher than for $RHAMM^{+/+}$ MDA-MB-231 cells.

$RHAMM^{-/-}$ MDA-MB-231 IC_{50}	0.05 µM
$RHAMM^{+/+}$ MDA-MB-231 IC_{50}	0.02 µM
P-value	<0.0001

Cells were plated at 1000 cells per well in 96-well plates and 24 hours later treated with doxorubicin for 72 hours and incubated with alamarBlue reagent for 4 hours before reading the fluorescent signal at 590 nm. Fluorescence intensity was proportional to the number of viable cells and the number of viable cells. Mean ± SEM; n=6 replicates. The data represent one of 2 experiments with similar results. IC_{50} values, the concentration of doxorubicin which kills 50% of cells, were determined via nonlinear regression using GraphPad Prism 4.0 software. $RHAMM^{+/+}$ MDA-MB-231 cell with IC_{50}: 0.02 µM were more sensitive to doxorubicin compared to $RHAMM^{-/-}$ MDA-MB-231 cell with IC_{50}: 0.05 µM ($P<0.05$).

3.6 RHAMM Modulates Intracellular Distribution of Activated ERK1/2

Cell surface RHAMM is required for formation of CD44-ERK1/2 complexes, and together with intracellular RHAMM sustains activation of the MEK-ERK1/2 signaling. Therefore, I determined the total activated ERK1/2 (Phospho-ERK1/2 or pERK1/2), the main component of the pathway, in whole cell lysates of $RHAMM^{-/-}$ and $RHAMM^{+/+}$ MDA-MB-231 cells by ELISA. There was no significant difference in the specific ERK1/2 activity (levels of pERK1/2 normalized against the total ERK1/2) in $RHAMM^{+/+}$ MDA-MB-231 cells compared to $RHAMM^{-/-}$ MDA-MB-231 cells ($p>0.05$). However, I tested the level of active ERK1/2 per cell using immunofluorescent staining of p-ERK1/2. $RHAMM^{+/+}$ MDA-MB-231 exhibited higher ERK1/2 activity per cell compared to $RHAMM^{-/-}$ MDA-MB-231 cells ($p<0.05$) (Figure 3.18).

Since RHAMM is required for nuclear translocation of pERK1/2[91, 97], I quantified the nuclear accumulation of pERK1/2 of $RHAMM^{-/-}$ and $RHAMM^{+/+}$ MDA-MB-231 cells using immunofluorescence staining of p-ERK1/2 (Figure 3.19). Approximately 75% of $RHAMM^{+/+}$ MDA-MB-231 showed nuclear accumulation of pERK1/2 compared to 35% of $RHAMM^{-/-}$

MDA-MB-231 cells ($p<0.05$). These results show that RHAMM expression is primarily affecting trafficking of pERK1/2 into the nucleus of MDA-MB-231 cells.

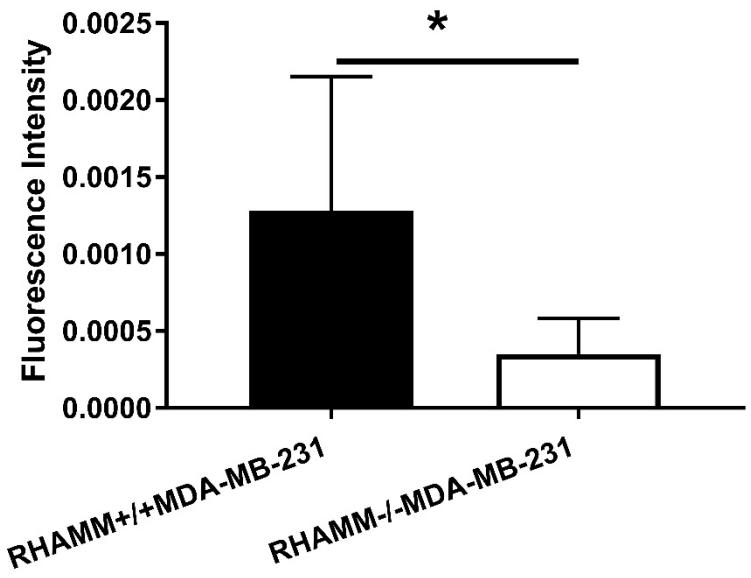

Figure 3.18. RHAMM$^{-/-}$MDA-MB-231 cells exhibit lower ERK1/2 activity than RHAMM$^{+/+}$MDA-MB-231 cells.

Cells were plated at 2000 cells per fibronectin-coated coverslip in 24-well plates for 24 hours and stained for pERK1/2 protein. Immunofluorescence images were captured (>20 per group) and fluorescence intensity which is proportional to pERK1/2 protein expression was quantified using ImageJ software. Mean ± SEM, *$P<0.05$ as determined by Student *t*-test.

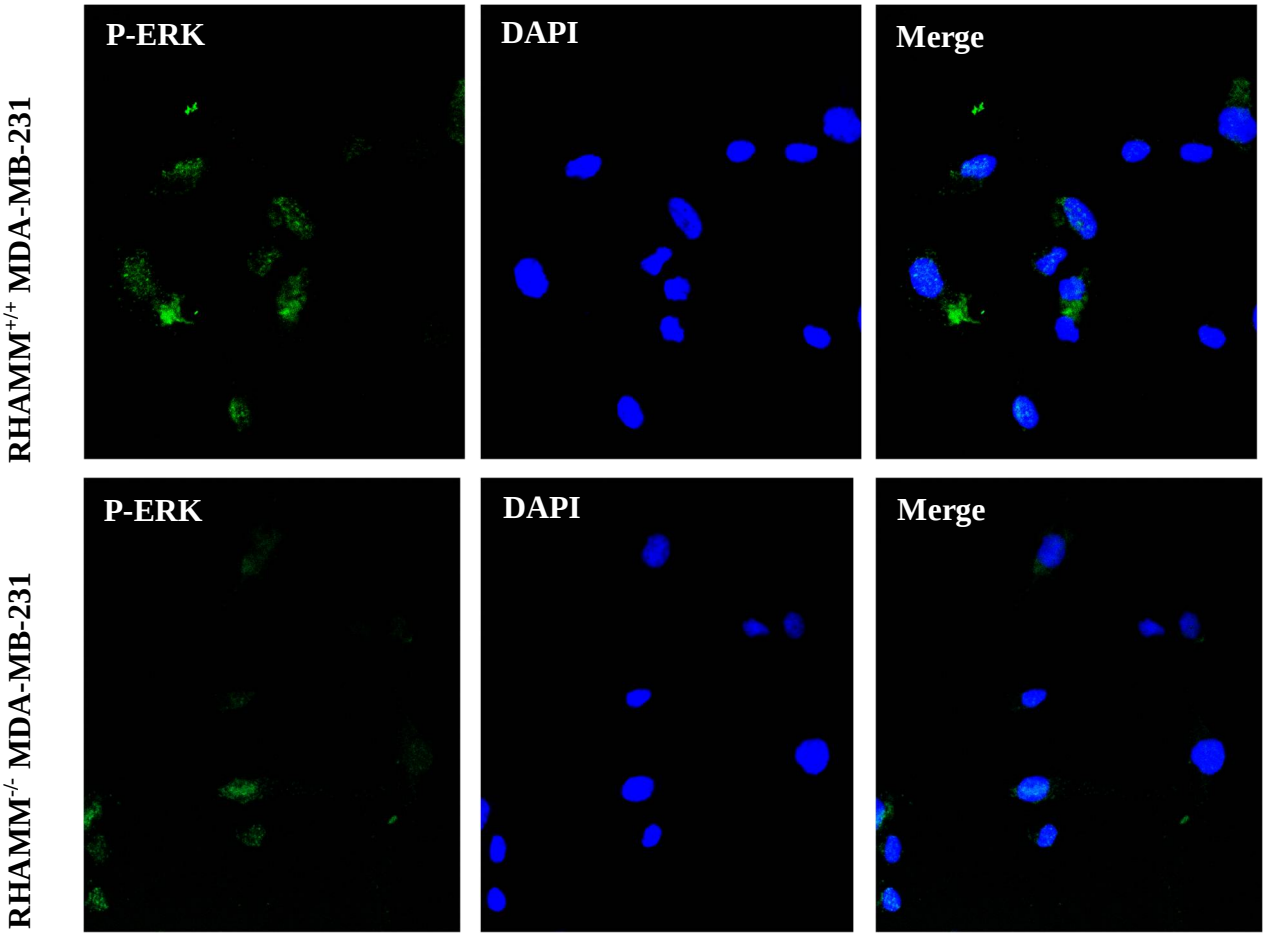

Figure 3.19. pERK1/2 protein localize in the nuclei in RHAMM$^{+/+}$MDA-MB-231 cells to a greater extent than in RHAMM$^{-/-}$MDA-MB-231 cells.

In immunofluorescence images, the percentage of cells with nuclear pERK1/2 is higher in RHAMM$^{+/+}$ compare to RHAMM$^{-/-}$ cells (approximately 75% and 35%, respectively).

3.7 Sensitivity of MDA-MB-231 Cells to MEK1/2 Inhibition Depends on RHAMM Expression

Since cell surface RHAMM regulates the Raf/MEK/ERK signaling pathway that promotes aggressive TNBC cell behavior[91, 218, 228] and since activation of this pathway is linked to poor outcome in TNBC[159, 229], I asked whether RHAMM expression may affect the sensitivity of these tumor cells to MEK inhibitors, which are increasingly being investigated as a therapeutic approach to managing some cancers. RHAMM plays several roles in regulating the ERK1/2 pathway. First, cell surface RHAMM is required for initial activation of ERK1/2 through its association with transmembrane receptors including growth factor receptors and CD44. As well, intracellular RHAMM acts as a scaffold protein that directly binds to ERK1 and forms a complex with ERK2 and MEK1[91] that sustains ERK activation. PD98059 was initially used to block ERK1/2 activity since it is a selective inhibitor of MEK1 activation that has been extensively used to inhibit ERK1/2 activity in a variety experimental tumor cell models[230-233]. Results show that PD98059 inhibited HA^{high} cell proliferation to a greater extent than HA^{low} cells suggesting that HA^{high} cells are significantly more sensitive to MEK1/2 inhibition than HA^{low} cells ($p<0.05$) (Figure 3.20). RHAMM deletion in MDA-MB-231 cells resulted in a decrease in tumor cell sensitivity to trametinib (trade name: Mekinist), an FDA-approved MEK1 kinase inhibitor for unresectable or metastatic melanoma with BRAF V600E or V600K mutation (a mutation at nucleotide 600 which converts a valine to a glutamic acid or lysine, respectively), and metastatic non-small cell lung cancer (NSCLC) with BRAF V600E mutation as detected by an FDA-approved test[234, 235]. Thus, trametinib inhibited $RHAMM^{+/+}$ and $RHAMM^{-/-}$ MDA-MB-231 cell proliferation with GI_{50} values of 0.6 nM and 2.0 nM, respectively (Table 3.3).

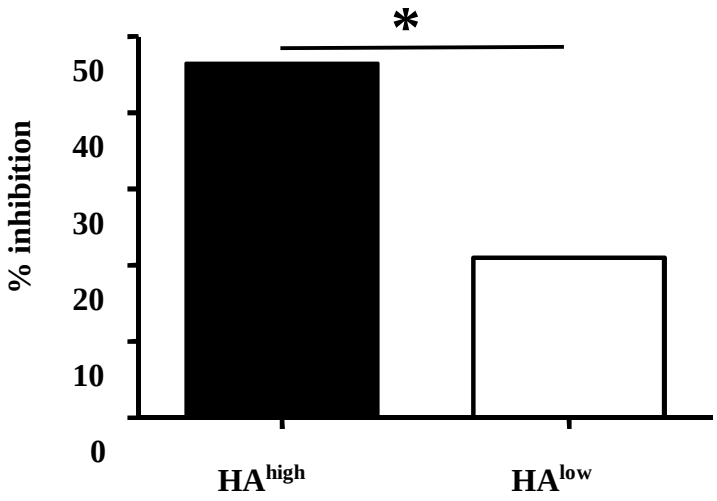

Figure 3.20. HA^{high} cells are inhibited approximately two-fold more by PD98059 compared to HA^{low} cells.

n=8 replicates, *P<0.05 HA^{low} and HA^{high} cells determined by Student's t-test. The data represent one of 3 experiments with similar results.

Table 3.3. $RHAMM^{+/+}$ MDA-MB-231 cells are more sensitive to trametinib than $RHAMM^{-/-}$MDA-MB-231.

$RHAMM^{-/-}$ MDA-MB-231 GI_{50}	2.0 nM
$RHAMM^{+/+}$ MDA-MB-231 GI_{50}	0.6 nM
P-value	<0.0005

The concentration of Trametinib, which suppresses 50% of cell proliferation (GI_{50}), was higher for $RHAMM^{-/-}$ than $RHAMM^{+/+}$ MDA-MB-231 cells. trametinib is an FDA-approved MEK inhibitor for treating advanced melanomas. Mean ± SEM; n=8 replicates. The data represent one of 3 experiments with similar results. GI_{50} values were determined via nonlinear regression using GraphPad Prism 4.0 software.

Chapter 4

4 « Discussion »

Hyaluronan is a major component of the tumor microenvironment in many cancer types and together with its cell-surface receptors, e.g. CD44 and RHAMM, is actively involved in tumor progression and development of chemoresistance. The binding of hyaluronan to breast cancer cell subtypes is heterogeneous[25]. Findings from the previous study[25] showed that tumor cell subsets that bind the highest levels of HA are highly aggressive in terms of invasion and metastasis. However, these same subsets proliferate slowly, prompting me to postulate that these aggressive cells are likely to be resistant to therapies that target proliferating tumor cells.

Here, I present four major findings. Firstly, I verified that the HA^{high} subset of MDA-MB-231 BCa cells is significantly less proliferative than the parental or HA^{low} subsets. Secondly, I discovered that the HA^{high} subset in this tumor cell line is more resistant to doxorubicin, a routinely used breast cancer chemotherapeutic drug that mainly targets DNA, than the HA^{low} subset. Thirdly, and in contrast to the effects of doxorubicin, I find that HA^{high} subset is more sensitive to targeting the MEK-ERK kinase pathway. Fourthly, I discovered that this sensitivity is controlled by RHAMM expression because knockout of RHAMM makes MDA-MB-231 cells more resistant to MEK inhibition. My overall conclusions are that the level of HA binding is linked to chemoresistance while the level of RHAMM display is linked to sensitivity to targeted therapy (MEK1 inhibition). I propose that these two properties may be useful biomarkers for the management of TNBC.

4.1 RHAMM as a Prognostic Factor for Response to Chemotherapy and Targeted Therapy

TNBC is the most lethal subtype of breast cancer due to lack of the effective treatment. It is resistant to chemotherapy and lacks clinically approved molecularly targeted therapies. The (intra- and inter-) tumor heterogeneity is a major hurdle to achieve effective treatment. I have

identified RHAMM as a potential marker for detecting subsets that are resistant to chemotherapy, but potentially targetable with molecularly directed therapies in clinical development.

RHAMM is an oncogenic protein that has been implicated in the progression of many cancers including TNBC[89]. The oncogenic effects of RHAMM on aggressive behavior like motility and invasion and resistance to therapy are mainly driven through the Raf/MEK/ERK pathway[89]. Cell surface RHAMM binds to HA and associates with CD44 and growth factor receptors. The resulting complexes, induce activation of the Raf/MEK/ERK pathway[89]. Intracellular RHAMM RHAMM binds directly to ERK1, forming complexes with ERK2 and MEK1 and is required for retention of activated ERK1/2 in the nucleus[236].

The Raf/MEK/ERK pathway, a pathway that is deregulated in TNBC, is organized by a variety of scaffold proteins, including RHAMM[237] . These scaffold proteins regulate the activity of the pathway (positively or negatively), localize its output, increase the efficiency of signal transmission, and/or isolate the pathway from crosstalk with other MAP kinase pathways. Intracellular RHAMM is proposed to function as a scaffold protein since it binds directly to ERK1 and complexes with ERK2, MEK1, and ERK1/2 substrates[238]. Furthermore, RHAMM as a scaffold protein is required for the translocation of ERK1/2 to the nucleus in the situations such as tissue injury responses, in particular in response to serum and PDGF-BB[57, 97]. ERK1/2 translocation to the nucleus requires phosphorylation by MEK, which causes formation of ERK dimers. This dimerization facilitates the translocation of activated ERK1/2 into the nucleus. The cell surface RHAMM in coordination with the intracellular form regulates sustained activation of MEK1-ERK1/2[237]. Results of the current study confirm that RHAMM expression is necessary for nuclear localization of pERK1/2. I found that RHAMM loss attenuated activated ERK1/2 in nuclei of $RHAMM^{-/-}$ compared to $RHAMM^{+/+}$ MDA-MB-231 cells. Nuclear localization of ERK1/2 is required for expression of target genes of the Raf/MEK/ERK pathway that promote TNBC aggression. Therefore, even though RHAMM does not appear to be essential for controlling total cellular ERK activity, my results suggest that it is critical for activation and nuclear retention of ERK1/2 in TNBC cells. Nuclear localization of ERK1/2 is required for manifestation of its oncogenic properties.

Although in my study RHAMM loss did not significantly reduce total cellular activated ERK1/2 compared to RHAMM$^{+/+}$ MDA-MB-231 cells, Wang *et al.*[103] showed that in MDA-MB-231 cells, down-regulation of RHAMM expression by lentivirus-mediated shRNA inhibited total cellular ERK1/2 activity. This discrepancy in my vs. Wang's results may be due to the variability of the results from the same cell line from two different laboratories. These variabilities originate from differences in cell banks and lots, dissimilarities between the two laboratories' cell culturing techniques and materials such as media and serum, as well as genotypic and phenotypic drift. More importantly, in the current study RHAMM was knocked out using CRISPR-Cas9 method while in the other study it was knocked down using shRNA, which did not completely inhibit RHAMM expression and thus may not have resulted in the enlistment of compensatory mechanisms. Furthermore, Wang *et al.*[103] did not look at the distribution of pERK1/2. As it has been mentioned, RHAMM is not only essential for ERK activation but also is associated with its cellular distribution.

HA^{high} cells are more resistant to doxorubicin than HA^{low} cells (Figure 3.3). The fact that the intracellular accumulation of doxorubicin is not different in both HA^{low} and HA^{high} subsets raises the possibility that HA^{high} cells tolerate higher concentration of doxorubicin compared to HA^{low} cells. This increased resistance to doxorubicin can be due to increased activation of cell survival and anti-apoptotic pathways in HA^{high} than in HA^{low} cells. The other possible mechanism contributing to this effect is the slow proliferation rate of HA^{high} cells. The slowly proliferative RHAMM$^{-/-}$ cells are resistant to doxorubicin consistent with the possibility that proliferation rate is a key factor in sensitivity to this chemotherapeutic reagent. Doxorubicin targets proliferative cells and both HA^{high} and RHAMM$^{-/-}$ are slow cycling. Therefore, their resistance to DNA targeting cytotoxic drugs is likely simply due to their slow proliferation.

HA^{high} subsets are RHAMM^{high} and although some studies predict that RHAMM should promote proliferation, this is controversial as studies have provided evidence that enriching cells with extracellular RHAMM reduces cell proliferation[134]. As well, others have shown that RHAMM deletion does not affect proliferation per se but rather the orientation of dividing cells. My results suggest that RHAMM does play a role in the proliferation of MDA-MB-231 cells. However, although it is likely that the increased accumulation of active nuclear ERK contributes to RHAMM-mediated proliferation, this was not addressed in my study and others have shown that

mitotic effects of RHAMM are mediated by unrelated signaling mechanisms. In my genome-wide mRNA screen, RHAMM level was not significantly different between HA^{high} and HA^{low} subpopulations. Since transcription and translation are far from having a linear and simple relationship, the two subsets might have different levels of RHAMM protein. It is also likely that HA^{high} subsets export RHAMM to the cell surface while HA^{low} cells do not without altering the total amount of either mRNA or protein.

Cell surface RHAMM in complex with CD44 and HA causes high basal motility in invasive breast cancer cells through the Raf/MEK/ERK pathway. Given that RHAMM display was higher in HA^{high} than HA^{low} cells, the best strategy to target the metastatic and chemoresistant HA^{high} cells was targeting the Raf/MEK/ERK pathway. To suppress this signaling cascade, I chose to inhibit MEK1/2 for several reasons[239, 240]. First, MEK inhibitors, unlike other kinase inhibitors, do not compete with ATP binding, which confers a high specificity. Second, effective targeting of MEK1/2 is highly specific as it does not have multiple downstream targets (ERK1/2 is its sole downstream target). Lastly, the most important advantage of inhibiting MEK is that it can be targeted without knowledge of the exact genetic mutation that results in its aberrant activation[240].

Since HA^{high} cells are resistant to chemotherapy and sensitive to MEK inhibition, targeting the Raf/MEK/ERK pathway could prove to be an effective treatment option. However, studies have shown that MEK-targeted therapies may fail due to activation of cell survival pathways[241-243]. Mirzoeva *et al.*[241] showed that MDA-MB-231 cells are particularly susceptible to growth inhibition by small-molecule MEK inhibitors, CI1040 and U0126. However, there is a cross-talk between the Raf/MEK/ERK and phosphatidylinositol 3-kinase (PI3K) pathways (Figure 4.1). In response to MEK inhibition, a negative MEK-EGFR-PI3K feedback loop activates the PI3K pathway. Because the PI3K pathway is a known promoter of the cell cycle and suppressor of apoptosis, its activation in response to MEK inhibition could counterpart therapeutically relevant effects of MEK inhibition. Consistent with their results, another group showed that treatment of MDA-MB-231 cells with the MEK inhibitor trametinib enhanced the levels of phospho-AKT, an essential component of the PI3K pathway[244]. Nonetheless, preclinical studies have shown that dual targeted inhibition of MEK and PI3K pathways can inhibit cell proliferation and induce apoptosis in normal and cancer cells[239, 241, 245]. Several clinical trials are underway to evaluate this promising combination for various cancer types including TNBC[246]. For example, targeting

PI3K and MEK with BYL719 and MEK162, respectively, in advanced solid tumors is being evaluated in phase II clinical trial[246].

In this study, I identified the possibility that detection of cell surface RHAMM expression is a predictive marker for the identification of chemoresistant subpopulations in breast cancer. This is concordant with other studies that have shown RHAMM is transported to the membrane in invasive cancer cell lines[227, 228]. This study also provides evidence that the use of MEK inhibitors in combination with conventional chemotherapeutic drugs may be an effective pharmaceutical strategy for treating TNBC.

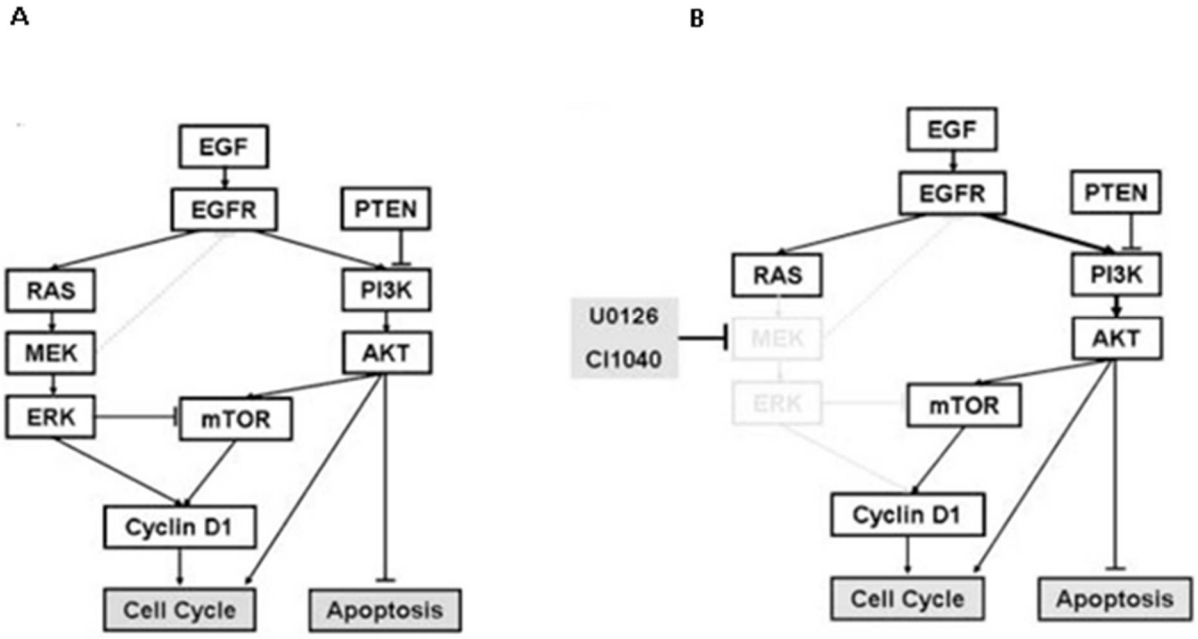

Figure 4.1. Schematic representation of the Raf/MEK/ERK and PI3K pathway interconnectivity.

The cross talk between the Raf/MEK/ERK and PI3K pathways in the absence (A) and presence (B) of MEK inhibitors. There is a negative regulatory feedback loop activating PI3K pathway in an EGFR-dependent mode in response to MEK inhibition (Figure adapted from Mirzoeva *et al.*[241]).

4.2 The phenotypic stability of HA^{low} and HA^{high} TNBC Phenotypes

The study by Veiseh *et al.*[25] postulates that the HA^{low} and HA^{high} phenotypes are stable, not dynamic as the phenotype of HA^{low} cells remained stable after growth in culture for 7 days and retained these phenotypes following growth in mammary fat pads of immune compromised mice for 2 months. Furthermore, a study from the Turley and McCarthy (UMN, USA) laboratories has shown that the HA^{low} and HA^{high} phenotypes in PC3MLN4 prostate cancer cells are stable after orthotopic growth in prostates for 3 months (manuscript in preparation). Nevertheless, in my study the purity of these two phenotypes was estimated to be 82-98% and the gradual reversion of HA^{high} subpopulation to a parental phenotype is likely due to overgrowth by contaminating subpopulations. To establish whether the phenotype is stable in culture, complementary purification strategies to FACS including cloning by limiting dilution and/or single-cell sorting methods.

4.3 The Transcriptome of HA^{low} and HA^{high} Cells

Comparison of microarray-based transcriptome profiles between HA^{high} and HA^{low} cells showed only a few significantly changed genes. Although unexpected, several factors indicate that this low level of transcriptome change is likely real. First, two of the 5 genes identified in the screen as increased in the HA^{high} subpopulation have been implicated in breast cancer and data mining show that these are linked to patient survival and poor response to chemotherapy. As well a similarly low number of changes were observed in the HA^{high} subset of PC3MLN4 prostate tumor cells. This prostate cancer cell subset exhibits a similar aggressive and poorly proliferative phenotype as MDA-MB-231 TNBC cells. The reasons why HA^{high} and HA^{low} cells exhibit only small differences an mRNA transcriptome yet have quite markedly different phenotypes is not clear. Purity could be one issue. However, the Affymetrix mRNA microarray used in my study is limited in that it does not detect splice variants and it may be that many of the genes responsible for the two phenotypes of HA^{high} and HA^{low} subsets are variants. E.g. RHAMM and CD44 are two HA receptors that are subject to alternative splicing which would not be detected by microarray and which result in different protein activity. As well, proteins are activated by post-

translational mechanisms and protein stability is also regulated, which are properties not detected by either RNAseq or Affymetrix arrays and proteome analyses might elucidate more accurately the signaling changes that are required to generate the two phenotypes. For example, HAS2 protein level is different in the two subpopulations and exhibits different subcellular localization.

My study implicates the role of PGA3 in TNBC chemoresistant and poor outcome. PGA3 is not well studied in BCa and could be the subject of the future studies.

4.4 Strategies for Increasing the Purity of Isolated HA^{low} and HA^{high} Subpopulations

This study has further characterized HA^{high} and HA^{low} phenotypes and has shown that the HA^{high} cells with higher HA binding levels, express more HAS2 and RHAMM protein at the plasma membrane. Therefore, sorting for HAS2 and RHAMM display may yield in isolating subpopulations with higher purity. Moreover, in the current study, a mixture of different sizes of HA molecules was used to isolate HA^{high} and HA^{low} cells. Using specific sizes of HA fragments may also result in higher purity of aggressive subpopulations.

4.5 Significance and Future Studies

Prognostic markers improve the accuracy of risk stratification of cancer patients and provide important data to optimize therapeutic decisions. The novel findings presented here suggest that the detection of cell surface RHAMM will aid in predicting the susceptibility of TNBC cells to targeted therapy, in this case MEK1/2 inhibition. As some studies have shown that inhibition of MEK results in resistance of the cancer cells by compensatory activation of PI3K pathway, future studies are required to explore status of PI3K pathway in HA^{high} cells exposed to MEK inhibition.

To the best of my knowledge, this is the first RHAMM study related to chemoresistant in TNBC, suggesting RHAMM as a marker of chemoresistant breast cancer cells. Results of the current study postulate that the subcellular localization of RHAMM might be more informative than its mRNA level for evaluating the susceptibility of TNBC cells towards chemotherapy. The chemoresistant HA^{high} cells express higher cell surface RHAMM than the chemo-sensitive HA^{low} subpopulation, while the mRNA levels are not significantly different.

To my knowledge, this is the second report that provides evidence that RHAMM regulates sensitivity to targeted therapy and the first involving TNBC brest cancer. The other study shows that loss of RHAMM in malignant peripheral nerve sheath tumors increases aurora kinase A (AURKA) activity and sensitizes tumor cells to AURKA inhibitors[247]. AURKA, an important regulator of the cell cycle, is essential for progression through mitosis. Despite the complexity of RHAMM functions in tumors, this study and the current study both suggest that its levels and distribution have a diagnostic/prognostic value such as identifying tumor subpopulations that are sensitive to targeted therapy such as AURKA and MEK inhibitors.

4.6 Limitations

The major limiting factor for performing some experiments was the the low number of sorted HA^{high} and HA^{low} cells. Each subset was composed of only 5-8% of the total population. The two sorted subpopulations were not 100% pure, making *in vitro* expansion of the sorted cells not an option.

Furthermore, the results of this study are limited due to use of only one TNBC cell line and lack of patient derived tumors. It will be important to validate the results in additional TNBC cell lines as well as breast cancer patient samples (e.g. TNBC patient xenografts in immune compromised mice) in order to draw firm conclusions as to the importance of HA^{high} subsets in TNBC aggression.

References

1. Torre LA, Bray F, Siegel RL, Ferlay J, Lortet-Tieulent J, Jemal A. Global cancer statistics, 2012. CA Cancer J Clin. 2015;65(2):87-108.

2. Society CC. Canadian Cancer Statistics. 2017.

3. Malhotra GK, Zhao X, Band H, Band V. Histological, molecular and functional subtypes of breast cancers. Cancer Biol Ther. 2010;10(10):955-60.

4. Li CI, Uribe DJ, Daling JR. Clinical characteristics of different histologic types of breast cancer. Br J Cancer. 2005;93(9):1046-52.

5. Lester SC, Bose S, Chen YY, Connolly JL, de Baca ME, Fitzgibbons PL, et al. Protocol for the examination of specimens from patients with invasive carcinoma of the breast. Arch Pathol Lab Med. 2009;133(10):1515-38.

6. Perou CM, Sorlie T, Eisen MB, van de Rijn M, Jeffrey SS, Rees CA, et al. Molecular portraits of human breast tumours. Nature. 2000;406(6797):747-52.

7. Herschkowitz JI, Simin K, Weigman VJ, Mikaelian I, Usary J, Hu Z, et al. Identification of conserved gene expression features between murine mammary carcinoma models and human breast tumors. Genome Biol. 2007;8(5):R76.

8. Prat A, Parker JS, Karginova O, Fan C, Livasy C, Herschkowitz JI, et al. Phenotypic and molecular characterization of the claudin-low intrinsic subtype of breast cancer. Breast Cancer Res. 2010;12(5):R68.

9. Curtis C. Genomic profiling of breast cancers. Curr Opin Obstet Gynecol. 2015;27(1):34-9.

10. Curtis C, Shah SP, Chin SF, Turashvili G, Rueda OM, Dunning MJ, et al. The genomic and transcriptomic architecture of 2,000 breast tumours reveals novel subgroups. Nature. 2012;486(7403):346-52.

11. Shah SP, Roth A, Goya R, Oloumi A, Ha G, Zhao Y, et al. The clonal and mutational evolution spectrum of primary triple-negative breast cancers. Nature. 2012;486(7403):395-9.

12. Kandoth C, McLellan MD, Vandin F, Ye K, Niu B, Lu C, et al. Mutational landscape and significance across 12 major cancer types. Nature. 2013;502(7471):333-9.

13. Banerji S, Cibulskis K, Rangel-Escareno C, Brown KK, Carter SL, Frederick AM, et al. Sequence analysis of mutations and translocations across breast cancer subtypes. Nature. 2012;486(7403):405-9.

14. Kaplan HG, Malmgren JA. Disease-specific survival in patient-detected breast cancer. Clin Breast Cancer. 2006;7(2):133-40.

15. Morris GJ, Naidu S, Topham AK, Guiles F, Xu Y, McCue P, et al. Differences in breast carcinoma characteristics in newly diagnosed African-American and Caucasian patients: a single-institution compilation compared with the National Cancer Institute's Surveillance, Epidemiology, and End Results database. Cancer. 2007;110(4):876-84.

16. Haffty BG, Yang Q, Reiss M, Kearney T, Higgins SA, Weidhaas J, et al. Locoregional relapse and distant metastasis in conservatively managed triple negative early-stage breast cancer. J Clin Oncol. 2006;24(36):5652-7.

17. Lehmann BD, Bauer JA, Chen X, Sanders ME, Chakravarthy AB, Shyr Y, et al. Identification of human triple-negative breast cancer subtypes and preclinical models for selection of targeted therapies. J Clin Invest. 2011;121(7):2750-67.

18. Prat A, Perou CM. Deconstructing the molecular portraits of breast cancer. Mol Oncol. 2010;5(1):5-23.

19. Collignon J, Lousberg L, Schroeder H, Jerusalem G. Triple-negative breast cancer: treatment challenges and solutions. Breast Cancer (Dove Med Press). 2016;8:93-107.

20. Hammond ME, Hayes DF, Dowsett M, Allred DC, Hagerty KL, Badve S, et al. American Society of Clinical Oncology/College of American Pathologists guideline recommendations for immunohistochemical testing of estrogen and progesterone receptors in breast cancer. Arch Pathol Lab Med. 2010;134(6):907-22.

21. Wolff AC, Hammond ME, Schwartz JN, Hagerty KL, Allred DC, Cote RJ, et al. American Society of Clinical Oncology/College of American Pathologists guideline recommendations for human epidermal growth factor receptor 2 testing in breast cancer. Arch Pathol Lab Med. 2007;131(1):18-43.

22. Misra S, Ghatak S, Zoltan-Jones A, Toole BP. Regulation of multidrug resistance in cancer cells by hyaluronan. J Biol Chem. 2003;278(28):25285-8.

23. Sironen RK, Tammi M, Tammi R, Auvinen PK, Anttila M, Kosma VM. Hyaluronan in human malignancies. Exp Cell Res. 2010;317(4):383-91.

24. Corte MD, Gonzalez LO, Junquera S, Bongera M, Allende MT, Vizoso FJ. Analysis of the expression of hyaluronan in intraductal and invasive carcinomas of the breast. J Cancer Res Clin Oncol. 2010;136(5):745-50.

25. Veiseh M, Kwon DH, Borowsky AD, Tolg C, Leong HS, Lewis JD, et al. Cellular heterogeneity profiling by hyaluronan probes reveals an invasive but slow-growing breast tumor subset. Proceedings of the National Academy of Sciences of the United States of America. 2014;111(17):E1731-9.

26. Schwertfeger KL, Cowman MK, Telmer PG, Turley EA, McCarthy JB. Hyaluronan, Inflammation, and Breast Cancer Progression. Front Immunol. 2015;6:236.

27. Bansal J, Kedige SD, Anand S. Hyaluronic acid: a promising mediator for periodontal regeneration. Indian J Dent Res. 2010;21(4):575-8.

28. Meyer K, Thompson R, Palmer JW, Khorazo D. The Nature of Lysozyme Action. Science. 1934;79(2038):61.

29. Weissmann B, Meyer K, Sampson P, Linker A. Isolation of oligosaccharides enzymatically produced from hyaluronic acid. J Biol Chem. 1954;208(1):417-29.

30. Toole BP. Hyaluronan: from extracellular glue to pericellular cue. Nat Rev Cancer. 2004;4(7):528-39.

31. Laurent TC, Dahl IM, Dahl LB, Engstrom-Laurent A, Eriksson S, Fraser JR, et al. The catabolic fate of hyaluronic acid. Connect Tissue Res. 1986;15(1-2):33-41.

32. Laurent TC, Fraser JR. The properties and turnover of hyaluronan. Ciba Found Symp. 1986;124:9-29.

33. Fraser JR, Laurent TC, Laurent UB. Hyaluronan: its nature, distribution, functions and turnover. J Intern Med. 1997;242(1):27-33.

34. Cleland RL. Ionic polysaccharides. II. Comparison of polyelectrolyte behavior of hyaluronate with that of carboxymethyl cellulose. Biopolymers. 1968;6(11):1519-29.

35. Scott JE. Secondary structures in hyaluronan solutions: chemical and biological implications. Ciba Found Symp. 1989;143:6-15; discussion -20, 281-5.

36. Weigel PH, Baggenstoss BA. What is special about 200 kDa hyaluronan that activates hyaluronan receptor signaling? Glycobiology. 2017;27(9):868-77.

37. Scott JE, Chen Y, Brass A. Secondary and tertiary structures involving chondroitin and chondroitin sulphates in solution, investigated by rotary shadowing/electron microscopy and computer simulation. Eur J Biochem. 1992;209(2):675-80.

38. Laurent TC, Fraser JR. Hyaluronan. FASEB J. 1992;6(7):2397-404.

39. Jiang D, Liang J, Noble PW. Hyaluronan in tissue injury and repair. Annu Rev Cell Dev Biol. 2007;23:435-61.

40. Coleman PJ, Scott D, Mason RM, Levick JR. Characterization of the effect of high molecular weight hyaluronan on trans-synovial flow in rabbit knees. J Physiol. 1999;514 (Pt 1):265-82.

41. Stern R, Asari AA, Sugahara KN. Hyaluronan fragments: an information-rich system. Eur J Cell Biol. 2006;85(8):699-715.

42. Stern R, Maibach HI. Hyaluronan in skin: aspects of aging and its pharmacologic modulation. Clin Dermatol. 2008;26(2):106-22.

43. Weigel PH, DeAngelis PL. Hyaluronan synthases: a decade-plus of novel glycosyltransferases. J Biol Chem. 2007;282(51):36777-81.

44. Spicer AP, Seldin MF, Olsen AS, Brown N, Wells DE, Doggett NA, et al. Chromosomal localization of the human and mouse hyaluronan synthase genes. Genomics. 1997;41(3):493-7.

45. Monslow J, Williams JD, Norton N, Guy CA, Price IK, Coleman SL, et al. The human hyaluronan synthase genes: genomic structures, proximal promoters and polymorphic microsatellite markers. Int J Biochem Cell Biol. 2003;35(8):1272-83.

46. Adamia S, Crainie M, Kriangkum J, Mant MJ, Belch AR, Pilarski LM. Abnormal expression of hyaluronan synthases in patients with Waldenstrom's macroglobulimenia. Semin Oncol. 2003;30(2):165-8.

47. Adamia S, Reiman T, Crainie M, Mant MJ, Belch AR, Pilarski LM. Intronic splicing of hyaluronan synthase 1 (HAS1): a biologically relevant indicator of poor outcome in multiple myeloma. Blood. 2005;105(12):4836-44.

48. Golshani R, Hautmann SH, Estrella V, Cohen BL, Kyle CC, Manoharan M, et al. HAS1 expression in bladder cancer and its relation to urinary HA test. Int J Cancer. 2007;120(8):1712-20.

49. Sayo T, Sugiyama Y, Takahashi Y, Ozawa N, Sakai S, Ishikawa O, et al. Hyaluronan synthase 3 regulates hyaluronan synthesis in cultured human keratinocytes. J Invest Dermatol. 2002;118(1):43-8.

50. Weigel PH, Hascall VC, Tammi M. Hyaluronan synthases. J Biol Chem. 1997;272(22):13997-4000.

51. Itano N, Kimata K. Mammalian hyaluronan synthases. IUBMB Life. 2002;54(4):195-9.

52. Prehm P. Hyaluronate is synthesized at plasma membranes. Biochem J. 1984;220(2):597-600.

53. Tammi RH, Passi AG, Rilla K, Karousou E, Vigetti D, Makkonen K, et al. Transcriptional and post-translational regulation of hyaluronan synthesis. FEBS J. 2011;278(9):1419-28.

54. Pummill PE, DeAngelis PL. Evaluation of critical structural elements of UDP-sugar substrates and certain cysteine residues of a vertebrate hyaluronan synthase. J Biol Chem. 2002;277(24):21610-6.

55. Turley EA, Moore D, Hayden LJ. Characterization of hyaluronate binding proteins isolated from 3T3 and murine sarcoma virus transformed 3T3 cells. Biochemistry. 1987;26(11):2997-3005.

56. Heldin P, Basu K, Olofsson B, Porsch H, Kozlova I, Kahata K. Deregulation of hyaluronan synthesis, degradation and binding promotes breast cancer. J Biochem. 2013;154(5):395-408.

57. Nikitovic D, Kouvidi K, Karamanos NK, Tzanakakis GN. The roles of hyaluronan/RHAMM/CD44 and their respective interactions along the insidious pathways of fibrosarcoma progression. BioMed research international. 2013;2013:929531.

58. McKee CM, Penno MB, Cowman M, Burdick MD, Strieter RM, Bao C, et al. Hyaluronan (HA) fragments induce chemokine gene expression in alveolar macrophages. The role of HA size and CD44. J Clin Invest. 1996;98(10):2403-13.

59. McKee CM, Lowenstein CJ, Horton MR, Wu J, Bao C, Chin BY, et al. Hyaluronan fragments induce nitric-oxide synthase in murine macrophages through a nuclear factor kappaB-dependent mechanism. J Biol Chem. 1997;272(12):8013-8.

60. West DC, Hampson IN, Arnold F, Kumar S. Angiogenesis induced by degradation products of hyaluronic acid. Science. 1985;228(4705):1324-6.

61. Perkins SJ, Nealis AS, Haris PI, Chapman D, Goundis D, Reid KB. Secondary structure in properdin of the complement cascade and related proteins: a study by Fourier transform infrared spectroscopy. Biochemistry. 1989;28(18):7176-82.

62. Yang B, Hall CL, Yang BL, Savani RC, Turley EA. Identification of a novel heparin binding domain in RHAMM and evidence that it modifies HA mediated locomotion of ras-transformed cells. J Cell Biochem. 1994;56(4):455-68.

63. Aruffo A, Stamenkovic I, Melnick M, Underhill CB, Seed B. CD44 is the principal cell surface receptor for hyaluronate. Cell. 1990;61(7):1303-13.

64. Toole BP. Hyaluronan-CD44 Interactions in Cancer: Paradoxes and Possibilities. Clin Cancer Res. 2009;15(24):7462-8.

65. Underhill C. CD44: the hyaluronan receptor. J Cell Sci. 1992;103 (Pt 2):293-8.

66. Iczkowski KA. Cell adhesion molecule CD44: its functional roles in prostate cancer. Am J Transl Res. 2010;3(1):1-7.

67. Jalkanen S, Wu N, Bargatze RF, Butcher EC. Human lymphocyte and lymphoma homing receptors. Annu Rev Med. 1987;38:467-76.

68. Stamenkovic I, Clark EA, Seed B. A B-lymphocyte activation molecule related to the nerve growth factor receptor and induced by cytokines in carcinomas. EMBO J. 1989;8(5):1403-10.

69. Goldstein LA, Zhou DF, Picker LJ, Minty CN, Bargatze RF, Ding JF, et al. A human lymphocyte homing receptor, the hermes antigen, is related to cartilage proteoglycan core and link proteins. Cell. 1989;56(6):1063-72.

70. Cichy J, Pure E. The liberation of CD44. J Cell Biol. 2003;161(5):839-43.

71. Ponta H, Sherman L, Herrlich PA. CD44: from adhesion molecules to signalling regulators. Nat Rev Mol Cell Biol. 2003;4(1):33-45.

72. Screaton GR, Bell MV, Jackson DG, Cornelis FB, Gerth U, Bell JI. Genomic structure of DNA encoding the lymphocyte homing receptor CD44 reveals at least 12 alternatively spliced exons. Proceedings of the National Academy of Sciences of the United States of America. 1992;89(24):12160-4.

73. Jackson DG, Buckley J, Bell JI. Multiple variants of the human lymphocyte homing receptor CD44 generated by insertions at a single site in the extracellular domain. J Biol Chem. 1992;267(7):4732-9.

74. Tolg C, Hofmann M, Herrlich P, Ponta H. Splicing choice from ten variant exons establishes CD44 variability. Nucleic Acids Res. 1993;21(5):1225-9.

75. Isacke CM, Yarwood H. The hyaluronan receptor, CD44. Int J Biochem Cell Biol. 2002;34(7):718-21.

76. Neame SJ, Isacke CM. Phosphorylation of CD44 in vivo requires both Ser323 and Ser325, but does not regulate membrane localization or cytoskeletal interaction in epithelial cells. EMBO J. 1992;11(13):4733-8.

77. Guo YJ, Lin SC, Wang JH, Bigby M, Sy MS. Palmitoylation of CD44 interferes with CD3-mediated signaling in human T lymphocytes. Int Immunol. 1994;6(2):213-21.

78. Okamoto I, Kawano Y, Tsuiki H, Sasaki J, Nakao M, Matsumoto M, et al. CD44 cleavage induced by a membrane-associated metalloprotease plays a critical role in tumor cell migration. Oncogene. 1999;18(7):1435-46.

79. Thorne RF, Legg JW, Isacke CM. The role of the CD44 transmembrane and cytoplasmic domains in co-ordinating adhesive and signalling events. J Cell Sci. 2004;117(Pt 3):373-80.

80. Heldin P, Karousou E, Bernert B, Porsch H, Nishitsuka K, Skandalis SS. Importance of hyaluronan-CD44 interactions in inflammation and tumorigenesis. Connect Tissue Res. 2008;49(3):215-8.

81. Zoller M. CD44: can a cancer-initiating cell profit from an abundantly expressed molecule? Nat Rev Cancer. 2011;11(4):254-67.

82. Inoue K, Fry EA. Aberrant Splicing of Estrogen Receptor, HER2, and CD44 Genes in Breast Cancer. Genet Epigenet. 2015;7:19-32.

83. Turley EA. Purification of a hyaluronate-binding protein fraction that modifies cell social behavior. Biochem Biophys Res Commun. 1982;108(3):1016-24.

84. Hardwick C, Hoare K, Owens R, Hohn HP, Hook M, Moore D, et al. Molecular cloning of a novel hyaluronan receptor that mediates tumor cell motility. J Cell Biol. 1992;117(6):1343-50.

85. Entwistle J, Hall CL, Turley EA. HA receptors: regulators of signalling to the cytoskeleton. J Cell Biochem. 1996;61(4):569-77.

86. Pilarski LM, Pruski E, Wizniak J, Paine D, Seeberger K, Mant MJ, et al. Potential role for hyaluronan and the hyaluronan receptor RHAMM in mobilization and trafficking of hematopoietic progenitor cells. Blood. 1999;93(9):2918-27.

87. Hofmann M, Assmann V, Fieber C, Sleeman JP, Moll J, Ponta H, et al. Problems with RHAMM: a new link between surface adhesion and oncogenesis? Cell. 1998;95(5):591-2; author reply 2-3.

88. Assmann V, Marshall JF, Fieber C, Hofmann M, Hart IR. The human hyaluronan receptor RHAMM is expressed as an intracellular protein in breast cancer cells. J Cell Sci. 1998;111 (Pt 12):1685-94.

89. Maxwell CA, McCarthy J, Turley E. Cell-surface and mitotic-spindle RHAMM: moonlighting or dual oncogenic functions? J Cell Sci. 2008;121(Pt 7):925-32.

90. Turley EA, Noble PW, Bourguignon LY. Signaling properties of hyaluronan receptors. J Biol Chem. 2002;277(7):4589-92.

91. Zhang S, Chang MC, Zylka D, Turley S, Harrison R, Turley EA. The hyaluronan receptor RHAMM regulates extracellular-regulated kinase. J Biol Chem. 1998;273(18):11342-8.

92. Cheung WF, Cruz TF, Turley EA. Receptor for hyaluronan-mediated motility (RHAMM), a hyaladherin that regulates cell responses to growth factors. Biochem Soc Trans. 1999;27(2):135-42.

93. Hall CL, Turley EA. Hyaluronan: RHAMM mediated cell locomotion and signaling in tumorigenesis. J Neurooncol. 1995;26(3):221-9.

94. Wang C, Entwistle J, Hou G, Li Q, Turley EA. The characterization of a human RHAMM cDNA: conservation of the hyaluronan-binding domains. Gene. 1996;174(2):299-306.

95. Park D, Kim Y, Kim H, Kim K, Lee YS, Choe J, et al. Hyaluronic acid promotes angiogenesis by inducing RHAMM-TGFbeta receptor interaction via CD44-PKCdelta. Molecules and cells. 2012;33(6):563-74.

96. Nikitovic D, Kouvidi K, Karamanos NK, Tzanakakis GN. The roles of hyaluronan/RHAMM/CD44 and their respective interactions along the insidious pathways of fibrosarcoma progression. BioMed research international.2013:929531.

97. Tolg C, Hamilton SR, Nakrieko KA, Kooshesh F, Walton P, McCarthy JB, et al. Rhamm-/- fibroblasts are defective in CD44-mediated ERK1,2 motogenic signaling, leading to defective skin wound repair. J Cell Biol. 2006;175(6):1017-28.

98. Hatano H, Shigeishi H, Kudo Y, Higashikawa K, Tobiume K, Takata T, et al. RHAMM/ERK interaction induces proliferative activities of cementifying fibroma cells through a mechanism based on the CD44-EGFR. Laboratory investigation; a journal of technical methods and pathology. 2011;91(3):379-91.

99. Du YC, Chou CK, Klimstra DS, Varmus H. Receptor for hyaluronan-mediated motility isoform B promotes liver metastasis in a mouse model of multistep tumorigenesis and a tail vein assay for metastasis. Proceedings of the National Academy of Sciences of the United States of America. 2011;108(40):16753-8.

100. Savani RC, Cao G, Pooler PM, Zaman A, Zhou Z, DeLisser HM. Differential involvement of the hyaluronan (HA) receptors CD44 and receptor for HA-mediated motility in endothelial cell function and angiogenesis. J Biol Chem. 2001;276(39):36770-8.

101. Manzanares D, Monzon ME, Savani RC, Salathe M. Apical oxidative hyaluronan degradation stimulates airway ciliary beating via RHAMM and RON. Am J Respir Cell Mol Biol. 2007;37(2):160-8.

102. Maxwell CA, Benitez J, Gomez-Baldo L, Osorio A, Bonifaci N, Fernandez-Ramires R, et al. Interplay between BRCA1 and RHAMM regulates epithelial apicobasal polarization and may influence risk of breast cancer. PLoS biology. 2011;9(11):e1001199.

103. Wang Z, Wu Y, Wang H, Zhang Y, Mei L, Fang X, et al. Interplay of mevalonate and Hippo pathways regulates RHAMM transcription via YAP to modulate breast cancer cell motility. Proceedings of the National Academy of Sciences of the United States of America. 2014;111(1):E89-98.

104. Joukov V, Groen AC, Prokhorova T, Gerson R, White E, Rodriguez A, et al. The BRCA1/BARD1 heterodimer modulates ran-dependent mitotic spindle assembly. Cell. 2006;127(3):539-52.

105. Amara FM, Entwistle J, Kuschak TI, Turley EA, Wright JA. Transforming growth factor-beta1 stimulates multiple protein interactions at a unique cis-element in the 3'-untranslated region of the hyaluronan receptor RHAMM mRNA. J Biol Chem. 1996;271(25):15279-84.

106. Samuel SK, Hurta RA, Spearman MA, Wright JA, Turley EA, Greenberg AH. TGF-beta 1 stimulation of cell locomotion utilizes the hyaluronan receptor RHAMM and hyaluronan. J Cell Biol. 1993;123(3):749-58.

107. Godar S, Weinberg RA. Filling the mosaic of p53 actions: p53 represses RHAMM expression. Cell Cycle. 2008;7(22):3479.

108. Sohr S, Engeland K. RHAMM is differentially expressed in the cell cycle and downregulated by the tumor suppressor p53. Cell Cycle. 2008;7(21):3448-60.

109. Tolg C, McCarthy JB, Yazdani A, Turley EA. Hyaluronan and RHAMM in wound repair and the "cancerization" of stromal tissues. BioMed research international. 2014;2014:103923.

110. Misra S, Hascall VC, Markwald RR, Ghatak S. Interactions between Hyaluronan and Its Receptors (CD44, RHAMM) Regulate the Activities of Inflammation and Cancer. Front Immunol. 2015;6:201.

111. Nikitovic D, Tzardi M, Berdiaki A, Tsatsakis A, Tzanakakis GN. Cancer microenvironment and inflammation: role of hyaluronan. Front Immunol. 2015;6:169.

112. Bharadwaj AG, Kovar JL, Loughman E, Elowsky C, Oakley GG, Simpson MA. Spontaneous metastasis of prostate cancer is promoted by excess hyaluronan synthesis and processing. Am J Pathol. 2009;174(3):1027-36.

113. Jaracz S, Chen J, Kuznetsova LV, Ojima I. Recent advances in tumor-targeting anticancer drug conjugates. Bioorg Med Chem. 2005;13(17):5043-54.

114. McBride WH, Bard JB. Hyaluronidase-sensitive halos around adherent cells. Their role in blocking lymphocyte-mediated cytolysis. J Exp Med. 1979;149(2):507-15.

115. Gately CL, Muul LM, Greenwood MA, Papazoglou S, Dick SJ, Kornblith PL, et al. In vitro studies on the cell-mediated immune response to human brain tumors. II. Leukocyte-induced coats of glycosaminoglycan increase the resistance of glioma cells to cellular immune attack. J Immunol. 1984;133(6):3387-95.

116. Naor D, Nedvetzki S, Walmsley M, Yayon A, Turley EA, Golan I, et al. CD44 involvement in autoimmune inflammations: the lesson to be learned from CD44-targeting by antibody or from knockout mice. Ann N Y Acad Sci. 2007;1110:233-47.

117. Jordan AR, Racine RR, Hennig MJ, Lokeshwar VB. The Role of CD44 in Disease Pathophysiology and Targeted Treatment. Front Immunol. 2015;6:182.

118. Chen L, Bourguignon LY. Hyaluronan-CD44 interaction promotes c-Jun signaling and miRNA21 expression leading to Bcl-2 expression and chemoresistance in breast cancer cells. Mol Cancer. 2014;13:52.

119. Bourguignon LY, Zhu D, Zhu H. CD44 isoform-cytoskeleton interaction in oncogenic signaling and tumor progression. Front Biosci. 1998;3:d637-49.

120. Lesley J, Hyman R, Kincade PW. CD44 and its interaction with extracellular matrix. Adv Immunol. 1993;54:271-335.

121. Bourguignon LY, Lokeshwar VB, He J, Chen X, Bourguignon GJ. A CD44-like endothelial cell transmembrane glycoprotein (GP116) interacts with extracellular matrix and ankyrin. Mol Cell Biol. 1992;12(10):4464-71.

122. Lokeshwar VB, Iida N, Bourguignon LY. The cell adhesion molecule, GP116, is a new CD44 variant (ex14/v10) involved in hyaluronic acid binding and endothelial cell proliferation. J Biol Chem. 1996;271(39):23853-64.

123. Lokeshwar VB, Selzer MG. Differences in hyaluronic acid-mediated functions and signaling in arterial, microvessel, and vein-derived human endothelial cells. J Biol Chem. 2000;275(36):27641-9.

124. Brecht M, Mayer U, Schlosser E, Prehm P. Increased hyaluronate synthesis is required for fibroblast detachment and mitosis. Biochem J. 1986;239(2):445-50.

125. Meran S, Luo DD, Simpson R, Martin J, Wells A, Steadman R, et al. Hyaluronan facilitates transforming growth factor-beta1-dependent proliferation via CD44 and epidermal growth factor receptor interaction. J Biol Chem. 2011;286(20):17618-30.

126. Tammi MI, Day AJ, Turley EA. Hyaluronan and homeostasis: a balancing act. J Biol Chem. 2002;277(7):4581-4.

127. Mueller BM, Schraufstatter IU, Goncharova V, Povaliy T, DiScipio R, Khaldoyanidi SK. Hyaluronan inhibits postchemotherapy tumor regrowth in a colon carcinoma xenograft model. Mol Cancer Ther. 2010;9(11):3024-32.

128. Bourguignon LY, Wong G, Earle CA, Xia W. Interaction of low molecular weight hyaluronan with CD44 and toll-like receptors promotes the actin filament-associated protein 110-actin binding and MyD88-NFkappaB signaling leading to proinflammatory cytokine/chemokine production and breast tumor invasion. Cytoskeleton (Hoboken). 2011;68(12):671-93.

129. Louderbough JM, Schroeder JA. Understanding the dual nature of CD44 in breast cancer progression. Mol Cancer Res. 2011;9(12):1573-86.

130. Gunthert U, Stauder R, Mayer B, Terpe HJ, Finke L, Friedrichs K. Are CD44 variant isoforms involved in human tumour progression? Cancer Surv. 1995;24:19-42.

131. Wang SJ, Wong G, de Heer AM, Xia W, Bourguignon LY. CD44 variant isoforms in head and neck squamous cell carcinoma progression. Laryngoscope. 2009;119(8):1518-30.

132. Greiner J, Bullinger L, Guinn BA, Dohner H, Schmitt M. Leukemia-associated antigens are critical for the proliferation of acute myeloid leukemia cells. Clin Cancer Res. 2008;14(22):7161-6.

133. Mantripragada KK, Spurlock G, Kluwe L, Chuzhanova N, Ferner RE, Frayling IM, et al. High-resolution DNA copy number profiling of malignant peripheral nerve sheath tumors using targeted microarray-based comparative genomic hybridization. Clin Cancer Res. 2008;14(4):1015-24.

134. Mohapatra S, Yang X, Wright JA, Turley EA, Greenberg AH. Soluble hyaluronan receptor RHAMM induces mitotic arrest by suppressing Cdc2 and cyclin B1 expression. J Exp Med. 1996;183(4):1663-8.

135. Oda Y, Takahira T, Kawaguchi K, Yamamoto H, Tamiya S, Matsuda S, et al. Altered expression of cell cycle regulators in myxofibrosarcoma, with special emphasis on their prognostic implications. Hum Pathol. 2003;34(10):1035-42.

136. Gottesman MM, Fojo T, Bates SE. Multidrug resistance in cancer: role of ATP-dependent transporters. Nat Rev Cancer. 2002;2(1):48-58.

137. Makin G, Dive C. Apoptosis and cancer chemotherapy. Trends Cell Biol. 2001;11(11):S22-6.

138. O'Gorman DM, Cotter TG. Molecular signals in anti-apoptotic survival pathways. Leukemia. 2001;15(1):21-34.

139. Ohwada C, Nakaseko C, Koizumi M, Takeuchi M, Ozawa S, Naito M, et al. CD44 and hyaluronan engagement promotes dexamethasone resistance in human myeloma cells. Eur J Haematol. 2008;80(3):245-50.

140. Liu CM, Chang CH, Yu CH, Hsu CC, Huang LL. Hyaluronan substratum induces multidrug resistance in human mesenchymal stem cells via CD44 signaling. Cell Tissue Res. 2009;336(3):465-75.

141. Ohashi R, Takahashi F, Cui R, Yoshioka M, Gu T, Sasaki S, et al. Interaction between CD44 and hyaluronate induces chemoresistance in non-small cell lung cancer cell. Cancer Lett. 2007;252(2):225-34.

142. Whatcott CJ, Han H, Posner RG, Hostetter G, Von Hoff DD. Targeting the tumor microenvironment in cancer: why hyaluronidase deserves a second look. Cancer Discov. 2011;1(4):291-6.

143. Misra S, Ghatak S, Toole BP. Regulation of MDR1 expression and drug resistance by a positive feedback loop involving hyaluronan, phosphoinositide 3-kinase, and ErbB2. J Biol Chem. 2005;280(21):20310-5.

144. Slomiany MG, Grass GD, Robertson AD, Yang XY, Maria BL, Beeson C, et al. Hyaluronan, CD44, and emmprin regulate lactate efflux and membrane localization of monocarboxylate transporters in human breast carcinoma cells. Cancer Res. 2009;69(4):1293-301.

145. Slomiany MG, Dai L, Bomar PA, Knackstedt TJ, Kranc DA, Tolliver L, et al. Abrogating drug resistance in malignant peripheral nerve sheath tumors by disrupting hyaluronan-CD44 interactions with small hyaluronan oligosaccharides. Cancer Res. 2009;69(12):4992-8.

146. Toole BP, Slomiany MG. Hyaluronan: a constitutive regulator of chemoresistance and malignancy in cancer cells. Semin Cancer Biol. 2008;18(4):244-50.

147. Takahashi E, Nagano O, Ishimoto T, Yae T, Suzuki Y, Shinoda T, et al. Tumor necrosis factor-alpha regulates transforming growth factor-beta-dependent epithelial-mesenchymal transition by promoting hyaluronan-CD44-moesin interaction. J Biol Chem. 2009;285(6):4060-73.

148. Xu Y, Stamenkovic I, Yu Q. CD44 attenuates activation of the hippo signaling pathway and is a prime therapeutic target for glioblastoma. Cancer Res. 2010;70(6):2455-64.

149. Goldie SJ, Mulder KW, Tan DW, Lyons SK, Sims AH, Watt FM. FRMD4A upregulation in human squamous cell carcinoma promotes tumor growth and metastasis and is associated with poor prognosis. Cancer Res. 2012;72(13):3424-36.

150. Zhang Y, Xia H, Ge X, Chen Q, Yuan D, Leng W, et al. CD44 acts through RhoA to regulate YAP signaling. Cell Signal. 2014;26(11):2504-13.

151. Meloche S, Pouyssegur J. The ERK1/2 mitogen-activated protein kinase pathway as a master regulator of the G1- to S-phase transition. Oncogene. 2007;26(22):3227-39.

152. Steelman LS, Navolanic PM, Franklin RA, Bonati A, Libra M, Stivala F, et al. Combining chemo-, hormonal and targeted therapies to treat breast cancer (Review). Mol Med Rep. 2008;1(2):139-60.

153. Navolanic PM, Steelman LS, McCubrey JA. EGFR family signaling and its association with breast cancer development and resistance to chemotherapy (Review). Int J Oncol. 2003;22(2):237-52.

154. Weinstein-Oppenheimer CR, Henriquez-Roldan CF, Davis JM, Navolanic PM, Saleh OA, Steelman LS, et al. Role of the Raf signal transduction cascade in the in vitro resistance to the anticancer drug doxorubicin. Clin Cancer Res. 2001;7(9):2898-907.

155. Davis JM, Navolanic PM, Weinstein-Oppenheimer CR, Steelman LS, Hu W, Konopleva M, et al. Raf-1 and Bcl-2 induce distinct and common pathways that contribute to breast cancer drug resistance. Clin Cancer Res. 2003;9(3):1161-70.

156. Hamilton SR, Fard SF, Paiwand FF, Tolg C, Veiseh M, Wang C, et al. The hyaluronan receptors CD44 and Rhamm (CD168) form complexes with ERK1,2 that sustain high basal motility in breast cancer cells. J Biol Chem. 2007;282(22):16667-80.

157. Chen H, Zhu G, Li Y, Padia RN, Dong Z, Pan ZK, et al. Extracellular signal-regulated kinase signaling pathway regulates breast cancer cell migration by maintaining slug expression. Cancer Res. 2009;69(24):9228-35.

158. Milde-Langosch K, Bamberger AM, Rieck G, Grund D, Hemminger G, Muller V, et al. Expression and prognostic relevance of activated extracellular-regulated kinases (ERK1/2) in breast cancer. Br J Cancer. 2005;92(12):2206-15.

159. Bartholomeusz C, Gonzalez-Angulo AM, Liu P, Hayashi N, Lluch A, Ferrer-Lozano J, et al. High ERK protein expression levels correlate with shorter survival in triple-negative breast cancer patients. Oncologist. 2012;17(6):766-74.

160. Adeyinka A, Nui Y, Cherlet T, Snell L, Watson PH, Murphy LC. Activated mitogen-activated protein kinase expression during human breast tumorigenesis and breast cancer progression. Clin Cancer Res. 2002;8(6):1747-53.

161. Corkery B, Crown J, Clynes M, O'Donovan N. Epidermal growth factor receptor as a potential therapeutic target in triple-negative breast cancer. Ann Oncol. 2009;20(5):862-7.

162. Eralp Y, Derin D, Ozluk Y, Yavuz E, Guney N, Saip P, et al. MAPK overexpression is associated with anthracycline resistance and increased risk for recurrence in patients with triple-negative breast cancer. Ann Oncol. 2008;19(4):669-74.

163. Sivaraman VS, Wang H, Nuovo GJ, Malbon CC. Hyperexpression of mitogen-activated protein kinase in human breast cancer. J Clin Invest. 1997;99(7):1478-83.

164. Prat A, Perou CM. Deconstructing the molecular portraits of breast cancer. Mol Oncol. 2011;5(1):5-23.

165. Prat A, Adamo B, Cheang MC, Anders CK, Carey LA, Perou CM. Molecular characterization of basal-like and non-basal-like triple-negative breast cancer. Oncologist. 2013;18(2):123-33.

166. Moriuchi S, Shimizu K, Miyao Y, Yamada M, Ohkawa M, Hayakawa T. In vitro assessment for neurotoxicity of antitumor agents before local administration into central nervous system. Anticancer Res. 1996;16(1):135-40.

167. Schondorf T, Kurbacher CM, Gohring UJ, Benz C, Becker M, Sartorius J, et al. Induction of MDR1-gene expression by antineoplastic agents in ovarian cancer cell lines. Anticancer Res. 2002;22(4):2199-203.

168. Gewirtz DA. A critical evaluation of the mechanisms of action proposed for the antitumor effects of the anthracycline antibiotics adriamycin and daunorubicin. Biochem Pharmacol. 1999;57(7):727-41.

169. Ginestier C, Hur MH, Charafe-Jauffret E, Monville F, Dutcher J, Brown M, et al. ALDH1 is a marker of normal and malignant human mammary stem cells and a predictor of poor clinical outcome. Cell Stem Cell. 2007;1(5):555-67.

170. Shen F, Chu S, Bence AK, Bailey B, Xue X, Erickson PA, et al. Quantitation of doxorubicin uptake, efflux, and modulation of multidrug resistance (MDR) in MDR human cancer cells. J Pharmacol Exp Ther. 2008;324(1):95-102.

171. GeneChip™ WT Terminal Labeling and Hybridization User Manual for use with the Ambion™ WT Expression Kit User Manual. 2017.

172. Irizarry RA, Bolstad BM, Collin F, Cope LM, Hobbs B, Speed TP. Summaries of Affymetrix GeneChip probe level data. Nucleic Acids Res. 2003;31(4):e15.

173. Cerami E, Gao J, Dogrusoz U, Gross BE, Sumer SO, Aksoy BA, et al. The cBio cancer genomics portal: an open platform for exploring multidimensional cancer genomics data. Cancer Discov. 2012;2(5):401-4.

174. Gao J, Aksoy BA, Dogrusoz U, Dresdner G, Gross B, Sumer SO, et al. Integrative analysis of complex cancer genomics and clinical profiles using the cBioPortal. Sci Signal. 2013;6(269):pl1.

175. Tsai CM, Chang KT, Wu LH, Chen JY, Gazdar AF, Mitsudomi T, et al. Correlations between intrinsic chemoresistance and HER-2/neu gene expression, p53 gene mutations, and cell proliferation characteristics in non-small cell lung cancer cell lines. Cancer Res. 1996;56(1):206-9.

176. Blagosklonny MV. Why therapeutic response may not prolong the life of a cancer patient: selection for oncogenic resistance. Cell Cycle. 2005;4(12):1693-8.

177. Jung Y, Lippard SJ. Direct cellular responses to platinum-induced DNA damage. Chem Rev. 2007;107(5):1387-407.

178. Papamichael D. The use of thymidylate synthase inhibitors in the treatment of advanced colorectal cancer: current status. Oncologist. 1999;4(6):478-87.

179. Smith L, Watson MB, O'Kane SL, Drew PJ, Lind MJ, Cawkwell L. The analysis of doxorubicin resistance in human breast cancer cells using antibody microarrays. Mol Cancer Ther. 2006;5(8):2115-20.

180. Chen NT, Wu CY, Chung CY, Hwu Y, Cheng SH, Mou CY, et al. Probing the dynamics of doxorubicin-DNA intercalation during the initial activation of apoptosis by fluorescence lifetime imaging microscopy (FLIM). PLoS One. 2012;7(9):e44947.

181. Zhang X, Chibli H, Mielke R, Nadeau J. Ultrasmall gold-doxorubicin conjugates rapidly kill apoptosis-resistant cancer cells. Bioconjug Chem. 2010;22(2):235-43.

182. Chen DR, Lu DY, Lin HY, Yeh WL. Mesenchymal stem cell-induced doxorubicin resistance in triple negative breast cancer. BioMed research international. 2014;2014:532161.

183. Reya T, Morrison SJ, Clarke MF, Weissman IL. Stem cells, cancer, and cancer stem cells. Nature. 2001;414(6859):105-11.

184. Visvader JE, Lindeman GJ. Cancer stem cells in solid tumours: accumulating evidence and unresolved questions. Nat Rev Cancer. 2008;8(10):755-68.

185. Al-Hajj M, Wicha MS, Benito-Hernandez A, Morrison SJ, Clarke MF. Prospective identification of tumorigenic breast cancer cells. Proceedings of the National Academy of Sciences of the United States of America. 2003;100(7):3983-8.

186. Croker AK, Goodale D, Chu J, Postenka C, Hedley BD, Hess DA, et al. High aldehyde dehydrogenase and expression of cancer stem cell markers selects for breast cancer cells with enhanced malignant and metastatic ability. J Cell Mol Med. 2009;13(8B):2236-52.

187. Sheridan C, Kishimoto H, Fuchs RK, Mehrotra S, Bhat-Nakshatri P, Turner CH, et al. CD44+/CD24- breast cancer cells exhibit enhanced invasive properties: an early step necessary for metastasis. Breast Cancer Res. 2006;8(5):R59.

188. Murohashi M, Hinohara K, Kuroda M, Isagawa T, Tsuji S, Kobayashi S, et al. Gene set enrichment analysis provides insight into novel signalling pathways in breast cancer stem cells. Br J Cancer. 2009;102(1):206-12.

189. Storms RW, Trujillo AP, Springer JB, Shah L, Colvin OM, Ludeman SM, et al. Isolation of primitive human hematopoietic progenitors on the basis of aldehyde dehydrogenase activity. Proceedings of the National Academy of Sciences of the United States of America. 1999;96(16):9118-23.

190. Auvinen P, Tammi R, Parkkinen J, Tammi M, Agren U, Johansson R, et al. Hyaluronan in peritumoral stroma and malignant cells associates with breast cancer spreading and predicts survival. Am J Pathol. 2000;156(2):529-36.

191. Jojovic M, Delpech B, Prehm P, Schumacher U. Expression of hyaluronate and hyaluronate synthase in human primary tumours and their metastases in scid mice. Cancer Lett. 2002;188(1-2):181-9.

192. Bernert B, Porsch H, Heldin P. Hyaluronan synthase 2 (HAS2) promotes breast cancer cell invasion by suppression of tissue metalloproteinase inhibitor 1 (TIMP-1). J Biol Chem. 2011;286(49):42349-59.

193. Udabage L, Brownlee GR, Waltham M, Blick T, Walker EC, Heldin P, et al. Antisense-mediated suppression of hyaluronan synthase 2 inhibits the tumorigenesis and progression of breast cancer. Cancer Res. 2005;65(14):6139-50.

194. Li Y, Li L, Brown TJ, Heldin P. Silencing of hyaluronan synthase 2 suppresses the malignant phenotype of invasive breast cancer cells. Int J Cancer. 2007;120(12):2557-67.

195. Vigetti D, Rizzi M, Viola M, Karousou E, Genasetti A, Clerici M, et al. The effects of 4-methylumbelliferone on hyaluronan synthesis, MMP2 activity, proliferation, and motility of human aortic smooth muscle cells. Glycobiology. 2009;19(5):537-46.

196. Goentzel BJ, Weigel PH, Steinberg RA. Recombinant human hyaluronan synthase 3 is phosphorylated in mammalian cells. Biochem J. 2006;396(2):347-54.

197. Karousou E, Kamiryo M, Skandalis SS, Ruusala A, Asteriou T, Passi A, et al. The activity of hyaluronan synthase 2 is regulated by dimerization and ubiquitination. J Biol Chem. 2010;285(31):23647-54.

198. Vigetti D, Deleonibus S, Moretto P, Karousou E, Viola M, Bartolini B, et al. Role of UDP-N-acetylglucosamine (GlcNAc) and O-GlcNAcylation of hyaluronan synthase 2 in the control of chondroitin sulfate and hyaluronan synthesis. J Biol Chem. 2012;287(42):35544-55.

199. Rilla K, Siiskonen H, Spicer AP, Hyttinen JM, Tammi MI, Tammi RH. Plasma membrane residence of hyaluronan synthase is coupled to its enzymatic activity. J Biol Chem. 2005;280(36):31890-7.

200. Gilg AG, Tye SL, Tolliver LB, Wheeler WG, Visconti RP, Duncan JD, et al. Targeting hyaluronan interactions in malignant gliomas and their drug-resistant multipotent progenitors. Clin Cancer Res. 2008;14(6):1804-13.

201. Cui R, Takahashi F, Ohashi R, Gu T, Yoshioka M, Nishio K, et al. Abrogation of the interaction between osteopontin and alphavbeta3 integrin reduces tumor growth of human lung cancer cells in mice. Lung Cancer. 2007;57(3):302-10.

202. Sato N, Cheng XB, Kohi S, Koga A, Hirata K. Targeting hyaluronan for the treatment of pancreatic ductal adenocarcinoma. Acta Pharm Sin B. 2016;6(2):101-5.

203. David-Raoudi M, Tranchepain F, Deschrevel B, Vincent JC, Bogdanowicz P, Boumediene K, et al. Differential effects of hyaluronan and its fragments on fibroblasts: relation to wound healing. Wound Repair Regen. 2008;16(2):274-87.

204. Zhao N, Wang X, Qin L, Guo Z, Li D. Effect of molecular weight and concentration of hyaluronan on cell proliferation and osteogenic differentiation in vitro. Biochem Biophys Res Commun. 2015;465(3):569-74.

205. Huang L, Cheng YY, Koo PL, Lee KM, Qin L, Cheng JC, et al. The effect of hyaluronan on osteoblast proliferation and differentiation in rat calvarial-derived cell cultures. J Biomed Mater Res A. 2003;66(4):880-4.

206. Takeda K, Sakai N, Shiba H, Nagahara T, Fujita T, Kajiya M, et al. Characteristics of high-molecular-weight hyaluronic acid as a brain-derived neurotrophic factor scaffold in periodontal tissue regeneration. Tissue Eng Part A. 2010;17(7-8):955-67.

207. Kudo D, Kon A, Yoshihara S, Kakizaki I, Sasaki M, Endo M, et al. Effect of a hyaluronan synthase suppressor, 4-methylumbelliferone, on B16F-10 melanoma cell adhesion and locomotion. Biochem Biophys Res Commun. 2004;321(4):783-7.

208. Hiraga T, Ito S, Nakamura H. Cancer stem-like cell marker CD44 promotes bone metastases by enhancing tumorigenicity, cell motility, and hyaluronan production. Cancer Res. 2013;73(13):4112-22.

209. Kultti A, Pasonen-Seppanen S, Jauhiainen M, Rilla KJ, Karna R, Pyoria E, et al. 4-Methylumbelliferone inhibits hyaluronan synthesis by depletion of cellular UDP-glucuronic acid and downregulation of hyaluronan synthase 2 and 3. Exp Cell Res. 2009;315(11):1914-23.

210. Clarkin CE, Allen S, Wheeler-Jones CP, Bastow ER, Pitsillides AA. Reduced chondrogenic matrix accumulation by 4-methylumbelliferone reveals the potential for selective targeting of UDP-glucose dehydrogenase. Matrix Biol. 2011;30(3):163-8.

211. Nagy N, Kuipers HF, Frymoyer AR, Ishak HD, Bollyky JB, Wight TN, et al. 4-methylumbelliferone treatment and hyaluronan inhibition as a therapeutic strategy in inflammation, autoimmunity, and cancer. Front Immunol. 2015;6:123.

212. Nakazawa H, Yoshihara S, Kudo D, Morohashi H, Kakizaki I, Kon A, et al. 4-methylumbelliferone, a hyaluronan synthase suppressor, enhances the anticancer activity of gemcitabine in human pancreatic cancer cells. Cancer Chemother Pharmacol. 2006;57(2):165-70.

213. Uchakina ON, Ban H, McKallip RJ. Targeting hyaluronic acid production for the treatment of leukemia: treatment with 4-methylumbelliferone leads to induction of MAPK-mediated apoptosis in K562 leukemia. Leuk Res. 2013;37(10):1294-301.

214. Shakya S, Wang Y, Mack JA, Maytin EV. Hyperglycemia-Induced Changes in Hyaluronan Contribute to Impaired Skin Wound Healing in Diabetes: Review and Perspective. Int J Cell Biol.2015:701738.

215. Wang Y, Lauer ME, Anand S, Mack JA, Maytin EV. Hyaluronan synthase 2 protects skin fibroblasts against apoptosis induced by environmental stress. J Biol Chem. 2014;289(46):32253-65.

216. Torronen K, Nikunen K, Karna R, Tammi M, Tammi R, Rilla K. Tissue distribution and subcellular localization of hyaluronan synthase isoenzymes. Histochem Cell Biol. 2013;141(1):17-31.

217. Turley EA. Hyaluronan and cell locomotion. Cancer Metastasis Rev. 1992;11(1):21-30.

218. Wang C, Thor AD, Moore DH, 2nd, Zhao Y, Kerschmann R, Stern R, et al. The overexpression of RHAMM, a hyaluronan-binding protein that regulates ras signaling, correlates with overexpression of mitogen-activated protein kinase and is a significant parameter in breast cancer progression. Clin Cancer Res. 1998;4(3):567-76.

219. Bourguignon LY. CD44-mediated oncogenic signaling and cytoskeleton activation during mammary tumor progression. J Mammary Gland Biol Neoplasia. 2001;6(3):287-97.

220. Bourguignon LY. Hyaluronan-mediated CD44 activation of RhoGTPase signaling and cytoskeleton function promotes tumor progression. Semin Cancer Biol. 2008;18(4):251-9.

221. Auvinen PK, Parkkinen JJ, Johansson RT, Agren UM, Tammi RH, Eskelinen MJ, et al. Expression of hyaluronan in benign and malignant breast lesions. Int J Cancer. 1997;74(5):477-81.

222. Matou-Nasri S, Gaffney J, Kumar S, Slevin M. Oligosaccharides of hyaluronan induce angiogenesis through distinct CD44 and RHAMM-mediated signalling pathways involving Cdc2 and gamma-adducin. Int J Oncol. 2009;35(4):761-73.

223. Ohta S, Yoshida J, Iwata H, Hamaguchi M. Hyaluronate activates tyrosine phosphorylation of cellular proteins including focal adhesion kinase via CD44 in human glioma cells. Int J Oncol. 1997;10(3):561-4.

224. Metzger-Filho O, Tutt A, de Azambuja E, Saini KS, Viale G, Loi S, et al. Dissecting the heterogeneity of triple-negative breast cancer. J Clin Oncol. 2012;30(15):1879-87.

225. Herrera-Gayol A, Jothy S. Effects of hyaluronan on the invasive properties of human breast cancer cells in vitro. Int J Exp Pathol. 2001;82(3):193-200.

226. Liu R, Wang X, Chen GY, Dalerba P, Gurney A, Hoey T, et al. The prognostic role of a gene signature from tumorigenic breast-cancer cells. N Engl J Med. 2007;356(3):217-26.

227. Hall CL, Yang B, Yang X, Zhang S, Turley M, Samuel S, et al. Overexpression of the hyaluronan receptor RHAMM is transforming and is also required for H-ras transformation. Cell. 1995;82(1):19-26.

228. Kouvidi K, Berdiaki A, Nikitovic D, Katonis P, Afratis N, Hascall VC, et al. Role of receptor for hyaluronic acid-mediated motility (RHAMM) in low molecular weight hyaluronan (LMWHA)-mediated fibrosarcoma cell adhesion. J Biol Chem. 2011;286(44):38509-20.

229. Bartholomeusz C, Xie X, Pitner MK, Kondo K, Dadbin A, Lee J, et al. MEK Inhibitor Selumetinib (AZD6244; ARRY-142886) Prevents Lung Metastasis in a Triple-Negative Breast Cancer Xenograft Model. Mol Cancer Ther. 2015;14(12):2773-81.

230. Crews CM, Alessandrini A, Erikson RL. The primary structure of MEK, a protein kinase that phosphorylates the ERK gene product. Science. 1992;258(5081):478-80.

231. Alessi DR, Saito Y, Campbell DG, Cohen P, Sithanandam G, Rapp U, et al. Identification of the sites in MAP kinase kinase-1 phosphorylated by p74raf-1. EMBO J. 1994;13(7):1610-9.

232. Rosen LB, Ginty DD, Weber MJ, Greenberg ME. Membrane depolarization and calcium influx stimulate MEK and MAP kinase via activation of Ras. Neuron. 1994;12(6):1207-21.

233. Cowley S, Paterson H, Kemp P, Marshall CJ. Activation of MAP kinase kinase is necessary and sufficient for PC12 differentiation and for transformation of NIH 3T3 cells. Cell. 1994;77(6):841-52.

234. Yamaguchi T, Kakefuda R, Tajima N, Sowa Y, Sakai T. Antitumor activities of JTP-74057 (GSK1120212), a novel MEK1/2 inhibitor, on colorectal cancer cell lines in vitro and in vivo. Int J Oncol. 2011;39(1):23-31.

235. FDA grants regular approval to dabrafenib and trametinib combination for metastatic NSCLC with BRAF V600E mutation 2017 [Available from: https://www.fda.gov/Drugs/InformationOnDrugs/ApprovedDrugs/ucm564331.htm.

236. Telmer PG, Tolg C, McCarthy JB, Turley EA. How does a protein with dual mitotic spindle and extracellular matrix receptor functions affect tumor susceptibility and progression? Commun Integr Biol. 2011;4(2):182-5.

237. Tolg C, Hamilton SR, Morningstar L, Zhang J, Zhang S, Esguerra KV, et al. RHAMM promotes interphase microtubule instability and mitotic spindle integrity through MEK1/ERK1/2 activity. J Biol Chem. 2010;285(34):26461-74.

238. Okuyama S, Aihara H. Hyperalgesic action in mice of intracerebroventricularly administered arachidonic acid, PG E2, PG F2 alpha and PG D2: effects of analgesic drugs on hyperalgesia. J Pharmacobiodyn. 1986;9(11):902-8.

239. Chappell WH, Steelman LS, Long JM, Kempf RC, Abrams SL, Franklin RA, et al. Ras/Raf/MEK/ERK and PI3K/PTEN/Akt/mTOR inhibitors: rationale and importance to inhibiting these pathways in human health. Oncotarget. 2011;2(3):135-64.

240. Delaney AM, Printen JA, Chen H, Fauman EB, Dudley DT. Identification of a novel mitogen-activated protein kinase kinase activation domain recognized by the inhibitor PD 184352. Mol Cell Biol. 2002;22(21):7593-602.

241. Mirzoeva OK, Das D, Heiser LM, Bhattacharya S, Siwak D, Gendelman R, et al. Basal subtype and MAPK/ERK kinase (MEK)-phosphoinositide 3-kinase feedback signaling determine susceptibility of breast cancer cells to MEK inhibition. Cancer Res. 2009;69(2):565-72.

242. Balmanno K, Chell SD, Gillings AS, Hayat S, Cook SJ. Intrinsic resistance to the MEK1/2 inhibitor AZD6244 (ARRY-142886) is associated with weak ERK1/2 signalling and/or strong PI3K signalling in colorectal cancer cell lines. Int J Cancer. 2009;125(10):2332-41.

243. Wee S, Jagani Z, Xiang KX, Loo A, Dorsch M, Yao YM, et al. PI3K pathway activation mediates resistance to MEK inhibitors in KRAS mutant cancers. Cancer Res. 2009;69(10):4286-93.

244. Ludwik KA, Campbell JP, Li M, Li Y, Sandusky ZM, Pasic L, et al. Development of a RSK Inhibitor as a Novel Therapy for Triple-Negative Breast Cancer. Mol Cancer Ther. 2016;15(11):2598-608.

245. Abrams SL, Steelman LS, Shelton JG, Wong EW, Chappell WH, Basecke J, et al. The Raf/MEK/ERK pathway can govern drug resistance, apoptosis and sensitivity to targeted therapy. Cell Cycle. 2010;9(9):1781-91.

246. Temraz S, Mukherji D, Shamseddine A. Dual Inhibition of MEK and PI3K Pathway in KRAS and BRAF Mutated Colorectal Cancers. Int J Mol Sci. 2015;16(9):22976-88.

247. Mohan P, Castellsague J, Jiang J, Allen K, Chen H, Nemirovsky O, et al. Genomic imbalance of HMMR/RHAMM regulates the sensitivity and response of malignant peripheral nerve sheath tumour cells to aurora kinase inhibition. Oncotarget. 2013;4(1):80-93.

Curriculum Vitae

Tahereh Vakili

EDUCATION

Master of Science in Biochemistry 2017
Western University, London, Canada
Master of Science in Clinical Biochemistry 2007
Urmia University of Medical Science, Urmia, Iran
Bachelor of Science in Biology 2003
Ferdowsi University of Mashhad, Mashhad, Iran

AWARDS AND DISTINCTIONS

CIHR Strategic Training Program in Cancer Research and Technology Transfer (CaRTT) 2013-2016
Translational Breast Cancer Research Unit (TBCRU) Award 2013-2016
Western Graduate Research Scholarship 2013-2016
Exceptional Talented Student Award, Urmia University of Medical Science, Iran 2007
Ranked 16th in the "National Graduate Entrance Exam" for Master of Science in Clinical Biochemistry, Iran 2004

TEACHING EXPERIENCES

Lecturer, Biochemistry for Midwifery, Maybod Azad University, Iran 2007-2010

RESEARCH EXPERIENCE

Western University, Canada Sept. 2013-Dec. 2018
Master of Science Thesis project: An invasive tumor cell subpopulation as a therapeutic target in breast cancer

Yazd University of Medical Science, Iran July 2009-Sept. 2011
Research Projects:

1) Effect of Turmeric water extract on GLUT4 translocation from intracellular compartments into the cytoplasmic membrane of C2C12 myotubes
2) Comparative efficacy of Hydrogen peroxide and Silver composition with Deconex as a hospital disinfectant
3) Antibacterial effects of Hydrogen peroxide and Silver composition on selected pathogenic enterobacteria
4) Effect of three selected trace elements on plasma coagulation and fibrinolysis indices

Urmia University of Medical Science, Iran Sept. 2005-Sept. 2007

Master of Science Thesis project: Relationship between inflammatory markers and the presence of angiographically verified coronary artery disease

Research Project: Relationship between Antioxidant markers and the presence of angiographically verified coronary artery disease

Bu-Ali Research Institute, Mashhad University of Medical Science, Iran Mar. 2001-Jan. 2002

Bachelor of Science Thesis project: Characterization of Rab-6 protein in Rat atrial myocytes

PUBLICATIONS

1. Ahmadipour F, **Vakili T**, Absalan A, Mohiti–Ardakani J, Hadinedoushan H, Khlili M, Pourrajab F, " C2C12 Cell Line Is a Good Model to Explore the Effects of Herbal Extracts on GLUT4 Expression and Translocation". Iranian journal of diabetes and obesity. 2012, 4(4): 143-151.
2. Davoudi M, Ehrampoush M, **Vakili T**, Absalan A, "Antibacterial effects of Hydrogen peroxide and Silver composition on selected pathogenic enterobacteria". International Journal of Environmental Health Engineering. 2012; 1(2).
3. Absalan A, **Vakili T**, Jalali Khanabadi B, "Effect of three selected trace elements on plasma coagulation and fibrinolysis indices". Journal of Shahid Sadoughi University of Medical Sciences, 2011; 19(3):323-8.
4. **Vakili T**, Khadem vatan K, Salari Lak Sh, Nourooz-zadeh J, "Association of C-reactive protein with the extent of angiographically verified coronary artery disease". Journal of Shahid Sadoughi University of Medical Sciences. 2010; 5(76):412-20.

PRESENTATIONS

1. **Vakili T**, Tolg C, Leith S, Turley E (2017) “An invasive tumor cell subpopulation as a therapeutic target in breast cancer”. (Poster) 11th International Conference on Hyaluronan, Cleveland, USA.
2. **Vakili T**, Tolg C, Hill K, Turley E (2016) “An invasive cell subpopulation as a model for triple negative breast cancer”. (Poster) TFRI-Ontario Node Research Symposium, Toronto, Canada.
3. **Vakili T**, Tolg C, Turley E (2015) “An invasive tumor cell subpopulation as a potential therapeutic target in breast cancer”. (Poster) London Health Research Day, London, Canada.
4. **Vakili T**, Turley E (2014) “An invasive but slow-growing tumor cell subset as a potential new diagnostic and therapeutic target in breast cancer”. (Poster) Oncology Research and Education Day, London, Canada.
5. **Vakili T**, Turley E (2014) “An invasive but slow-growing tumor cell subset as a potential new diagnostic and therapeutic target in breast cancer”. (Poster) London Health Research Day, London, Canada.
6. Absalan A, Mohiti J, **Vakili T** (2011) "C2C12 cell line is a good model to explore the effects of

herbal extracts on muscular GLUT4 metabolism". (Poster) The 12th Iranian Congress of Biochemistry & 4th International Congress of Biochemistry & Molecular Biology, Mashhad, Iran, Published Abstract: Clin Biochem 44(13):0 (2011).

7. Absalan A, **Vakili T,** Jalali Khanabadi B (2010) "Effect of three selected trace elements on plasma coagulation and fibrinolysis indices". (Poster) The 2nd congress of Iranian trace elements, Tehran, Iran.
8. Servat H, Nourooz-Zadeh J, **Vakili T** (2009)"Gamma glutamyltransferase (GGT) is a novel risk factor for CAD". (Poster) The 10th Iranian Congress of Biochemistry & the 3rd International Congress of Biochemistry & Molecular Biology, Tehran, Iran.
9. **Vakili T**, Nourooz-zadeh J (2009) "Relationship between inflammatory markers and the presence of angiographically verified coronary artery disease". (Poster) The 8th International Congress on Coronary Artery Disease, Prague, Czech Republic.
10. Nourooz-Zadeh J, Eftekhar E, Haghparast F, Khadem vatan K, **Vakili T** (2007) "Enhanced lipid peroxidation and impaired antioxidant balance in patients with coronary artery disease proven angiographically". (Poster) The 9th Iranian Congress of Biochemistry & the 2nd International Congress of Biochemistry and Molecular Biology, Shiraz, Iran.
11. **Vakili T**, Sarafraz yazdi E (2002) "Small GTP-binding proteins, Rab 6 in secretary granules of Rat atrial myocytes". (Oral talk) The 1st Student Congress of Biology and Biotechnology, Isfahan, Iran.